Investigations of the Interplay of Molecule Structures, Crystal Packing, Solar Cell, and Field-Effect Transistor Characteristics in Novel Polymeric Semiconductors

Yiho Kim

Department of Energy Engineering

Graduate School of UNIST

Investigations of the Interplay of Molecule Structures, Crystal Packing, Solar Cell, and Field-Effect Transistor Characteristics in Novel Polymeric Semiconductors

A thesis submitted to the Graduate School of UNIST
in partial fulfillment of
the requirements for the degree of
Doctor of Philosophy

Yiho Kim

12. 16. 2014 of submission
Approved by

Major Advisor
Changduk Yang

Investigations of the Interplay of Molecule Structures, Crystal Packing, Solar Cell, and Field-Effect Transistor Characteristics in Novel Polymeric Semiconductors

Yiho Kim

This certifies that the thesis of Yiho Kim is approved.

12. 16. 2014 of submission

Thesis supervisor [Changduk Yang]

[Hyun-Kon Song]

[Kwanyong Seo]

[Tae-Hyuk Kwon]

[Minseok Kwak]

Acknowledgements

Foremost, I would like to express my sincere gratitude to the chairman of ISU Group, Sang-Beom Kim for providing me with the opportunity that I explored new world, also the president of ISU Chemical, Kyu-Chul Lee and the former president of ISU Chemical, In-Koo Kang for their continuous support until I finished my dissertation.

I would like to thank the director of ISU Chemical Research Center, Dr. In-Chul Oh, the team reader, Chang-Kuk Kim and all members of R&D Team, I would never have been able to finish my dissertation without their help.

I would like express my deepest gratitude and veneration to my advisor, Prof. Changduk Yang for his excellent guidance, caring, patience and personal support throughout all my years in graduate school of UNIST and I believe that the instruction of Prof. Changduk Yang will be the steadfast foundation to make me overcome every infliction which will have been waiting for me in the future. Also, I am grateful to all of Yang Group's members.

Finally, I would like express my warmest gratitude to my whole family, especially my wife Sungshin and two daughters, Taehee and Minkyeong. They were always there cheering me up and stood by me through the good and bad time.

Table of Contents

List of Figures

Chapter 1

Chapter 2

Chapter 3

Chapter 4

List of Schemes

Chapter 2

Chapter 3

Chapter 4

List of Table

Chapter 2

Chapter 3

Chapter 4

Glossary of Abbreviations

AFM	Atomic force microscopy
BHJ	Bulk-heterojunction
Bz	Benzene
CF	Chloroform
CN	1-Chloronaphthalene
CT	Charge transfer
CV	Cyclic voltammetry
D-A	Donor-Acceptor
DFT	Density functional theory
DIO	1,8-Diiodooctane
DPE	Diphenylether
EDTA	Ethylenediaminetetraacetic acid
FF	Fill factor
GIXD	Grazing incidence X-ray diffraction
GPC	Gel permeation chromatography
HOMO	Highest occupied molecular orbital
ICT	Intramolecular charge transfer
IPCE	Incident photon-to-electron conversion efficiency
ITO	Indium tin oxide
J	Coupling constants
$\mathbf{J_{sc}}$	Short-circuit current

LUMO	Lowest occupied molecular orbital
Mn	Number-averaged molecular weight
NDI	Naphthalene diimide
NEXAFS	Near-edge X-ray absorption fine structure
NMR	Nuclear magnetic resonance
Np	Naphthalene
***o*-DCB**	o-dichlorobenzene
2OD	2-Octyldodecyl
ODT	1,8-Octanedithiol
OFETs	Organic field-effect transistors
OTS	n-Octadecyltrimethoxysilane
P(NDI2SiC6-T2)	Poly((N,N'-bis(1,1,1,3,5,5,5-heptamethyltrisiloxane)-1,4,5,8-naphthalenediimide-2,6-diyl)-alt-5,5'-bithiophene)
P(NDI2SiC6-TVT)	Poly((N,N'-bis(1,1,1,3,5,5,5-heptamethyltrisiloxane)-1,4,5,8-naphthalenediimide-2,6-diyl)-alt-5,5'-(E)-2-(2-(thiophene-2-yl)-vinyl)thiophene)
$PC_{71}BM$	[6,6]-Phenyl C_{71}-butyric acid methyl ester
PCE	Power conversion efficiency
PDI	Polydispersity index
PEDOT	Poly(3,4-ethylenedioxythiophene)
PNDI-Bz	Poly((N,N'-bis(2-octyldodecyl)-1,4,5,8-naphthalene diimide-2,6-diyl)-alt-1,4-benzene)
PNDI-Np	Poly((N,N'-bis(2-octyldodecyl)-1,4,5,8-naphthalene diimide-2,6-diyl)-alt-2,6-naphthalene)
PNDI-Py	Poly((N,N'-bis(2-octyldodecyl)-1,4,5,8-naphthalene diimide-2,6-diyl)-alt-2,7-pyrene)

PNDI-Se	Poly((N,N'-bis(2-octyldodecyl)-1,4,5,8-naphthalenedicarboximide-2,6-diyl)-2,5-selenophene)
PNDI-Th	Poly((N,N'-bis(2-octyldodecyl)-1,4,5,8-naphthalenedicarboximide-2,6-diyl)-2,5-thiophene)
PSCs	Polymer solar cells
PSS	Poly(styrenesulfonate)
Py	Pyrene
RMS	Root-mean-square
SCLC	Space-charge-limited current
Se	Selenophene
T2	Bithiophene
TCB	Trichlorobenzene
TDM	Transition dipole moment
TEM	Transmission electron microscopy
TG/BC	Top-gate, bottom-contact
Th	Thiophene
THF	Tetrahydrofuran
TQ1	Poly[2,3-bis-(3-octyloxyphenyl)-quinoxaline-5,8-alt-thiophene-2,5-dyl]
TVT	(E)-2-(2-(thiophen-2-yl)-vinyl)thiophene
V_{oc}	Open-circuit voltage
XRD	X-ray diffraction
YFM	Y-functin method

Chapter 1

Introduction

1.1. Semiconducting polymer

Due to the interesting electronic properties similar to metals or semiconductor, alongside the easy processability and mechanical properties, conjugated or conducting polymers have been widely investigated. Since the electrical properties of polyaniline obtained through the anodic oxidation method of aniline were reported, a lot of interesting research results have been being reported as results of efforts to find new materials with high efficiency of charge transport. As a example of the simplest conjugated polymer, polyacetylene, especially trans configuration, doped with iodine was reported to exhibit high conductivity by Hideki Shirakawa, Alan G. MacDiamd and Alan J. Heeger in 1977, (see Figure 1.1 they demonstrate that the high conductivity could be granted to polyacetylene with the simplest π-conjugated system just merely applying iodine doping method.[1-3] These three pioneers were awarded the Novel Prize in recognition of their distinguished research results in 2000.

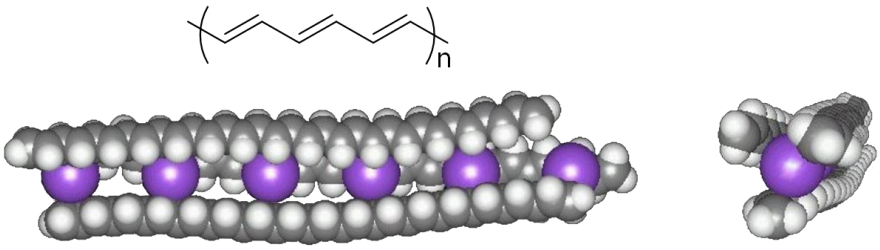

Figure 1.1 *rans*-Polyacetylene doped with iodine.

Two types of electrons exist in polyacetylene forming the chemical bondings. These two

types of electrons involve in the formation of σ- and π-bonding in polyacetylene called as σ and π electron respectively. General π-conjugated system is composed of alternating single and multi bonds like double or triple bond. Especially, the conjugation system of polyacetylene is constructed by the combination of these two kinds of bondings, single and double bond. The energy level of σ-bonding electron is quite low, meanwhile π-bonding electron resides higher energy level orbital compare with σ-bonding electron. Also these energy levels of π-bonding electrons are getting higher and π-bonding electrons are getting more delocalized as the conjugation length increase allowing π electrons easily to move. Because the unique electronic properties of conducting polymers are attributed to the π-conjugated system, studies on synthesis and evaluation of conducting polymers have been extensively carried out using diverse materials to control of electronic properties of conjugated polymer. Electric properties of semiconducting polymers can be well depicted with the simplified energy band diagram described in Figure 1.2 As shown in Figure 1.2, this energy band diagram is constructed by many energy bands to be originated from anti-bonding and bonding energy levels associated with forming the σ-bonds and π-bonds in the molecule.

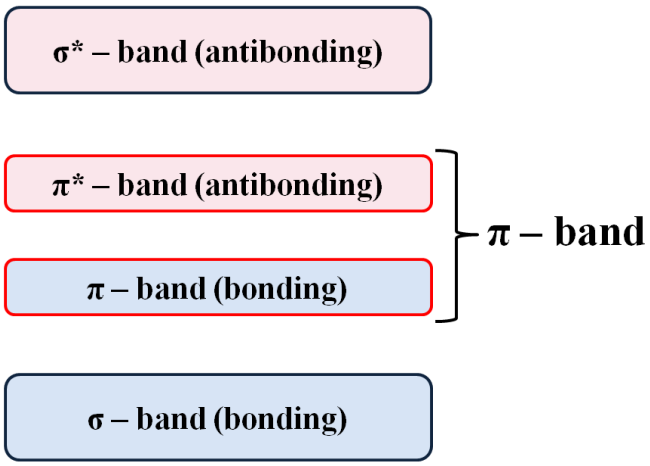

Figure 1.2 simplified band diagram for π-conjugated polymers.

However these two types of bonds exhibit the different characteristics, σ-bonds generally contribute to the structure of molecule, while the π-bonds present the electric properties to conjugated polymer as semiconducting polymer. Semiconducting polymer, as one kind of these conjugated polymers has recently come into the spotlight for the application of electronic devices, organic photovoltaic devices (OPVs) or organic field-effect transistors (OFETs) and other electronic devices.

1.1.1. Quinoxaline-based copolymer for the application of OPVs

Recently, the sustainability of energy sources is getting more important due to the oil price rise and environmental pollution. These needs for renewable energy sources have enlivened development of photovoltaic energy conversion. Although there are some kinds of photovoltaic conversion technology, polymer solar cell is one of the most powerful methods for solar energy conversion considering its advantages in low cost, convenient fabrication process like solution processing technique, light weight and possibility for the application to flexible devices.[4-9] Since the concept of bulk heterojunction (BHJ) successfully worked on polymer solar cells, almost polymer solar cells having high efficiency have been fabricated based on this BHJ concept, which uses mixture of electron donating polymer as p-type semiconducting material and electron accepting material; [6,6]-phenyl-C_{61}-butyrid acid methyl ester ($PC_{61}BM$) or [6,6]-phenyl-C_{71}-butyrid acid methyl ester ($PC_{71}BM$)), as n-type semiconducting material.[10-15] Not only the large interfacial area but also high light absorption by light scattering can be obtained through BHJ method.[16,17] Notwithstanding these advantages of polymer solar cell, in order to improve PCE, synthesis of low energy bandgap polymer with broad absorption property have been intensively investigated.[15,18-21] Recently,

low energy band-gap polymers having Donor-Acceptor structure have been developed and these materials exhibited 7-8 % of PCE. PTB7 is the first and most representative low band-gap polymer showing over 7% PCE and these great research achievements have played the role of pioneer in commercialization of polymer solar cells.[22-26] From this point of view, Poly[2,3-bis-(3-octyloxyphenyl)quinoxaline-5,8-dyl-alt-thiophene-2,5-diyl] (TQ1) to be reported as CT(charge-transferred)-type copolymer firstly by Takakazu Yamamoto in 2003 have been considered as one of the most promising materials for OPVs due to its favorable characteristics for OPVs just like simple synthetic route, low energy bandgap energy (~1.7 eV), low lying HOMO level (-5.5 eV).[27] (see Figure 1.3)

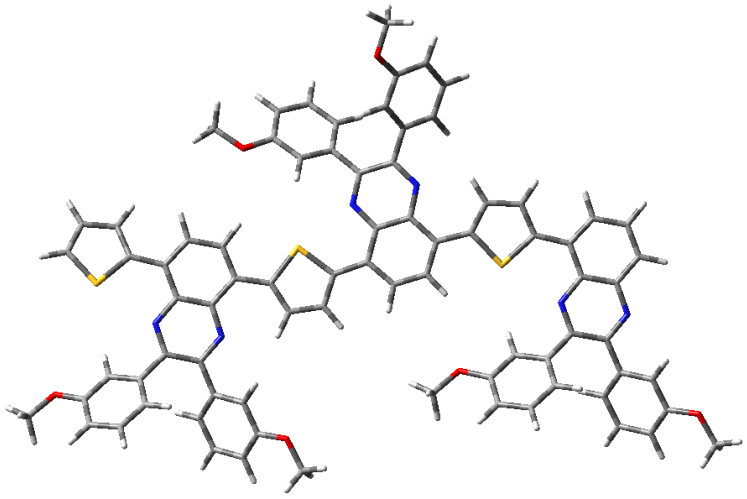

Figure 1.3 Molecular structure of TQ1.

Since Mats R. Andersson demonstrated the high efficiency over 6% using TQ1 as active material in BHJ solar cell in 2010, this material have attracted attention of many researchers for the application of polymer solar cell.[28] The goal of this study is to evaluate the effect of additives on surface morphology and crystallnity in thin film in order to obtain highest efficiency of TQ1-based solar cell through the maximization of the virtues of TQ1.

1.1.2. Naphthalene Diimide copolymer for the application of OFETs

Recently, as the consumer's desire for potable smart-electronics to make them access any information or data which they want without restriction of place and time explosively increase, the development of advanced technologies and synthesis of new materials to satisfy these demands for new generation electronics have been required continuously. Solution-processing technique has been evaluated as one of most cost-effective fabrication methods and this printing technology has been opening our daily life to new world, called as ubiquitous that we never experienced before.[29-36] However, despite appearance of incredible technique to fabricate electronic devices at a low cost, the synthesis of new efficient polymeric materials based on rational design concept cannot be too emphasized for the manufacture of large area and flexible devices. Especially, organic thin-film transistor (OTFT) fabricated with polymeric materials as active layer have widely been investigated by academic and industrial researchers for the realization of flexible and ultralow-cost logic circuits. On the strength of tremendous investigation results, although some polymeric materials with excellent hole mobilities have been reported for the application of p-channel OFETs,[29,37-39] there is a lack of researches on polymeric semiconductors to exhibit n-type dominant property and also, the focuses of these studies are limited to change the donor moieties in order to control n-type property resulted in the increased electron mobility.[40-50] Therefore, the development of design concept and syntheses of n-type polymeric materials still remains challenging and fascinating. Among n-type materials, especially with PDI (Perylene Diimide), NDI (Naphthalene Diimide) to have unique tetracarboxylic diimide structure has been widely studied for the application of strong electron accepting unit and the resulting donor (D)-acceptor (A) type copolymers have been evaluated as leading candidate

materials for the fabrication of organic electronics for example, organic thin-film transistor (OTFT). Due to its strong electron withdrawing ability, NDI derivatives have been adapted for n-type characteristic materials from small-molecule to polymeric semiconductors. Since Facchetti's group showed the possibility that NDI based D-A type copolymers could be applicable to p-n junction logic circuit through the fabrication of top-gate bottom contact OTFT device exhibiting electron mobility near integer levels, 0.85cm^2/Vs, lots of studies have been conducted by individual research groups.[51,52] In spite of these well defined study results, the investigation of NDI copolymers have primarily been focused on thiophene and its derivatives as electron donating unit. It is no exaggeration to say that these limits to study controlling LUMO levels of D-A type NDI copolymers have resulted from the steadfast results of experiment reported by lots of research groups.[53] Notwithstanding, the researching trends up to now have been stressed on the evaluation of effects that the change of donor moieties influence the LUMO level, electron mobility of NDI based copolymers, and formation of morphology in thin film state, although it is generally known that turning LUMO level of intended copolymers is very difficult with only substitution of donor moiety exploring lots of NDI based copolymers having different structure from each other. In spite of the limit of NDI based copolymer as mentioned above, NDI core unit as electron accepting unit is still one of the fascinating material because of the intrinsic property of NDI core unit allowing LUMO level lowering. As a endeavor overcoming this limit in tuning in the energy level at molecular level, and a trial widening the understanding of intrinsic conformation properties, recently research results on structural properties and optoelectrochemical properties have been published by individual research groups. Especially, the research conducted by Dieter Neher and co-workers shows very interesting and important information

on the intrinsic properties with regard to physical state in solution and thin film formation of NDI based copolymer. According to their research results, the physical states of NDI-bithiophene copolymer (P(NDI2OD-T2), N2200) in solution are apparently different each other depending on solvents used, meaning the degree of aggregation varies from amorphous to aggregated state, also furthermore these physical state in solution decide the crystalline structure of thin film state. (see Figure 1.4) From this point of view, it is the goal of this study to investigate the relationship between the molecular structure of NDI-based copolymer or the degree of aggregation from solution state to thin film state and the efficiency of OFETs, and to propose the unprecedented design strategy to obtain high electron mobility compared with existing NDI-based copolymers having general branched alkyl groups.

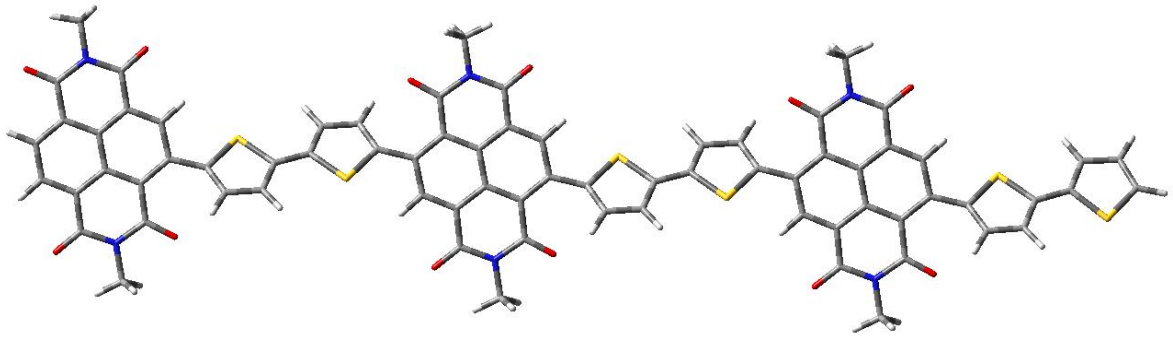

Figure 1.4 Molecular structure of P(NDI2OD-T2).

1.2. Palladium-catalysed reaction for Carbon-Carbon bond formation

Even though there are many carbon-carbon (C-C) coupling reaction, Some coupling reactions especially catalysed by palladium have been widely investigated using different substrates and the representative reactions are summarized in Figure 1.5.

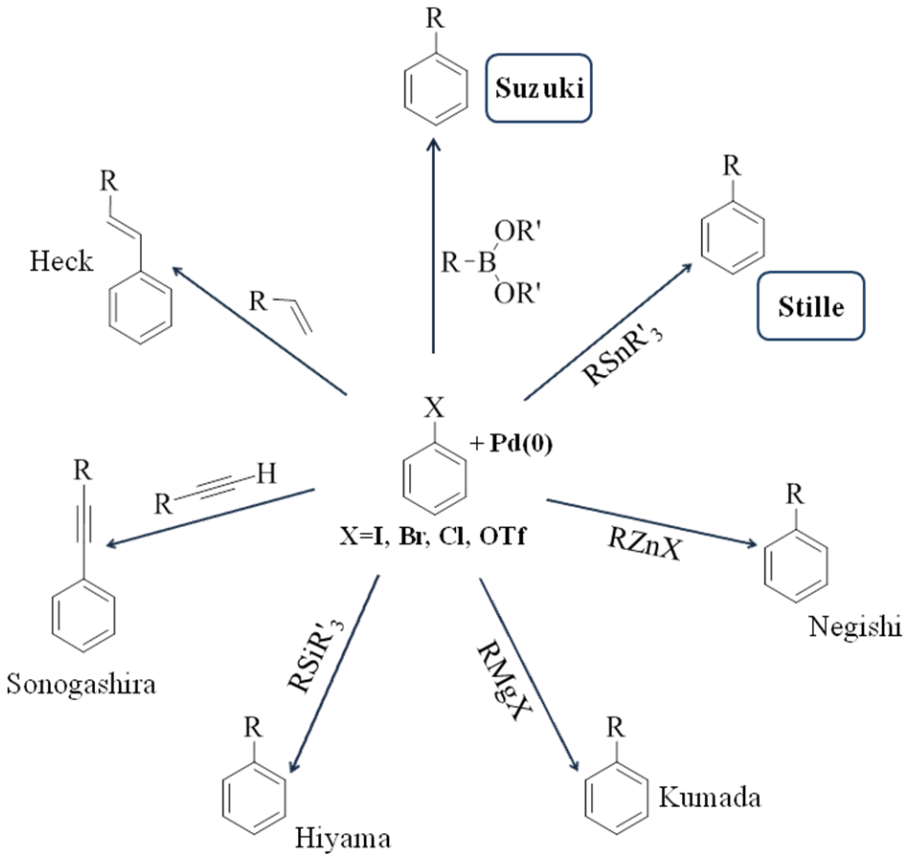

Figure 1.5 Palladium-catalysed reaction for Carbon-Carbon bond formation.

A similar catalytic reaction cycle as described in Figure 1.6 is suggested to be involved in the most palladium catalysed reactions. Pd2(dba)3, Pd(OAc)2 are used together with ligand as palladium sources, while Pd(PPh3)4 or Pd(PtBu3)2 are used as performed catalyst without activation procedure of catalyst.

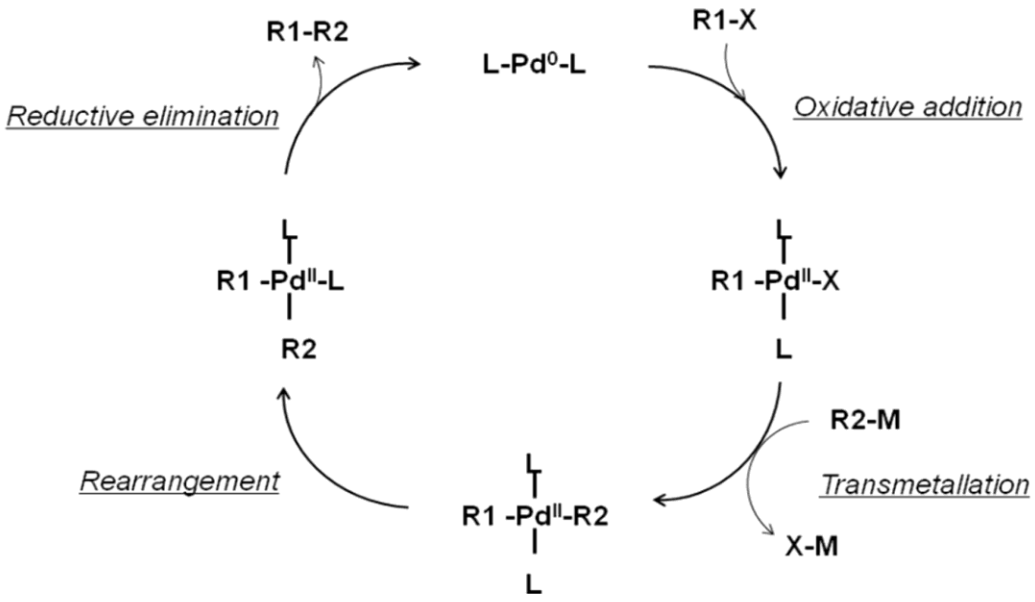

Figure 1.6 Palladium-catalyzed cross-coupling reaction cycle.

These two palladium-catalysed reactions for the formation of C-C bonds have been widely used in the synthesis of conjugated polymers. Depending on the chosen ligands incorporating palladium catalyst, two steps of catalytic cycle are facilitated. Generally, the strong σ-donating ligands incorporating catalyst like trialkylphosphines induce the increase of electron density around the metal, and electronic environment of prepared catalyst like this increase the rate of the oxidative addition of catalyst to the substrate. This is suggested to be the rate determining step of palladium-catalyzed reaction using ligand. The choice of ligand affect not only oxidative addition step but also accelerate the elimination step especially when the bulky ligands are used. Among a lot of these useful palladium-catalysed (C-C) coupling reaction, Suzuki and Stille reaction is distinguished for its versatile C-C bond forming ability between halides compound and organoboronic acid for Suzuki reaction or organotin compound for Stille reaction. In this study, target copolymers were synthesized by Suzuki and Stille reaction.

1.2.1. Suzuki reaction

Suzuki reaction was named after Akira Suzuki who had firstly reported this reaction using organohalides and organoboron reagents under basic aqueous condition for the formation C-C bond. This reaction shows high tolerance of many different functional groups and is considered to be one of the most effect aryl-aryl coupling methods. When compared with Stille reaction, the only different thing is that the organoboron reagent should be activated first. The activated boron atom induces the polarization of the organic ligand bonded to palladium catalyst then facilitates transmetallation, one of the four steps in reaction cycle. In this study three NDI based copolymers were synthesized with Suzuki reaction for the application of OPVs and OFETs.

1.2.2. Stille reaction

The Stille reaction is one of the extremely powerful reactions which have widely used for the formation of C-C bond with organotin compounds. The Stille reaction is considered as a complementary method to Suzuki reaction, and also to have very few limitations on the R-group. Toxicity of the organotin compounds is recognized as the main disadvantage of Stille reaction, however the most strong point of this reaction is that it is possible to carry out the reaction under neutral conditions. In this study, five copolymers were synthesized with Stiller action for the application of OPVs and OFETs.

1.3. Reference

(1) Heeger, A. J.; Kivelson, S.; Schrieffer, J.; Su, W.-P. *Rev. Mod. Phys.* **1988**, *60*, 781.

(2) Heeger, A. J. *Rev. Mod. Phys.* **2001**, *73*, 681.

(3) Heeger, A. J. *Angew. Chem. Int. Ed.* **2001**, *40*, 2591.

(4) Brabec, C. J.; Sariciftci, N. S.; Hummelen, J. C. *Adv. Funct. Mater.* **2001**, *11*, 15.

(5) Coakley, K. M.; McGehee, M. D. *Chem. Mater.* **2004**, *16*, 4533.

(6) Gunes, S.; Neugebauer, H.; Sariciftci, N. S. *Chem. Rev.* **2007**, *107*, 1324.

(7) Lewis, N. S. *Science* **2007**, *315*, 798.

(8) Scharber, M. C.; Wuhlbacher, D.; Koppe, M.; Denk, P.; Waldauf, C.; Heeger, A. J.; Brabec, C. L. *Adv. Mater.* **2006**, *18*, 789.

(9) Helgesen, M.; Sondergaard, R.; Krebs, F. C. *J. Mater. Chem.* **2010**, *20*, 36.

(10) Campoy-Quiles, M.; Ferenczi, T.; Agostinelli, T.; Etchegoin, P. G.; Kim, Y.; Anthopoulos, T. D.; Stavrinou, P. N.; Bradley, D. D. C.; Nelson, J. *Nat. Mater.* **2008**, *7*, 158.

(11) Ma, W.; Yang, C.; Gong, X.; Lee, K.; Heeger, A. J. *Adv. Funct. Mater.* **2005**, *15*, 1617.

(12) Moulé, A. J.; Meerholz, K. *Adv. Mater.* **2008**, *20*, 240.

(13) Thompson, B. C.; Frechet, J. M. J. *Angew. Chem. Int. Ed.* **2008**, *47*, 58.

(14) Yang, X.; Loos, J. *Macromolecules* **2007**, *40*, 1353.

(15) Chen, M.-H.; Hou, J.; Hong, Z.; Yang, G.; Sista, S.; Chen, L.-M.; Yang, Y. *Adv. Mater.* **2009**, *21*, 4238.

(16) Dennler, G.; Scharber, M. C.; Brabec, C. J. *Adv. Mater.* **2009**, *21*, 1323.

(17) Yu, G.; Gao, J.; Hummelen, J. C.; Wudl, F.; Heeger, A. J. *Science* **1995**, *270*, 1789.

(18) Svensson, M.; Zhang, F. L.; Veenstra, S. C.; Verhees, W. J. H.; Hummelen, J. C.; Kroon, J. M.; Inganas, O.; Andersson, M. R. *Adv. Mater.* **2003**, *15*, 988.

(19) Chen, H.-Y.; Hou, J.; Zhang, S.; Liang, Y.; Yang, G.; Yang, Y.; Yu, L.; Wu, Y.; Li, G. *Nat. Photonics* **2009**, *3*, 649.

(20) Wang, E.; Wang, M.; Wang, L.; Duan, C.; Zhang, J.; Cai, W.; He, C.; Wu, H.; Cao, Y. *Macromolecules* **2009**, *42*, 4410.

(21) Zhang, F. L.; Bijleveld, J.; Perzon, E.; Tvingstedt, K.; Barrau, S.; Inganas, O.; Andersson, M. R. *J. Mater. Chem.* **2008**, *18*, 5468.

(22) Wang, E. G.; Wang, L.; Lan, L. F.; Luo, C.; Zhuang, W. L.; Peng, J. B.; Cao, Y. *Appl. Phys. Lett.* **2008**, *92*.

(23) Hou, J.; Chen, H.-Y.; Zhang, S.; Li, G.; Yang, Y. *J. Am. Chem. Soc.* **2008**, *130*, 16144.

(24) Liang, Y.; Feng, D.; Wu, Y.; Tsai, S.-T.; Li, G.; Ray, C.; Yu, L. *J. Am. Chem. Soc.* **2009**, *131*, 7792.

(25) Qin, R.; Li, W.; Li, C.; Du, C.; Veit, C.; Schleiermacher, H.-F.; Andersson, M.; Bo, Z.; Liu, Z.; Inganäs, O.; Wuerfel, U.; Zhang, F. *J. Am. Chem. Soc.* **2009**, *131*, 14612.

(26) Liang, Y.; Xu, Z.; Xia, J.; Tsai, S.-T.; Wu, Y.; Li, G.; Ray, C.; Yu, L. *Adv. Mater.* **2010**, *22*, E135.

(27) Yamamoto, T.; Lee, B.-L.; Kokubo, H.; Kishida, H.; Hirota, K.; Wakabayashi, T.; Okamoto, H. *Macromol. Rapid. Commun.* **2003**, *24*, 440.

(28) Wang, E.; Hou, L.; Wang, Z.; Hellström, S.; Zhang, F.; Inganäs, O.; Andersson, M. R. *Adv. Mater.* **2010**, *22*, 5240.

(29) Kim, G.; Kang, S.-J.; Dutta, G. K.; Han, Y.-K.; Shin, T. J.; Noh, Y.-Y.; Yang, C. *J. Am. Chem. Soc.* **2014**, *136*, 9477.

(30) Lee, J.; Han, A.-R.; Kim, J.; Kim, Y.; Oh, J. H.; Yang, C. *J. Am. Chem. Soc.* **2012**, *134*, 20713.

(31) Lee, J.; Han, A.-R.; Yu, H.; Shin, T. J.; Yang, C.; Oh, J. H. *J. Am. Chem. Soc.* **2013**, *135*, 9540.

(32) Baeg, K.-J.; Caironi, M.; Noh, Y.-Y. *Adv. Mater.* **2013**, *25*, 4210.

(33) Olivier, Y.; Niedzialek, D.; Lemaur, V.; Pisula, W.; Müllen, K.; Koldemir, U.; Reynolds, J. R.; Lazzaroni, R.; Cornil, J.; Beljonne, D. *Adv. Mater.* **2014**, *26*, 2119.

(34) Tsao, H. N.; Cho, D. M.; Park, I.; Hansen, M. R.; Mavrinskiy, A.; Yoon, D. Y.; Graf, R.; Pisula, W.; Spiess, H. W.; Müllen, K. *J. Am. Chem. Soc.* **2011**, *133*, 2605.

(35) Sirringhaus, H. *Adv. Mater.* **2014**, *26*, 1319.

(36) Mei, J.; Diao, Y.; Appleton, A. L.; Fang, L.; Bao, Z. *J. Am. Chem. Soc.* **2013**, *135*, 6724.

(37) Tseng, H.-R.; Phan, H.; Luo, C.; Wang, M.; Perez, L. A.; Patel, S. N.; Ying, L.; Kramer, E. J.; Nguyen, T.-Q.; Bazan, G. C.; Heeger, A. J. *Adv. Mater.* **2014**, *26*, 2993.

(38) Li, J.; Zhao, Y.; Tan, H. S.; Guo, Y.; Di, C.-A.; Yu, G.; Liu, Y.; Lin, M.; Lim, S. H.; Zhou, Y.; Su, H.; Ong, B. S. *Sci. Rep.* **2012**, *2*.

(39) Kang, I.; Yun, H.-J.; Chung, D. S.; Kwon, S.-K.; Kim, Y.-H. *J. Am. Chem. Soc.* **2013**, *135*, 14896.

(40) Newman, C. R.; Frisbie, C. D.; da Silva Filho, D. A.; Brédas, J.-L.; Ewbank, P. C.; Mann, K. R. *Chem. Mater.* **2004**, *16*, 4436.

(41) Chua, L.-L.; Zaumseil, J.; Chang, J.-F.; Ou, E. C. W.; Ho, P. K. H.; Sirringhaus, H.; Friend, R. H. *Nature* **2005**, *434*, 194.

(42) Oh, J. H.; Lee, H. W.; Mannsfeld, S.; Stoltenberg, R. M.; Jung, E.; Jin, Y. W.; Kim, J. M.; Yoo, J.-B.; Bao, Z. *Proc. Natl. Acad. Sci. U.S.A.* **2009**, *106*, 6065.

(43) Usta, H.; Risko, C.; Wang, Z.; Huang, H.; Deliomeroglu, M. K.; Zhukhovitskiy, A.; Facchetti, A.; Marks, T. J. *J. Am. Chem. Soc.* **2009**, *131*, 5586.

(44) Steyrleuthner, R.; Di Pietro, R.; Collins, B. A.; Polzer, F.; Himmelberger, S.; Schubert, M.; Chen, Z.; Zhang, S.; Salleo, A.; Ade, H.; Facchetti, A.; Neher, D. *J. Am. Chem. Soc.* **2014**, *136*, 4245.

(45) Chen, H.; Guo, Y.; Mao, Z.; Yu, G.; Huang, J.; Zhao, Y.; Liu, Y. *Chem. Mater.* **2013**, *25*, 3589.

(46) Kim, R.; Amegadze, P. S. K.; Kang, I.; Yun, H.-J.; Noh, Y.-Y.; Kwon, S.-K.; Kim, Y.-H. *Adv. Funct. Mater.* **2013**, *23*, 5719.

(47) Anthony, J. E.; Facchetti, A.; Heeney, M.; Marder, S. R.; Zhan, X. *Adv. Mater.* **2010**, *22*, 3876.

(48) Sun, B.; Hong, W.; Yan, Z.; Aziz, H.; Li, Y. *Adv. Mater.* **2014**, *26*, 2636.

(49) Sonar, P.; Singh, S. P.; Li, Y.; Soh, M. S.; Dodabalapur, A. *Adv. Mater.* **2010**, *22*, 5409.

(50) Di Pietro, R.; Fazzi, D.; Kehoe, T. B.; Sirringhaus, H. *J. Am. Chem. Soc.* **2012**, *134*, 14877.

(51) Yan, H.; Chen, Z.; Zheng, Y.; Newman, C.; Quinn, J. R.; Dötz, F.; Kastler, M.; Facchetti, A. *Nature* **2009**, *457*, 679.

(52) Chen, Z.; Zheng, Y.; Yan, H.; Facchetti, A. *J. Am. Chem. Soc.* **2008**, *131*, 8.

(53) Steyrleuthner, R.; Schubert, M.; Howard, I.; Klaumünzer, B.; Schilling, K.; Chen, Z.; Saalfrank, P.; Laquai, F.; Facchetti, A.; Neher, D. *J. Am. Chem. Soc.* **2012**, *134*, 18303.

High-Efficiency Polymer Solar Cells with a Cost-Effective Quinoxaline Polymer through Nanoscale Morphology Control Induced by Practical Processing Additives

2.1. Abstract

In the quest to improve the performance of polymer solar cells (PSCs) with a view to realizing economically viable, various solvent additives such as 1,8-octanedithiol (ODT), 1,8-diiodooctane (DIO), diphenylether (DPE) and 1-chloronaphthalene (CN) are used in easily obtainable poly(2,3-bis-(3-octyloxyphenyl)quinoxaline-5,8-dyl-*alt*-thiophene-2,5-diyl) (TQ1)-based systems with [6,6]-phenyl C_{71}-butyric acid methyl ester ($PC_{71}BM$) as an acceptor to optimize the active layer nanomorphology. Utilizing a combination of X-ray diffraction (XRD), atomic force microscopy (AFM), and transmission electron microscopy (TEM), we find that the addition of 5% (v/v) CN leads to smoother films, less heterogeneous surface features, and well-distributed TQ1:$PC_{71}BM$ phases, resulting in more balanced charge transport in the devices and a highly efficient power conversion efficiency (PCE) of 7.08%. This is a record for quinoxaline-based PCSs and also comparable the hitherto reported highest efficiency of the PSCs in single junction devices. In addition, the PSCs using an inverted device structure show a respectable PCE of 5.83% with high stability to ambient exposure, maintaining over 80% of its initial PCE, even after storage in air for more than 1 month.

Chapter 2

2.2. Introduction

Bulk-heterojunction (BHJ) polymer solar cells (PSCs) based on conjugated donor polymers and acceptor fullerenes are promising devices for alternative energy sources because of their potential applications in flexible, light-weight, and low-cost large-area devices through roll-to-roll printing.[1-6] Primarily thanks to the development of new low bandgap donor polymers[7-10] and better control of the nanoscale morphology of the interpenetrating electron donor/acceptor networks,[11-19] great progress has been made in this field, and the power conversion efficiencies (PCEs) of solution-processed PSCs have reached 7-8%.[20] In principle, to push the PCEs of PSCs towards the theoretical limit,[21] achieving both a high short-circuit current (J_{SC}) and a high open-circuit voltage (V_{OC}) is critical, indeed essential. This has succeeded by using low bandgap polymers with deeper highest occupied molecular orbital (HOMO) levels[22,23] such as PSiFDTBT,[24] PFDTBT,[25] and PCDTBT.[26,27] On the other hand, many largely empirical strategies have been applied to achieve the aforementioned nanoscale morphology, including postproduction annealing,[28,29] solvent annealing,[30,31] and the introduction of processing additives or mixed solvents.[16,32] Alongside higher PCEs, for enhancing the confidence in the commercialization of PSCs, it is of critical importance to synthesize inexpensive polymers as well as to minimize processing cost.

In this regard, we focus our attention to an easily synthesized poly(2,3-bis-(3-octyloxyphenyl)quinoxaline-5,8-dyl-*alt*-thiophene-2,5-diyl) (TQ1) that simultaneously possesses a deep HOMO (~ -5.5 eV) and low bandgap (~ 1.7 eV)[33] as required by the proposed 'ideal polymers'[26,34] as well as the processing additives capable of modifying the BHJ organization in that they do not require additional fabrication steps. Despite the initial high PCE of up to 6.0% in a typical BHJ device from TQ1 and [6,6]-phenyl C_{71}-butyric acid

methyl ester ($PC_{71}BM$)[33] as well as another study reporting comparative tests on TQ1:$PC_{71}BM$ using mixed solvents,[35] no attempt has been made to create the optimal blend nanomorphology by using such techniques listed above for more efficient PCE operation.

In this contribution, we have comprehensively studied the effect of various solvent additives (1,8-octanedithiol (ODT), 1,8-diiodooctane (DIO), diphenylether (DPE) and 1-chloronaphthalene (CN)) on the BHJ PSCs based on TQ1:$PC_{71}BM$. Upon adding 5% (v/v) CN to the BHJ active layer, a PCE as high as 7.08% with J_{SC} of 12 mA/cm^2 and V_{OC} of 0.91 V is achieved. To the best of our knowledge, this is the highest value among quinoxaline-based PCSs reported to date. The techniques of X-ray diffraction (XRD), atomic force microscopy (AFM), and transmission electron microscopy (TEM) have been applied to study the influence of CN on the nanomorphology and crystallinity of TQ1:$PC_{71}BM$ blend. Besides, since long-term stability is another primary area of concern for commercial PSCs, the potential utilization of TQ1:$PC_{71}BM$ into inverted PSCs with ZnO and MoO_3 as electron-selective and hole-selective layers is explored, resulting in a high PCE of up to 5.83%. The inverted device using Au electrode retains over 80% of its original conversion efficiency after 30 days while the conventional one shows negligible photovoltaic activity within 7 days. From a manufacturing perspective, our studies boast a promising pathway for constructing low-cost PSCs with high efficiency as well as long-term stability.

2.3. Results and Discussion

2.3.1. Synthesis and Characterization

In Figure 2.1 a)-c), the molecular sturctures of TQ1, $PC_{71}BM$, and solvent additives used in this study together with the evergy level diagrams of the component materials are described. TQ1 was synthesized by Stille coupling according to literature reports, [33,36,37] (see Scheme 2.1) which shows a relatively high molecular weight (*Mn*) of 48kg/mole with polydispersity index (PDI) of 3.6, as determined by gel permeation chromatography (GPC).

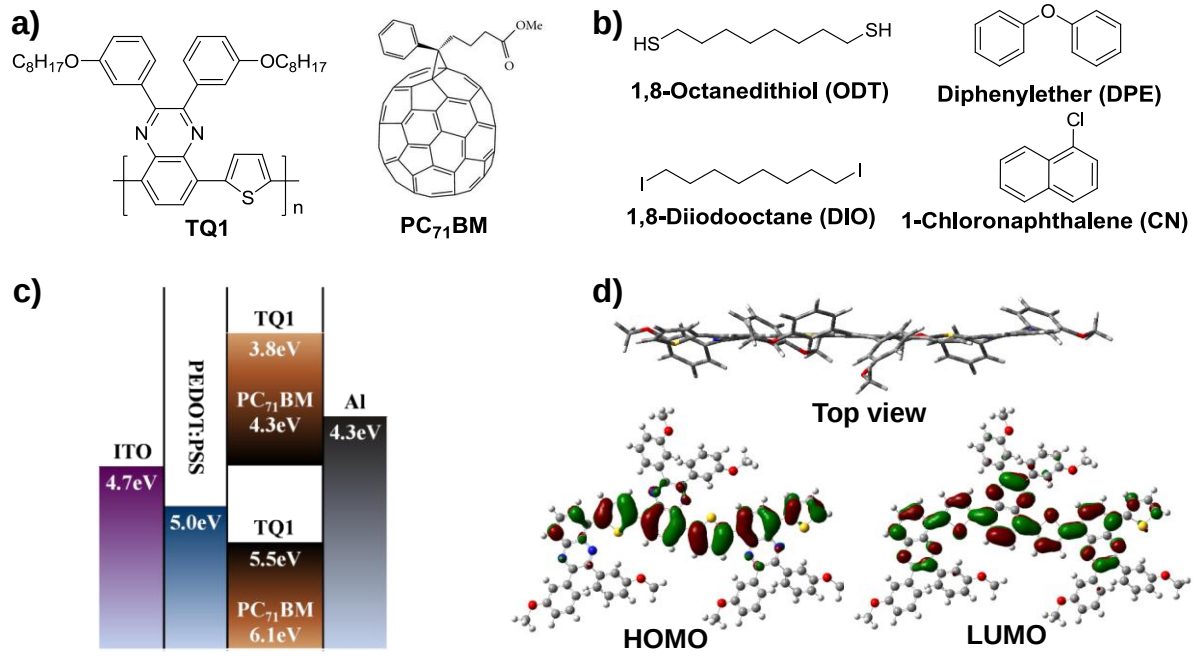

Figure 2.1 Molecular structure and DFT-optimized geometries. a) Molecular structures of TQ1, $PC_{71}BM$, and b) various solvent additives used in this study. c) Energy level diagram of the components. d) DFT-optimized geometries and charge-density iso-surfaces for the HOMO and LUMO levels of TQ1 trimer.

Scheme 2.1 Synthesis of monomer intermediates and target polymer TQ1

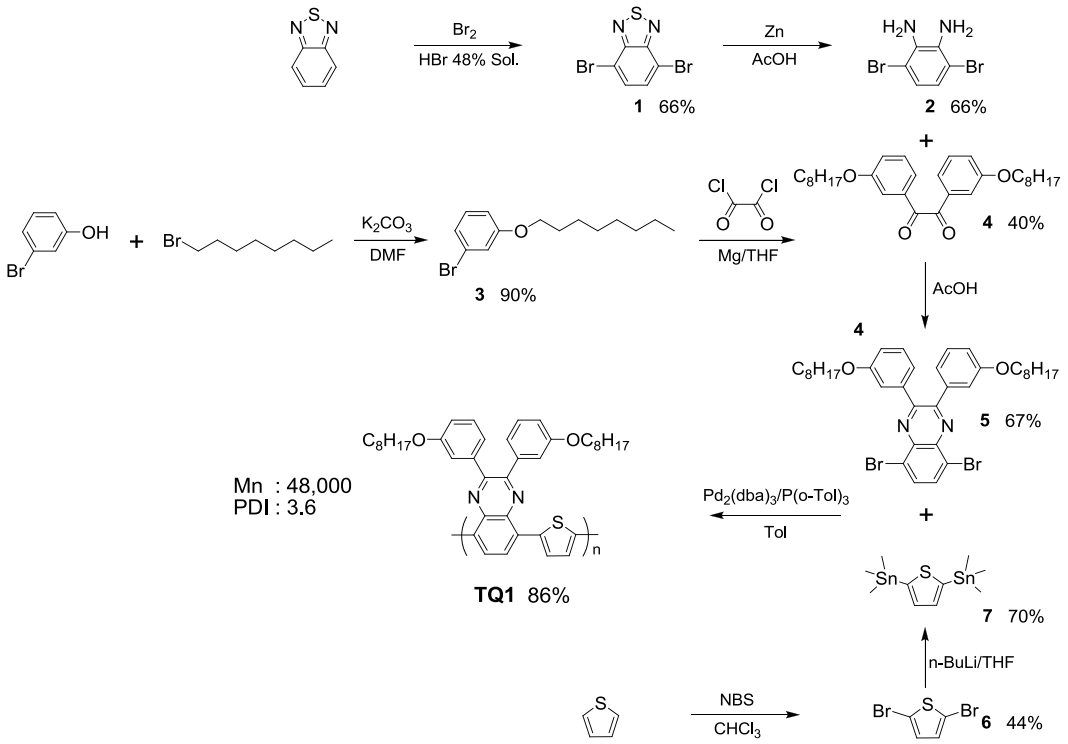

2.3.2. Photophysical and Electrochemical Properties as Computational Studies

On the basis of the photophysical and electrochemical stidies (see Figure 2.2), the highest occupied molecular orbital (HOMO) energy level, -5.5 eV is calculated using oxidation potential of TQ1 thin film and the lowest unoccupied molecular orbital (LUMO) is calculated from HOMO energy and the optical band gap (1.7 eV). [33]

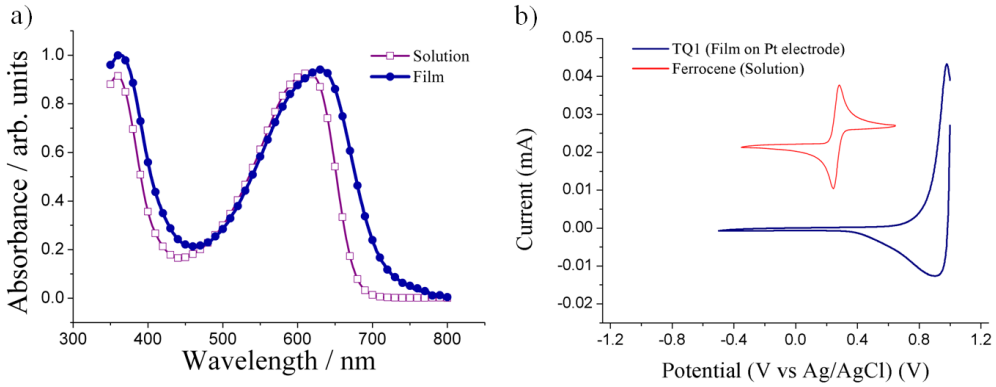

Figure 2.2 a) UV-Vis absorption spectra of TQ1 in dilute chloroform solution and thin films on glass plate. b) Cyclic voltammograms of TQ1 in the films.

Upon utilizing a model trimeric system containing methoxy groups instead of octyloxyl chains for simplicity, the optimized molecular geometry of TQ1 and its molecular orbitals of the calculated HOMO and LUMO isosurfaces were computed by density functional theory (DFT, B3LYP/6-31G) (Figure 2.1 d)). Interestingly, both the HOMO and LUMO are well spread over the whole conjugated backbone, implying a 'strong donor-weak acceptor' system of TQ1. This is in contrast to many other donor-acceptor polymers in which the LUMO is localized upon the electron accepting core of the polymer backbone. The localization can hinder interchain electron transport, since hopping requires good alignment of the localized LUMO levels.[38,39] As well, good coplanarity exists between the comonomers (see the top view in Figure 2.1 d)).

2.3.3. Photovoltaic Performance of TQ1 Solar cell and Thin-Film Morphology

For the investigation of Photovoltaic effects of TQ1 in BHJ PSCs, the standard configuration glass/ITO/PEDOT:PSS/TQ1:$PC_{71}BM$/Al was employed. Following the optimized fibrication process of PSCs as reported inn pevious work, [33] the casting solution of TQ1:$PC_{71}BM$ as active layer was prepared in a 1:3 (w/w) ratio using *o*-dichlorobenzene (*o*-DCB) and PSCs of TQ1 was fabricated under the same conditions, firstly (see the experimental section for the detailed information).

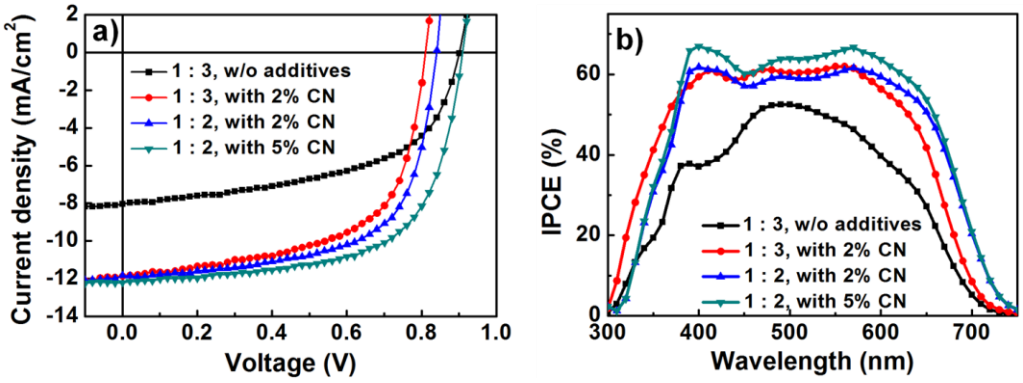

Figure 2.3 a) *J-V* characteristics and b) incident photon-to-current efficiency (IPCE) of PSCs based on TQ1:$PC_{71}BM$ without or with different concentrations of CN.

The representative current-density-voltage (*J-V*) characteristics of the devices under the illumination of simulated AM 1.5G conditions (100 mW/cm^2) are shown in Figure 2.3 (see Figure 2.4) and the parameters are summarized in Table 2.1.

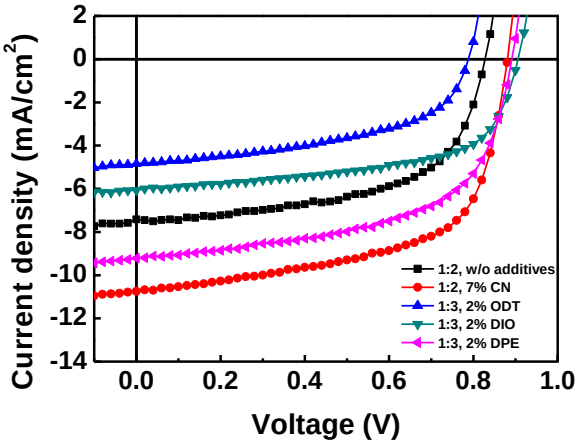

Figure 2.4 *J-V* characteristics of PSCs based on TQ1:$PC_{71}BM$ without or with various additives.

Table 2.1 Photovoltaic parameters of the devices.[a]

TQ1:$PC_{71}BM$	J_{SC} [mA/cm^2]	V_{OC} [V]	*FF*	PCE [%]
1:3 (w/w), w/o additives	8.03	0.90	0.54	3.94
1:3 (w/w), with 2% ODT	4.84	0.79	0.51	1.93
1:3 (w/w), with 2% DIO	6.07	0.91	0.59	3.27
1:3 (w/w), with 2% DPE	9.22	0.89	0.58	4.77
1:3 (w/w), with 2% CN	10.9	0.81	0.56	4.94
1:2 (w/w), w/o additives	7.42	0.83	0.59	3.61
1:2 (w/w), with 2% CN	11.8	0.84	0.64	6.38
1:2 (w/w), with 5% CN	12.2	0.91	0.64	7.08[b]
1:2 (w/w), with 7% CN	10.8	0.88	0.61	5.78

[a]2 wt% from *o*-DCB and the device performance was consistent and reproducible (see Experimental Section).
[b]Note the statistical data analysis shown in (5-6%: 72 cells, 6-7%: 58 cells, over 7%: 3 cells)

In this condition, the fabricated TQ1 solar cell exhibit PCE of 3.94% with a V_{OC} of 0.90 V, a J_{SC} of 8.03 mA/cm^2, and a fill factor (*FF*) of 0.54. As the next step, various solvent additives (1,8-octanedithiol (ODT), 1,8-diiodooctane (DIO), diphenylether (DPE) and 1-chloronaphthalene (CN)) were addided for the purpose of investigation the effect of 2% addition (v/v) of solvent additives on the TQ1 and $PC_{71}BM$ (1:3 (w/w)). Interestingly, among the devices containing solvent additives, we find adding CN into the *o*-DCB solution of TQ1:$PC_{71}BM$ prior to spin coating, the PCE dramatically increased up to 4.94%. The performance of BHJ PSCs could be determined by the morphology of the active thin layer.[40] With large interfacial area and bicontinuous interpenetrating networks, small phase domains enable maximum charge separation from donor polymer to acceptor fullerene derivative and enhance the collection of charge carriers from the active layer to each electrode. Additionally, in order to elucidate the effect of additives on the phase separation of thin films of TQ1:$PC_{71}BM$,[41] atomic force microscopy (AFM) images were exained. The morphology of the thin films with ODT, DIO and DPE shows very rough, while the film with CN has small

phase domains as shown in Figure 2.5, where the root-mean-square (RMS) roughness values of each film are 6.08, 1.62, 1.10, and 0.75 nm, respectively. Regardless of a complete mechanistic understanding at this stage, it is evident that CN plays an imporant role in control of the optimal morphology and formation of a better interprenetrating network in TQ1:$PC_{71}BM$ through the decreased donor and acceptor domain sizes. This is reasonably advocated by the fact that the efficiently induced uniform film morphology with CN displays relative to those with other additives.

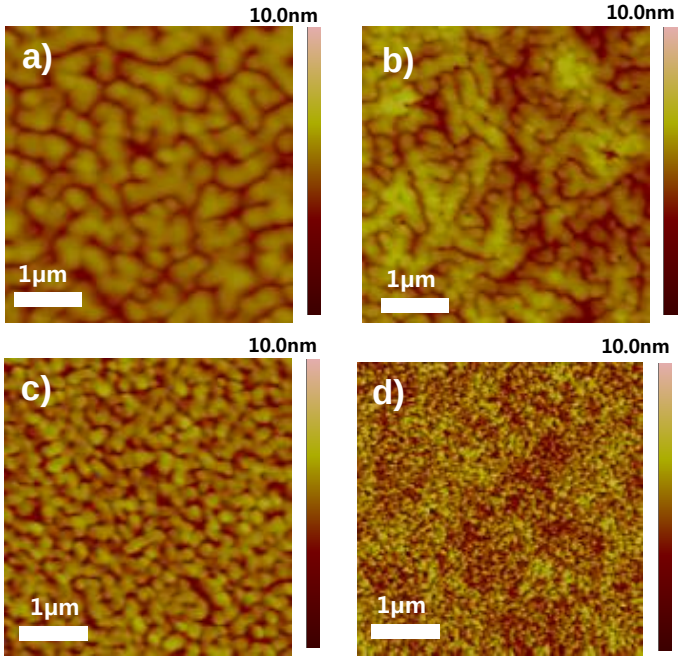

Figure 2.5 Surface morphology of TQ1:$PC_{71}BM$ blend films; 1:3 w/w with a) 2% (v/v) ODT b) 2% (v/v) DIO c) 2% (v/v) DPE d) 2% (v/v) CN from tapping mode AFM (the RMS roughness values are 6.08, 1.62, 1.10, and 0.75 nm, respectively.)

Therefore, in the course of the planned nanomorphology study, not only do we further investigate the influence of CN on the film morphology and device performance, but also seek to understand the mechanism for improvement and thereby identify guidelines for

selecting appropriate solvent additives for use in similar BHJ PSCs. It is revealed that the device perofrmance can bel futher improved not only by changing the weight ratios of TQ1:$PC_{71}BM$ but also by different volume fractions of CN. Through the fully optimization of the device architecture process, the best device, prepared using 5% (v/v) CN additive with a weight ratio of 1:2, reaches an overall PCE of 7.08%, with V_{OC} = 0.91 V, J_{SC} = 12.2 mA/cm^2, and *FF* = 0.64, which is the highest PCE reported to date for PSCs fabricated polymers containing quinoxaline unit. This work is valuable to maximaze the great potential of the low cost polymer to realize high-performance PSCs by taking advantage of the practical process as an additional driving force to further optimize the active layer nanomorphology. The integrated incident photon-to-electron conversion efficiency (IPCE) for these devices matches the measured short-circuit current to within 1% error (Figure 2.3 b)). The J_{SC} and *FF* values are primarily affected by the charge carrier mobilities and blend morphology when the absorbing materials and film thicknesses are kept constant.[42,43] Therefore, the mobility and morphology of the BHJ blends with and without CN were investigated to probe what was the function of CN addition as solvent additive efficiently to obtain the increased PCE. The electron as well as hole mobilities were measured by using the space-charge-limited current (SCLC) method,[44,45] as shown in Figure 2.6 and Table 2.2.

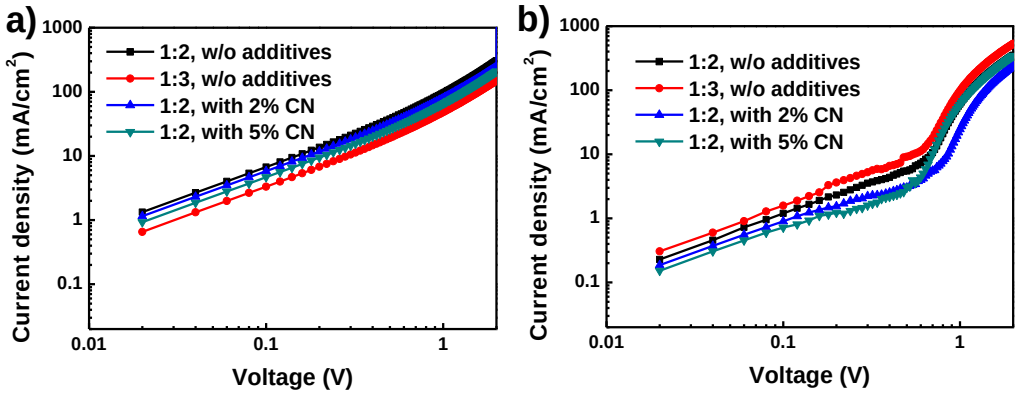

Figure 2.6 Measured *J-V* characteristics by the space-charge-limited current (SCLC) method with TQ1:$PC_{71}BM$ films under dark conditions without or with different concentrations of CN for hole-only device a) and electron-only device b).

Table 2.2 Calculated electron and hole mobility values for TQ1:$PC_{71}BM$ devices without or with different concentrations of CN.[a]

TQ1:$PC_{71}BM$[a]	Hole mobility [m^2/Vs]	Electron mobility [m^2/Vs]	Hole/Electron ratio
1:3, w/o additives	6.23×10^{-4}	1.27×10^{-3}	0.49
1:2, w/o additives	9.64×10^{-4}	3.62×10^{-4}	2.66
1:2, with CN 2%	9.47×10^{-4}	3.61×10^{-4}	2.63
1:2, with CN 5%	5.97×10^{-4}	5.36×10^{-4}	1.11

[a] 2 wt% from *o*-DCB

In the case of the blend films without CN, the hole mobilities (μ_h) are generally an order of magnitude lower than the electron mobilities (μ_e). Notably, the μ_h for the films with CN drops slightly, and meanwhile the μ_e is improved, leading to a smaller value between the mobility ratio. This support that the CN addition beneficially affect TQ1:$PC_{71}BM$ system. The large increase in J*sc* and *FF*, at least partially is deemed to be resulted from the well-balanced charge transport in the optimized blends (TQ1:$PC_{71}BM$ of 1:2 (w/w)) processed with 5% (v/v) CN.[46,47] For the purpose of mimute investgation on thin film morphologies in the TQ1:$PC_{71}BM$ blends upon the addition of CN, X-ray diffraction (XRD), AFM and

transmission elecron microscopy (TEM) were applied. The AFM height images without CN presented in Figure 2.7 a)-d) show large features with RMS of 1.51nm, while in the case of with CN addition, the significantly reduced feature sizes are observed. This suggests that the majority of CN additive far leads to rougher surfaces. In the case of TQ1:$PC_{71}BM$ (1:2 (w/w)) with 5% (v/v) of CN (see Figure 2.7 d)), the large domains are not observed but the finest features with RMS of 0.47nm are observed. The role of CN in thin film is believed to improve the miscibility between TQ1:$PC_{71}BM$ and formation of interpenetrating networks highly. Considering the current understanding of PSCs, the enhanced photocurrents (7.42 vs 12.2 mA/cm^2) and *FF* (0.59 vs 0.64) of the optimized TQ1:$PC_{71}BM$ of 1:2 (w/w) blend processed with CN can be explained by the improved morphology. When compared to the devices without CN.

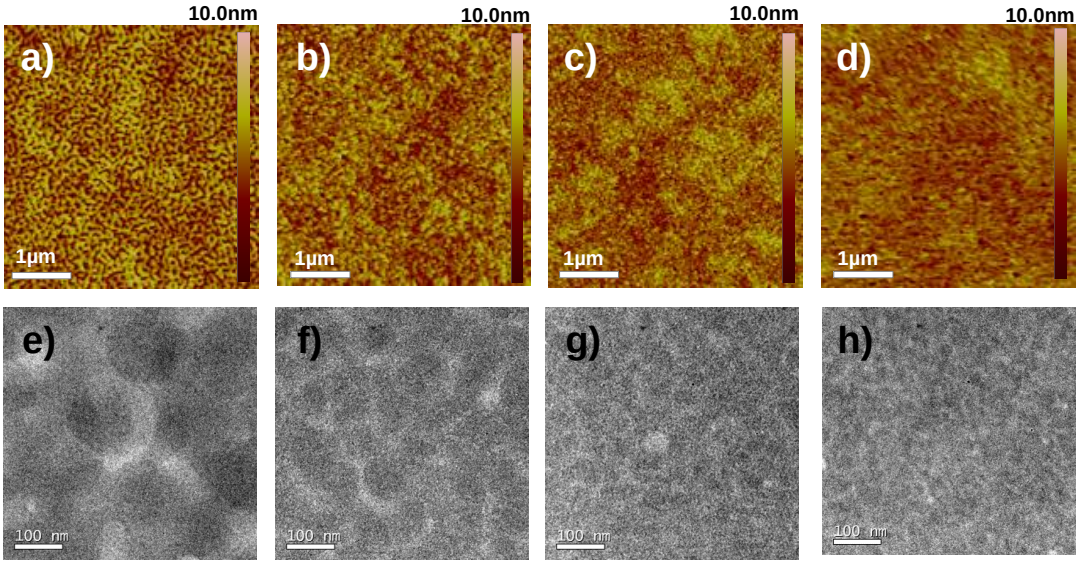

Figure 2.7 Surface morphology of TQ1:$PC_{71}BM$ blend films; a) 1:3 (w/w) without additives, b) 1:3 (w/w) with 2% (v/v) CN, c) 1:2 (w/w) with 2% (v/v) CN, and d) 1:2 (w/w) with 5% (v/v) CN from tapping mode AFM (the rms roughness values are 1.51, 0.75, 0.68, and 0.47 nm, respectively.). e-f) The TEM images to corresponding to the AFMs.

The effect of CN on the improved morphology is visualized by TEM (Figure 2.7 e)-h)).

Large scale phase separation with a continuous darker phase embedded with discrete micrometer-size light domains (~100-200 nm in diameter) is seen in the films processed without CN additive. In the films, processed with CN, large fullerene domains are absent, indeed, creating elongated nanofibrous networks through the promotion of the demixing of the TQ1 and $PC_{71}BM$, in qualitative agreement with the above AFM results.[48]

2.3.4. Nanostructural Order in Thin Films

In order clearly to elucidate the structural heterogeneity and the dynamics of ordering of TQ1 with $PC_{71}BM$ being forced into the intercrystaline, the out-of-plane XRD of films annealed at 120 ^{o}C was monitored corresponding to the imates of Figure 2.8.

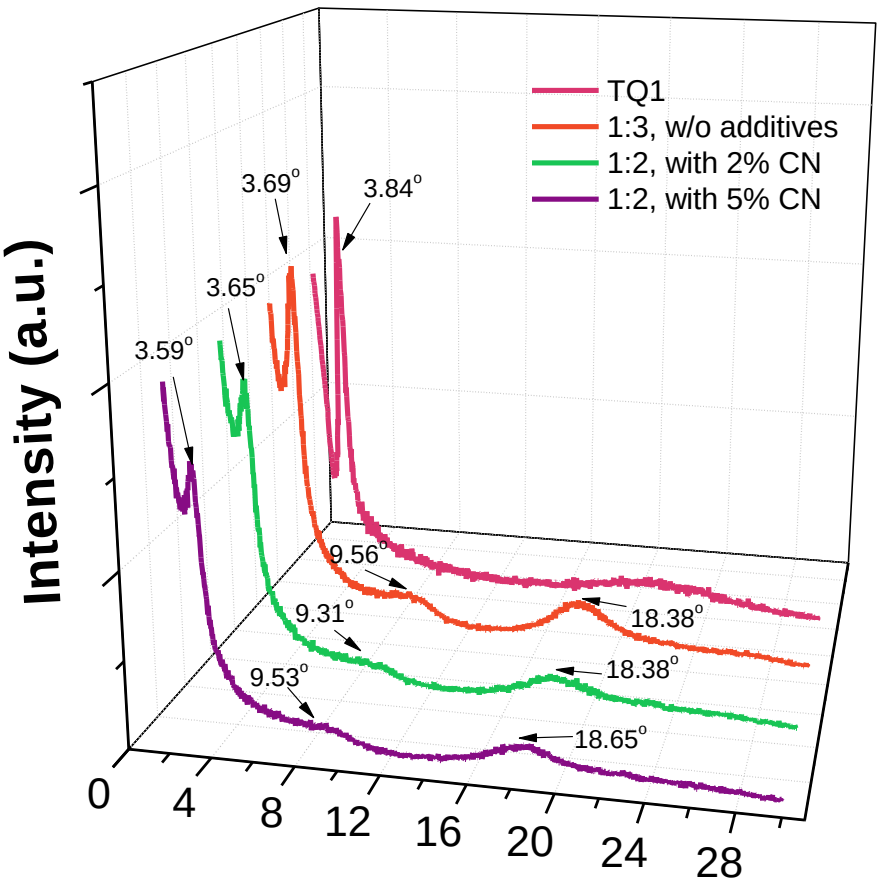

Figure 2.8 XRD patterns of (a) TQ1 and TQ1:$PC_{71}BM$ blend films without or without or with different concentrations of CN.

Distinct primary diffraction (100) peaks of pristine TQ1 films are detected at 2θ = 3.84°, corresponding to *d*-spacing of 23.0 Å, indicating that the orientation of (100) plane is preferentially prependicular to the substrates. However another diffraction peaks of secod-order or π-stacking planes cannot be detected. These above XRD results suggest the signature of ordered lamellar packing motif with a presumably edge-on orientation for the pristine TQ1 films.[49,50] When the $PC_{71}BM$ and TQ1 are mixed with CN or not, the *d*-spacing peaks are somewhat shifted, which is expanded by ~1.6 Å. Such an expansion f the lattice as shown Figure 2.8 is most likely ascribed to the intercalation of PC71BM between the side-chains of the TQ1. [51] The most facinating thing is that the new diffraction peaks emerge at 2θ = ~9.5° (~9 Å) in the blends, which probably arises from the intercalated TQ1:$PC_{71}BM$ lamellar structure.[52] Another possible approch for the explanation of this phenomenon is that the $PC_{71}BM$ molecles can diffuse through the polymer matrix and form large single crystals. [53-55] Notably, the broad featureless peaks (010) caused by the characteristics of the π-π interchain stacking in the profiles of blended samples are observed, which is probably deu to the occurrence of intercalation between the polymer side chains and fullerene.[51,52,56,57] In additiion, this suggests that the pllymer chains in the blends of TQ1:PC71BM have either a slight preference in the face-on orientation or a co-existence of the face-on and other tiled chain orientations.[58] Besides, the (010) peaks of the blend films with the 5% (v/v) of CN shift from 18.38° (π-stacking distance of 4.82 Å) to 18.65° (π-stacking distance of 4.75 Å). The reduction of the interlayer spacing in the blend cast films using the solvent with additive could be helpful for charge transportation in the corresponding device.[59]

2.3.5. Photovoltaic Performance of Inverted Solar Cell

For the comparison of conventional PSCs, inverted-type devices were fabricated and these inverted-type devices demontrate better long-term ambient stability by avoiding the need for the corrosive and hygroscopic hole-transporting PEDOT:PSS and low-work-function metal cathode, both of which are detrimental to device lifetime.[60-62] The inverted PSCs architecture (ITO/ZnO/TQ1:$PC_{71}BM$/MoO_3/Ag) employed in this study is presented in Figure 2.9 a) (see the experimental section for the detailed fabrication).

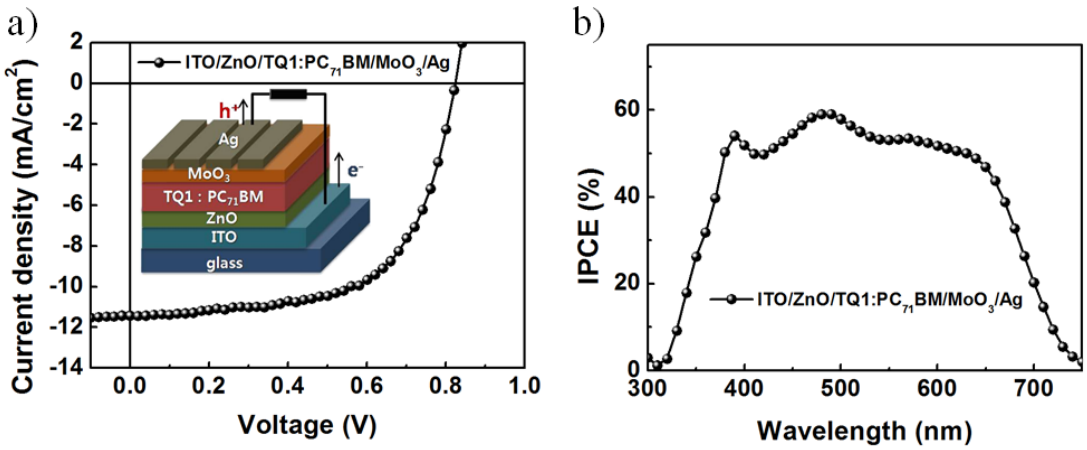

Figure 2.9 a) *J-V* characteristics and b) IPCE of the inverted PSCs (ITO/ZnO/TQ1:$PC_{71}BM$/MoO_3/Ag). Insert; the inverted device architecture.

Following BHJ cell fabrication conditions, for the optimized active layer components, TQ1:$PC_{71}BM$ (1:2(w/w)) processed with 5% (v/v) CN were chosen for the inverted BHJ PScs. A PCE of up to 5.83% is observed for the inverted PSCs with a V_{OC} of 0.82 V, a J_{SC} of 11.4 mA/cm^2, and a *FF* of 0.62. Note that the measured J_{SC} is in a good agreement with IPCE measurements (Figure 2.9 b)). The preliminary results can be comparable with those of the high-performance inverted PSCs.[63-67] However, PCE of current inverted PSCs fabricated

based on TQ1:PC71BM is slightly lower than that of the best conventional PSCs above, because the J_{SC} and V_{OC} are reduced. This suggests that the fabricatin method which is emprically optimized for the cnventional architectures is quite different from that for the invented cells because a PSCs to have an inverted sturcture are sinsitive to the electrical properties of the interfaces between the buffer layer and the photoactive layer.

On the other hand, other inverted PScs were fabricated by replacing the MoO_3/Ag with a MoO_3/Au electrode, which would produce more environmentallu stanle devices due to the stability of electrodes. [64]

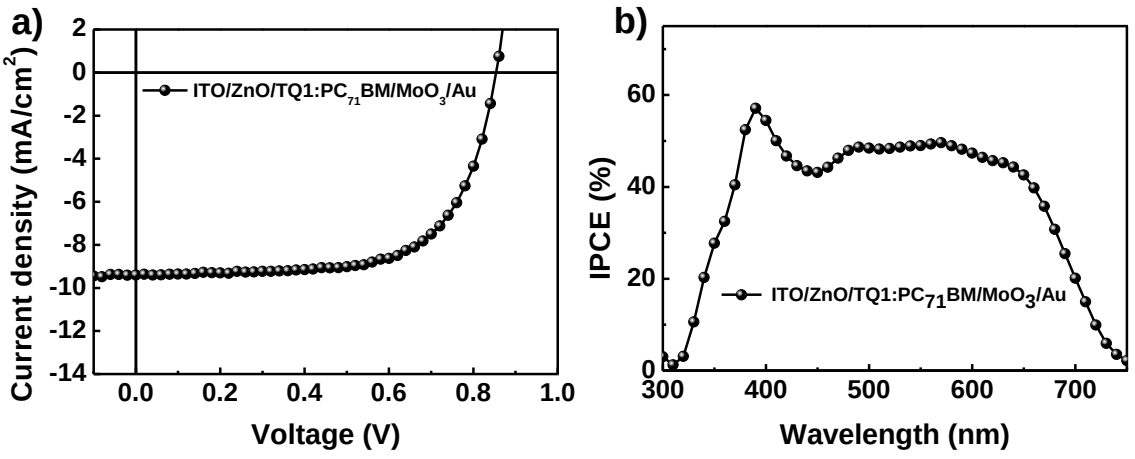

Figure 2.10 (a) *J-V* characteristics and (b) IPCE of the inverted TQ1:$PC_{71}BM$ PSCs using Au. J_{SC} = 9.40 mA/cm^2, V_{OC} = 0.85 V, *FF* = 0.67, PCE = 5.35%.

Although the PCE value 0.48% of Au devices is slightly smaller that that of Ag devices (see Figure 2.10), which is suggested to be resulted from the decreased reflectivity in the visible region of Au, [68] the PCS exhibit high stability in air, sustaining more than 83% of initial efficiency over 30 days of ambient exposure (Figure 2.11 a)). However the other hand, the devieces with the conventional sturcture fall from 7.08% to 1.06% (over 85%) after only 1 day and lose their efficiency within 7 days after ambient exposure (see Figure 2.11 b)).

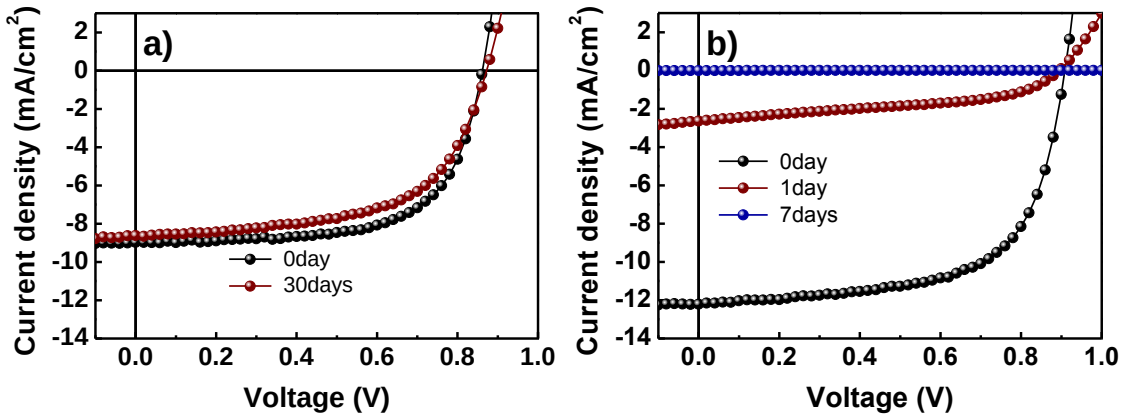

Figure 2.11 a) *J-V* characteristics of the unencapsulated inverted PSCs (ITO/ZnO/TQ1:$PC_{71}BM$/MoO_3/Au) and b) the unencapsulated conventional PSCs over a certain period time in air under ambient conditions.

2.4. Conclusions

In summary, high-performance PSCs using the structure of an easily synthesized low bandgap polymer, TQ1, adopting the solvent additives, such as ODT, DIO, DPE and CN to play a critical role in enhancing their PCEs. When compared with performance of the devices processed without the solvent aditives, the devices with the solvent additives exhibit efficiency of higher than 7% ny means of engineering of acitive layer nanomophology upon the addition of 5% (v/v) CN. This is the highest value among other qinoxaline-based polymer solar cells to have been reported on single junction devices. By systematic experimental study using the combination with XRD, AFM, and TEM, it has been found that the addition of CN promotes small scale phase separation, less heterogeneous surface features through the improved miscibility of the TQ1 and $PC_{71}BM$, resulting in well-intercalated polymer/fullerene networks. Additionally, without both fully optimal morphology control and processing optimization, the corresponding inverted PSCs show still respectable PCE of 5.83%, and also the inverted devices with Au electrode retains over 83% of the original efficiency after 30 days. Considering based on an easy and practical perspective, these research results offer a bright future for commercializatin of PSCs, although guidelines for selecting an appropriate solvent additive remain relatively unclear in various materials systems.

2.5. Experimental Section

2.5.1. Materials and Characterizations

Unless state otherwise, all reagents were purchased either from Aldrich or Acros and used without further purification. THF was distilled over sodium/benzophenone. ^{1}H NMR spectra were acquired from a VNMRS 600 (Varian, USA) NMR spectrometer. Tetramethylsilane was used as an internal reference with deuterated chloroform as solvent. Gel Permeation Chromatography (GPC) was performed on Agilent technologies 1200 series (UV detector at 500nm). THF and PS was used respectively as eluent and standard for GPC analysis. UV-Vis absorption was measured with Cary 5000 UV/Vis-NIR spectrometer (Varian USA). Cyclic voltammetry measurements were carried out on Solartron electrochemical station (METEK, Versa STAT3) at a scan rate of 100 mV/s at room temperature under argon. A three-electrode setup was used with platinum wire both as counter and working electrode and Ag/AgCl used as reference electrode to be calibrated using a ferrocene/ferrocenium redox couple as an external standard, whose oxidation potential is set at -4.8 eV with respect to zero vacuum level. A 0.1 M solution of *n*-tetrabutylammonium hexafluorophosphate (n-Bu_4NPF_6) in degassed anhydrous acetonitrile was used as supporting electrolyte. The polymer thin film was deposited on PT working electrode.

2.5.2. Synthesis of TQ1

The monomer intermediates were prepared according to the literature procedure.[33,36,37](see Scheme 2.1) The target polymer TQ1 was synthesized by a Stille coupling using 5,8-dibromo-2,3-bis(3-(octyloxy)phenyl)quinoxaline (250 mg, 0.36mmole) and 2,5-bis(trimethylstannyl)thiophene (147 mg, 0.36 mmole) as monomers. For the synthesis of TQ1,

4.3 mg (1.3 mole%) of tris(dibenzylideneacetone)dipalladium(0) ($Pd_2(dba)_3$) and 7.16 mg of tri(*o*-toyl)phosphine ($P(o\text{-}Tol)_3$) were used as catalyst and ligand under argon atmosphere at 100 ^oC for three days. After the reaction, the crude polymer precipitated in methanol-ammonia water solution (700 ml:100 ml) was collected by filtration through 0.5 μm Tefron membrane filter. The collected polymer was dried in vacuum drying oven for 12 hours, then sequential Soxhlet-extracted with methanol, acetone, hexane, and chloroform. The chloroform fraction was poured into aqueous EDTA solution then stirred for 12 hours followed by extraction with demineralized water twice. After phase separation, the concentrated chloroform fraction was precipitated in methanol. Finally, the purified polymer was collected by filtration through 0.5 μm Tefron membrane filter and dried in vacuum drying oven for 24 hours. (190 mg, 85.6%). ^1H NMR (600MHz, $CDCl_3$, δ): 7.83 (br, 2H), 7.35 (br, 2H), 7.21-7.10 (br, 6H), 6.85 (br, 2H), 3.70 (br, 4H), 1.55 (br, 4H), 1.17 (br, 20H), 0.80 (br, 6H). M_n = 48 kg/mol, M_w = 173 kg/mol, PDI = 3.6.

2.5.3. Fabrication of Photovoltaic Cells

PSC devices were fabricated according to the following procedure: First, the ITO coated glass substrate was cleaned with detergent, then sequentially ultrasonicated in distilled water, acetone and isopropyl alcohol, and then dried overnight in an oven at 100 ^oC. Poly(3,4-ethylenedioxythiophene):poly(styrenesulfonate) (PEDOT:PSS) (Baytron PH) was spin-cast at 5000 rpm for 40 s. The substrate was dried at 140 ^oC in air for 10 min. Subsequently, it is moved into a glove box for spin-coating the active layer. A mixed solution of TQ1:$PC_{71}BM$ in *o*-dichlorobenzene (*o*-DCB) with various additives (1,8-octanedithiol (ODT), 1,8-diiodooctane (DIO), diphenylether (DPE) and 1-chloronaphthalene (CN)) was spin coated at

1400 rpm for 60 s on the top of the PEDOT:PSS layer to obtain a BHJ film. These samples were brought into a vacuum system (about 10^{-7} Torr), and an Al electrode (100 nm) was deposited on the top of the BHJ layer. In the case of inverted structure cells, ZnO is applied as electron transport layer. ZnO layer was deposited on ITO coated glass by spin coating with 3000 rpm for 40 s and dried at 120 ^{o}C in air for 15 min. The active layer was coated with the same method explained above. Then, a thin layer of MoO_3 film (~5 nm) was evaporated on the top of the active layer. Finally, the anode (Ag or Au, ~95 nm) was deposited on the active layer in a vacuum (about 10^{-7} Torr) thermal evaporator. Measurements were carried out with the solar cells in the glove-box by using a high quality optical fiber to guide the light from the solar simulator equipped with a Keithley 2635 A source. The solar cell devices were illuminated at an intensity of 100 mW/cm^2. For the accurate information, the IPCE measurements were carried out with QEX7. The device structures of the hole and electron only devices are ITO/PEDOT:PSS/TQ1:PC_{71}BM/Au and FTO/TQ1:PC_{71}BM/Al, respectively. The space-charge-limited current (SCLC) mobilities were estimated the Mott-Gurney square law $J_{SCLC} = 9(\varepsilon_r\varepsilon_0\mu)/8 \times (V^2/L^3)$, where ε_r is the dielectric constant of the material, ε_0 is the permittivity of free space, L is the distance between the cathode and anode, which is equivalent to the film thickness, and V is the applied voltage. In order to optimize the performance as well as to probe the reproducibility and trend of the devices in our study, we not only fabricated more than 500 devices, but also carried out the experiments in strictly controlled circumstance and using high grade reagent.

2.6. Reference

(1) Szarko, J. M.; Guo, J.; Liang, Y.; Lee, B.; Rolczynski, B. S.; Strzalka, J.; Xu, T.; Loser, S.; Marks, T. J.; Yu, L.; Chen, L. X. *Adv. Mater.* **2010**, *22*, 5468.

(2) Yu, G.; Gao, J.; Hummelen, J. C.; Wudl, F.; Heeger, A. J. *Science* **1995**, *270*, 1789.

(3) Krebs, F. C. *Sol. Energ. Mat. Sol. C.* **2009**, *93*, 394.

(4) Chen, J.; Cao, Y. *Acc. Chem. Res.* **2009**, *42*, 1709.

(5) Li, C.; Liu, M.; Pschirer, N. G.; Baumgarten, M.; Müllen, K. *Chem. Rev.* **2010**, *110*, 6817.

(6) Dennler, G.; Scharber, M. C.; Brabec, C. J. *Adv. Mater.* **2009**, *21*, 1323.

(7) Kim, J.; Yun, M. H.; Anant, P.; Cho, S.; Jacob, J.; Kim, J. Y.; Yang, C. *Chem. Eur. J.* **2011**, *17*, 14681.

(8) Liang, Y.; Xu, Z.; Xia, J.; Tsai, S.-T.; Wu, Y.; Li, G.; Ray, C.; Yu, L. *Adv. Mater.* **2010**, *22*, E135.

(9) Chen, H.-Y.; Hou, J.; Zhang, S.; Liang, Y.; Yang, G.; Yang, Y.; Yu, L.; Wu, Y.; Li, G. *Nat. Photon.* **2009**, *3*, 649.

(10) Kim, B.; Yeom, H. R.; Yun, M. H.; Kim, J. Y.; Yang, C. *Macromolecules* **2012**, *45*, 8658.

(11) Chen, W.; Nikiforov, M. P.; Darling, S. B. *Energy Environ. Sci.* **2012**, *5*, 8045.

(12) Yip, H.-L.; Jen, A. K. Y. *Energy Environ. Sci.* **2012**, *5*, 5994.

(13) Su, M.-S.; Kuo, C.-Y.; Yuan, M.-C.; Jeng, U. S.; Su, C.-J.; Wei, K.-H. *Adv. Mater.* **2011**, *23*, 3315.

(14) Li, G.; Shrotriya, V.; Huang, J. S.; Yao, Y.; Moriarty, T.; Emery, K.; Yang, Y. *Nat. Mater.* **2005**, *4*, 864.

(15) Ma, W.; Yang, C.; Gong, X.; Lee, K.; Heeger, A. J. *Adv. Funct. Mater.* **2005**, *15*, 1617.

(16) Hoven, C. V.; Dang, X.-D.; Coffin, R. C.; Peet, J.; Nguyen, T.-Q.; Bazan, G. C. *Adv. Mater.* **2010**, *22*, E63.

(17) Lee, J. K.; Ma, W. L.; Brabec, C. J.; Yuen, J.; Moon, J. S.; Kim, J. Y.; Lee, K.; Bazan, G. C.; Heeger, A. J. *J. Am. Chem. Soc.* **2008**, *130*, 3619.

(18) Liu, J.; Tanaka, T.; Sivula, K.; Alivisatos, A. P.; Fréchet, J. M. J. *J. Am. Chem. Soc.* **2004**, *126*, 6550.

(19) Peet, J.; Kim, J. Y.; Coates, N. E.; Ma, W. L.; Moses, D.; Heeger, A. J.; Bazan, G. C. *Nat. Mater.* **2007**, *6*, 497.

(20) Henson, Z. B.; Mullen, K.; Bazan, G. C. *Nat. Chem.* **2012**, *4*, 699.

(21) Scharber, M. C.; Mühlbacher, D.; Koppe, M.; Denk, P.; Waldauf, C.; Heeger, A. J.; Brabec, C. J. *Adv. Mater.* **2006**, *18*, 789.

(22) Yang, L.; Tumbleston, J. R.; Zhou, H.; Ade, H.; You, W. *Energy Environ. Sci.* **2013**, *6*, 316.

(23) Kim, G.; Yeom, H. R.; Cho, S.; Seo, J. H.; Kim, J. Y.; Yang, C. *Macromolecules* **2012**, *45*, 1847.

(24) Wang, E.; Wang, L.; Lan, L.; Luo, C.; Zhuang, W.; Peng, J.; Cao, Y. *Appl. Phys. Lett.* **2008**, *92*, 033307.

(25) Svensson, M.; Zhang, F.; Veenstra, S. C.; Verhees, W. J. H.; Hummelen, J. C.; Kroon, J. M.; Inganäs, O.; Andersson, M. R. *Adv. Mater.* **2003**, *15*, 988.

(26) Blouin, N.; Michaud, A.; Gendron, D.; Wakim, S.; Blair, E.; Neagu-Plesu, R.; Belletête, M.; Durocher, G.; Tao, Y.; Leclerc, M. *J. Am. Chem. Soc.* **2008**, *130*, 732.

(27) Park, S. H.; Roy, A.; Beaupre, S.; Cho, S.; Coates, N.; Moon, J. S.; Moses, D.; Leclerc, M.; Lee, K.; Heeger, A. J. *Nat. Photon.* **2009**, *3*, 297.

(28) Wang, T.; Pearson, A. J.; Lidzey, D. G.; Jones, R. A. L. *Adv. Funct. Mater.* **2011**, *21*, 1383.

(29) Loser, S.; Bruns, C. J.; Miyauchi, H.; Ortiz, R. P.; Facchetti, A.; Stupp, S. I.; Marks, T. J. *J. Am. Chem. Soc.* **2011**, *133*, 8142.

(30) Miller, S.; Fanchini, G.; Lin, Y.-Y.; Li, C.; Chen, C.-W.; Su, W.-F.; Chhowalla, M. *J. Mater. Chem.* **2008**, *18*, 306.

(31) Li, G.; Yao, Y.; Yang, H.; Shrotriya, V.; Yang, G.; Yang, Y. *Adv. Funct. Mater.* **2007**, *17*, 1636.

(32) Etzold, F.; Howard, I. A.; Forler, N.; Cho, D. M.; Meister, M.; Mangold, H.; Shu, J.; Hansen, M. R.; Müllen, K.; Laquai, F. *J. Am. Chem. Soc.* **2012**, *134*, 10569.

(33) Wang, E.; Hou, L.; Wang, Z.; Hellström, S.; Zhang, F.; Inganäs, O.; Andersson, M. R. *Adv. Mater.* **2010**, *22*, 5240.

(34) Zhou, H.; Yang, L.; Price, S. C.; Knight, K. J.; You, W. *Angew. Chem. Int. Ed.* **2010**, *49*, 7992.

(35) Wang, Z.; Wang, E.; Hou, L.; Zhang, F.; Andersson, M.; Inganäs, O. *J. Photon. Energy.* **2011**, *1*, 011122.

(36) Yamamoto, T.; Lee, B.-L.; Kokubo, H.; Kishida, H.; Hirota, K.; Wakabayashi, T.; Okamoto, H. *Macromol. Rapid. Commun.* **2003**, *24*, 440.

(37) Gadisa, A.; Mammo, W.; Andersson, L. M.; Admassie, S.; Zhang, F.; Andersson, M. R.; Inganäs, O. *Adv. Funct. Mater.* **2007**, *17*, 3836.

(38) Donley, C. L.; Zaumseil, J.; Andreasen, J. W.; Nielsen, M. M.; Sirringhaus, H.; Friend, R. H.; Kim, J.-S. *J. Am. Chem. Soc.* **2005**, *127*, 12890.

(39) Kronemeijer, A. J.; Gili, E.; Shahid, M.; Rivnay, J.; Salleo, A.; Heeney, M.; Sirringhaus, H. *Adv. Mater.* **2012**, *24*, 1558.

(40) Thompson, B. C.; Fréchet, J. M. *Angew. Chem. Int. Ed.* **2008**, *47*, 58.

(41) Lee, J. K.; Wang, Y.-M.; Cho, S.; Wudl, F.; Heeger, A. J. *Org. Electrons.* **2009**, *10*, 1223.

(42) Chiu, M.-Y.; Jeng, U.-S.; Su, M.-S.; Wei, K.-H. *Macromolecules* **2009**, *43*, 428.

(43) Chiu, M. Y.; Jeng, U.; Su, C. H.; Liang, K. S.; Wei, K. H. *Adv. Mater.* **2008**, *20*, 2573.

(44) Mihailetchi, V. D.; Koster, L. J. A.; Blom, P. W.; Melzer, C.; de Boer, B.; van Duren, J. K.; Janssen, R. A. *Adv. Funct. Mater.* **2005**, *15*, 795.

(45) Zhao, G.; He, Y.; Xu, Z.; Hou, J.; Zhang, M.; Min, J.; Chen, H. Y.; Ye, M.; Hong, Z.; Yang, Y. *Adv. Funct. Mater.* **2010**, *20*, 1480.

(46) Bundgaard, E.; Krebs, F. C. *Sol. Energ. Mat. Sol. C.* **2007**, *91*, 954.

(47) Yun, M. H.; Kim, G.-H.; Yang, C.; Kim, J. Y. *J. Mater. Chem.* **2010**, *20*, 7710.

(48) Yang, C.; Lee, J. K.; Heeger, A. J.; Wudl, F. *J. Mater. Chem.* **2009**, *19*, 5416.

(49) Sonar, P.; Singh, S. P.; Li, Y.; Soh, M. S.; Dodabalapur, A. *Adv. Mater.* **2010**, *22*, 5409.

(50) Lu, G.; Usta, H.; Risko, C.; Wang, L.; Facchetti, A.; Ratner, M. A.; Marks, T. J. *J. Am. Chem. Soc.* **2008**, *130*, 7670.

(51) Mayer, A.; Toney, M. F.; Scully, S. R.; Rivnay, J.; Brabec, C. J.; Scharber, M.; Koppe, M.; Heeney, M.; McCulloch, I.; McGehee, M. D. *Adv. Funct. Mater.* **2009**, *19*, 1173.

(52) Xin, H.; Guo, X.; Ren, G.; Watson, M. D.; Jenekhe, S. A. *Adv. Eng. Mater.* **2012**, *2*, 575.

(53) Erb, T.; Zhokhavets, U.; Gobsch, G.; Raleva, S.; Stühn, B.; Schilinsky, P.; Waldauf, C.; Brabec, C. J. *Adv. Funct. Mater.* **2005**, *15*, 1193.

(54) Yang, X.; van Duren, J. K. J.; Janssen, R. A. J.; Michels, M. A. J.; Loos, J. *Macromolecules* **2004**, *37*, 2151.

(55) Yang, X.; van Duren, J. K. J.; Rispens, M. T.; Hummelen, J. C.; Janssen, R. A. J.; Michels, M. A. J.; Loos, J. *Adv. Mater.* **2004**, *16*, 802.

(56) Cates, N. C.; Gysel, R.; Beiley, Z.; Miller, C. E.; Toney, M. F.; Heeney, M.; McCulloch, I.; McGehee, M. D. *Nano Lett.* **2009**, *9*, 4153.

(57) Cates, N. C.; Gysel, R.; Dahl, J. E. P.; Sellinger, A.; McGehee, M. D. *Chem. Mater.* **2010**, *22*, 3543.

(58) Li, Y.; Sonar, P.; Singh, S. P.; Zeng, W.; Soh, M. S. *J. Mater. Chem.* **2011**, *21*, 10829.

(59) Lee, O. P.; Yiu, A. T.; Beaujuge, P. M.; Woo, C. H.; Holcombe, T. W.; Millstone, J. E.; Douglas, J. D.; Chen, M. S.; Fréchet, J. M. J. *Adv. Mater.* **2011**, *23*, 5359.

(60) Hsieh, C.-H.; Cheng, Y.-J.; Li, P.-J.; Chen, C.-H.; Dubosc, M.; Liang, R.-M.; Hsu, C.-S. *J. Am. Chem. Soc.* **2010**, *132*, 4887.

(61) Xu, Z.; Chen, L.-M.; Yang, G.; Huang, C.-H.; Hou, J.; Wu, Y.; Li, G.; Hsu, C.-S.; Yang, Y. *Adv. Funct. Mater.* **2009**, *19*, 1227.

(62) Yang, L.; Sontag, S. K.; LaJoie, T. W.; Li, W.; Huddleston, N. E.; Locklin, J.; You, W. *ACS Appl. Mater. Interfaces.* **2012**, *4*, 5069.

(63) Sun, Y.; Takacs, C. J.; Cowan, S. R.; Seo, J. H.; Gong, X.; Roy, A.; Heeger, A. J. *Adv. Mater.* **2011**, *23*, 2226.

(64) Chen, L.-M.; Hong, Z.; Li, G.; Yang, Y. *Adv. Mater.* **2009**, *21*, 1434.

(65) Cheng, Y.-J.; Hsieh, C.-H.; He, Y.; Hsu, C.-S.; Li, Y. *J. Am. Chem. Soc.* **2010**, *132*, 17381.

(66) Small, C. E.; Chen, S.; Subbiah, J.; Amb, C. M.; Tsang, S.-W.; Lai, T.-H.; Reynolds, J. R.; So, F. *Nat. Photon.* **2012**, *6*, 115.

(67) Tan, Z. a.; Zhang, W.; Zhang, Z.; Qian, D.; Huang, Y.; Hou, J.; Li, Y. *Adv. Mater.* **2012**, *24*, 1476.

(68) Shih, P.-I.; Shu, C.-F.; Tung, Y.-L.; Chi, Y. *Appl. Phys. Lett.* **2006**, *88*, 251110.

Naphthalene Diimide Incorporated Thiophene-Free Copolymers with Acene and Heteroacene Units: Comparison of Geometric Features and Electron-Donating Strength of Co-Units

3.1. Abstract

A family of naphthalene diimide (NDI)-based donor (D)-acceptor (A) copolymers having various acene- (benzene (Bz), naphthalene (Np), and pyrene (Py)) and heteroacene-type (selenophene (Se) and thiophene (Th)) donor rings has been designed and synthesized, for the purpose of understanding understand structure-property relationships on the subject of the structural factor systematically and electron-donating capability of the donor portions for applications in organic field-effect transistors (OFETs) fabricated by NDI-based copolymers to have been synthesized following our new design strategy. The resulting copolymers are categorized by the lack or existence of the heteroatoms in the donor framework, and also can be classified into 'thiophene-free' D-A copolymers (**PNDI-Bz**, **PNDI-Np**, **PNDI-Py**, and **PNDI-Se**) and thiophene-containing copolymer (**PNDI-Th**).

When considering from the results of optical and electronic properties, the determination that the empirical electron-donating strength of donor co-units is in the order of Bz < Np < Py < Th < Se. Even though the resulting copolymers show the similarity of the LUMO levels (-3.73 ~ -3.82 eV), the dominant contribution of NDI unit to the polymer backbone lead to that the HOMO levels are sensitive to the relative electron-donating ability and shown to primarily influence whether unipolar n-channel (**PNDI-Bz** and **PNDI-Np**) or ambipolar charge transport (**PNDI-Py**, **PNDI-Se**, and **PNDI-Th**) is observed in OFETs of the NDI-

based copolymers. Interestingly, the best OFET performance is observed in the acene-based centrosymmetric copolymer **PNDI-Np** (5.63×10^{-2} $cm^2V^{-1}s^{-1}$), regardless of the strong electron donors toward efficient intramolecular charge transfer (ICT) when compared to those of the other copolymers with axisymmetric units. Thus, the present work highlights that the geometric features of the donors in NDI D-A copolymers strongly reflect the carrier mobility dynamics rather than inserting electron-rich donor moieties into the backbone to lower the band gap and further strengthen ICT.

Chapter 3

3.2. Introduction

Recently increased needs for organic electronic materials and devices have enlivened the development of solution-processable high-performance materials and fabrication of low-cost and flexible organic electronic devices. Prompted by the fast-growing need for innovative display technologies, significant efforts have been made toward the development of solution-processable polymeric materials for both p- and n-channel organic field-effect transistors (OFETs). Although current state-of-the-art polymeric materials for p-channel OFETs have shown excellent hole mobilities in the ranges of 1–8 $cm^2V^{-1}s^{-1}$ with good ambient stability,[1-19] even recently reaching 10.5 $cm^2V^{-1}s^{-1}$,[20] there is a lack of polymeric semiconductors with comparable processing and performance characteristics for n-channel OFETs. Therefore, the development of high-performance, ambient-stable n-channel polymeric semiconductors still remains challenging. Especially with PDI (Perylene Diimide), NDI (Naphthalene Diimide) to have unique tetracarboxylic diimide structure has been widely studied for the application to organic electronics for example, OTFT and evaluated as leading candidate material. Due to its strong electron withdrawing ability, NDI derivatives have been adapted for n-type characteristic materials from small-molecule to polymeric semiconductors. To the best of our knowledge, the best performing structure pioneered by Facchetti and co-workers is the recently reported donor (D)-acceptor (A) copolymer P(NDI2OD-T2) (also known as Polyera ActivInk N2200) containing naphthalene diimide (NDI) and bithiophene repeat units, achieving a promising electron mobility of up to 0.85 $cm^2V^{-1}s^{-1}$ with an encapsulated active layer in top-gate/bottom-contact OFETs.[21] In order to quantify and understand the outstanding performance of this material, a series of publications followed, shedding light on the injection and transport of charge carriers,[22-27] energetic disorder,[28-30] and film morphology

or texture.[31-35] It is believed that superior n-type OFETs performance is possible through implementation of electron-deficient NDI core to copolymerize with suitable electron-rich co-units. The intramolecular charge transfer (ICT) induced by the D-A structued polymer can facilitate the π-electrons delocalization along the conjugated backbone, thus greatly impacting the molecular packing and charge carrier mobilities.[36-42] Furthermore, more planar resonance structures and low LUMO energy level of NDI-based copolymers can also be considered as critical factors to enhance electron transport and operational stability. One other practical way to increase ICT in D-A copolymers having an identical acceptor unit is to strengthen the electron-donating capability of the donor moieties. Thereby, judging from the viewpoint of molecular design, various thiophene-based moieties (e.g. different number of thiophene rings and modified thiophene derivatives providing varied electron-donating strength) as the strong donor moieties within the main backbone have been prevailingly introduced in constructing NDI-based D-A copolymers for applications in OFETs.[43-45]

To date, however, there is no single report on NDI-containing D-A copolymers based on directly connecting ‘acenes’ with moderate electron-donating properties as well as ‘heteroacenes’ as a thiophene analogue with enhanced electron-donating characteristics relative to thiophene, which raises a host of very interesting questions: Does the empirical electron-donating ability of the donor companions matter? Are thiophene-based components required to render promising OFETs performance? What is the relative importance of counterpart co-monomers other than their overall electron-donating ability? Our studies on a structure-property relationship study of systematically designed NDI-based D-A copolymers with various acene and selenophene rings may give answers to all of these important questions. For the accurate and meaningful comparison, the thiophene-based copolymer

(**PNDI-Th**) has been chosen as reference substance, herein we report the synthesis and detailed characterization of the electronic properties of a series of 'thiophene-free' D-A copolymers, **PNDI-Bz**, **PNDI-Np**, **PNDI-Py**, and **PNDI-Se**, by copolymerizing various acene- and heteroacene-type donor units with NDI acceptor moiety. We hope these studies, relating to molecular packing, energetics, carrier transport, and morphology in the family of the copolymer films, are meaningful by giving a timely analysis on NDI-based copolymers, to guide the rational design and synthesis of novel, high-performance n-channel polymeric semiconductors, and advance their practical applications in OFETs.

3.3. Results and Discussion

3.3.1. Design, Synthesis, and Characterization

As presented in Scheme 3.1, benzene (Bz), naphthalene (Np), pyrene (Py), selenophene (Se), and thiophene (Th) were chosen to examine the influence of electron-donating properties of the counterpart co-monomers and the physical features (different conjugation length and conformation/geometry/physical size) on the nature of NDI-based D-A copolymers. Firstly, the core NDI monomer, 2,6-dibromonaphthalene diimides (Br2-NDI), was synthesized from dibrominated 1,4,5,8-naphthalenetetracarboxylic dianhydride[46] and 2-octyldodecylamine[47] using the previously reported methods (see Scheme 3.1). The donor co-monomers, benzene-1,4-bis(boronate), naphthalene-2,6-bis(boronate), 2,5-bis(trimethylstannyl)selenophene, and 2,5-bis(trimethylstannyl)thiophene were prepared by the minor modifications of the literature procedures[48,49]; except for pyrene-2,7-bis(boronate) obtained from the direct borylation of pyrene using iridium-based catalyst,[50] lithiation and subsequent quenching with trimethyltin chloride or 2-isopropoxy-4,4,5,5-tetramethyl-1,3,2-dioxaborolane were used in other cases (see Scheme 3.1). The target copolymers were synthesized by either a palladium (Pd)-catalyzed Stille or Suzuki type-coupling reaction with 1:1 monomer ratio, respectively. (see Scheme 3.2 and details in Experimental section). The crude copolymers were precipitated from ammonia solution-methanol (100ml:700ml) and collected, followed by washing with methanol. Further purification was accomplished by successive Soxhlet extortions with methanol, acetone, hexane and chloroform.

Scheme 3.1 Synthesis of comonomers[a]

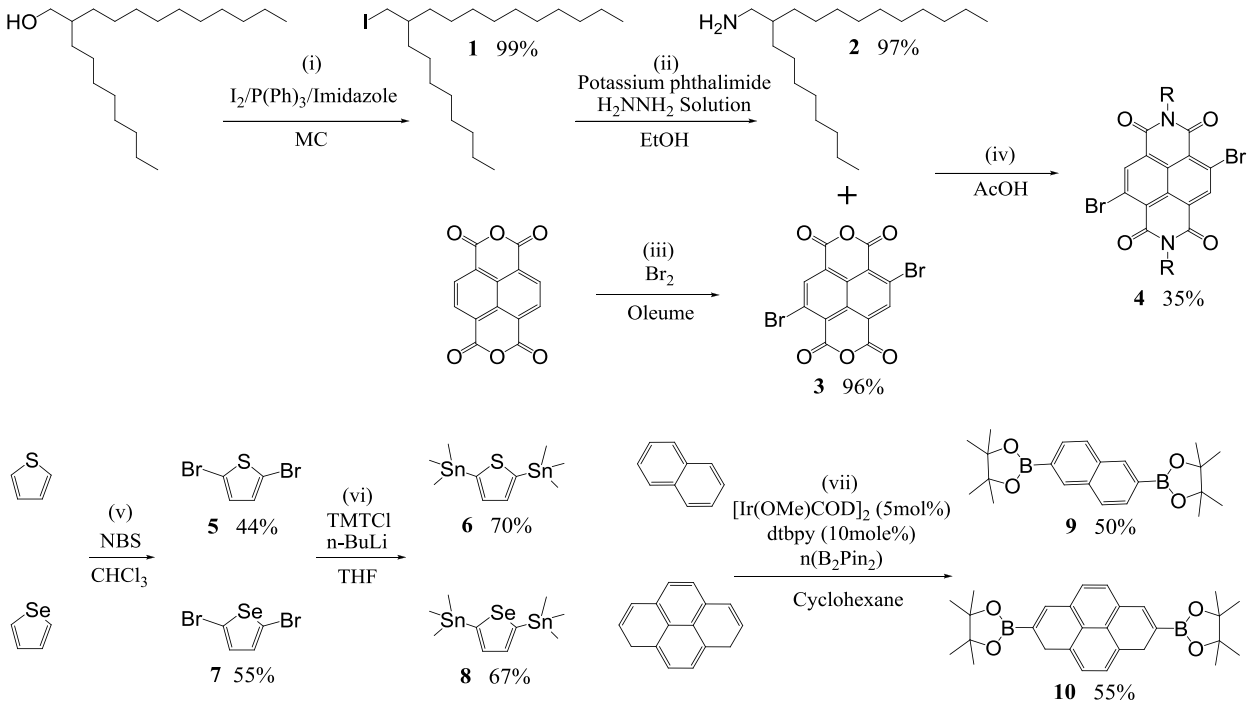

[a]Reagents and conditions: (i) Iodine, triphenylphosphine, imidazole, Na_2SO_3, dichloromethane, 0℃, 99% (ii) Potassium phthalimide, DMF, 25℃, hydrazine hydrate, ethanol, reflux, 97% (iii) Bromine, Oleum (25% SO_3), 95℃, 96% (iv) Acetic acid, 120℃ 35% (v) NBS, $CHCl_3$, dark, r.t, thiophene; 44%, selenophene; 55% (vi) n-butyllithium, trimethylthin chloride, -76℃, thiophene; 70%, selenophene; 67% (vii) $[Ir(OMe)COD]_2$ (5mole%) / dtbpy (10mole%) / n(B_2Pin_2), cyclohexane, 80℃, naphthalene; 50%, pyrene; 55%.

The chloroform fraction was washed with ethylenediaminetetraacetic acid (EDTA) saturated solution then the extracted chloroform fraction was reduced in volume, and the NDI-based D-A copolymers (**NDI-Bz**, **PNDI-Np**, **PNDI-Py**, **PNDI-Se**, and **PNDI-Th**) were collected by precipitation from methanol. Reactions resulted in satisfactory yields (82 - 94%) with the exception of **PNDI-Py**, which was isolated in 38% yield. In the case of **PNDI-Py**, even with the short reaction period and/or large amounts of catalyst, a significant amount of insoluble material remained in the Soxhlet thimble.

Scheme 3.2 Synthesis of NDI copolymers[a]

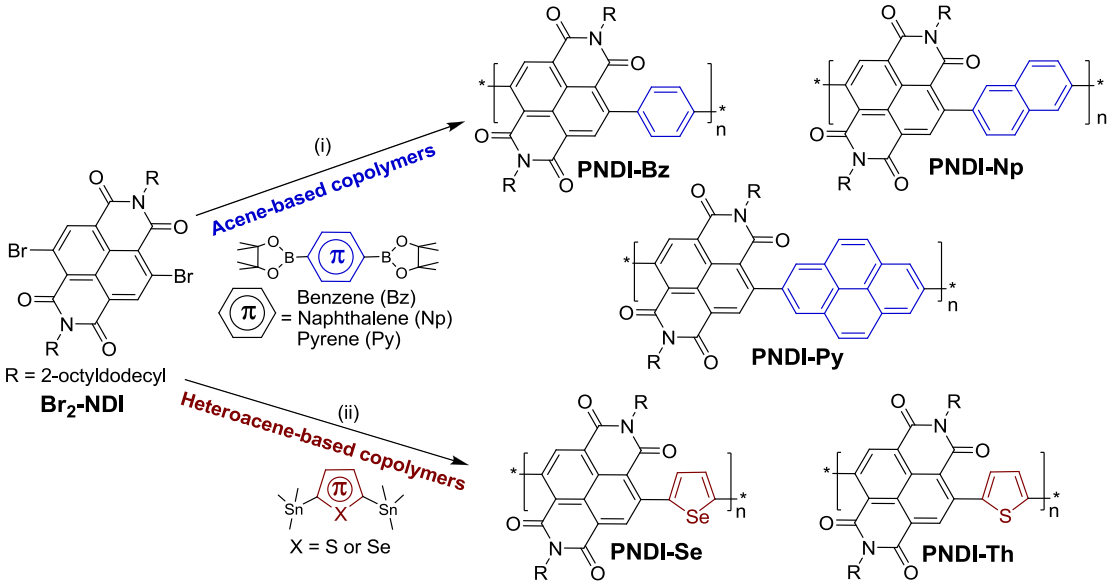

[a]Reagents and conditions: (i) $Pd(PPh_3)_4$, 2M K_2CO_3 aqueous solution, toluene, 100 °C, 72h; (ii) $Pd_2(dba)_3$, P(*o*-tolyl)$_3$, toluene, 100 °C, 72h.

Thus, the reported yields only represent the readily soluble fraction of each sample. Gel-permeation chromatography (GPC) analysis against polystyrene standard using THF as the eluent exhibits reasonably high number-averaged molecular weight (M_n) values in the range of 3.3 ~ 87.8 kDa and polydispersity indices (PDIs) of 1.4 ~ 8.6 for the NDI copolymers. All the data are summarized in Table 3.1. The estimated molecular weights as well as the PDIs might be overestimated due to the potential formation of aggregates in THF, nevertheless, which indicated that copolymerizations produced copolymers (**NDI-Bz**, **PNDI-Np**, **PNDI-Se**, and **PNDI-Th**) with moderate to high molecular weights, due to the good solubility and efficient Pd-mediated coupling reaction. In contrast, copolymerizations always resulted in low molecular weight materials (M_n = 3.0 - 4.0 kDa) for **PNDI-Py**, despite various synthetic attempts, such as the utilization of microwave-assisted heating protocol, use of tiny amounts of catalyst, variation of solution concentrations, and replacement of $Pd_2(dba)_3$ with $Pd(PPh_3)_4$

as a catalyst. The rational reason for the low molecular weights is likely the poor solubility of the resulting copolymer **PNDI-Py**, which is mainly ascribed to the rigid and flat π-conjugated Py units along the main backbone.

Table 3.1 Optical and electrochemical properties of NDI-based D-A copolymers.

Copolymer	M_n(kDa) /PDI[a]	λ_{max} soln (nm)[b]	λ_{max} film (nm)[c]	E_g^{opt} (eV)[d]	LUMO (eV)[e]	HOMO (eV)[f]
PNDI-Bz	30.8/3.3	457	472	2.36	-3.74	-6.10
PNDI-Np	18.4/2.8	488	514	2.11	-3.78	-5.89
PNDI-Py	3.3/1.4	464	474	1.96	-3.78	-5.73
PNDI-Se	87.8/8.6	574	614	1.79	-3.73	-5.52
PNDI-Th	62.7/5.1	547	600	1.83	-3.82	-5.65

[a]GPC versus polystyrene standards in THF as eluent; [b]Solution absorption spectra in chloroform; [c]Thin film absorption spectra from spin-cast from chloroform solution; [d]Optical energy gap estimated from the absorption onset of the thin films; [e]Cyclic voltammetry determined with Fc/Fc+ as an internal reference (LUMO = -4.8 - ($E_{1/2red}^{first}$ - $E_{1/2ox}^{Fc/Fc+}$)); [f]Estimated from HOMO = LUMO – E_g^{opt}.

3.3.2. Photophysical and Electrochemical Properties as well as Computational Studies

Electronic absorption spectra of copolymers in the chloroform solutions and drop-cast films were measured, and the details are summarized in Table 3.1. All D-A type copolymers (**PNDI-Bz**, **PNDI-Np**, **PNDI-Py**, **PNDI-Se**, and **PNDI-Th**) both in solution and as films prepared by chloroform solution exhibit two/three main characteristic absorption bands consisting of broader ones in the low-energy region (500–950 nm), corresponding to the intramolecular charge transfer (ICT) transition, and another relatively sharp ones in the high-energy region (330–470 nm) arising from π-π* transitions between the electron-donor blocks and the NDI electron-deficient segments. (Figure 3.1). The absorption spectra of the copolymer films show obvious red-shift relative to those of their solutions, which can be

explained by a common phenomenon for conjugated polymers owing to the molecular organization in the solid films to form more ordered structures.

a) b)

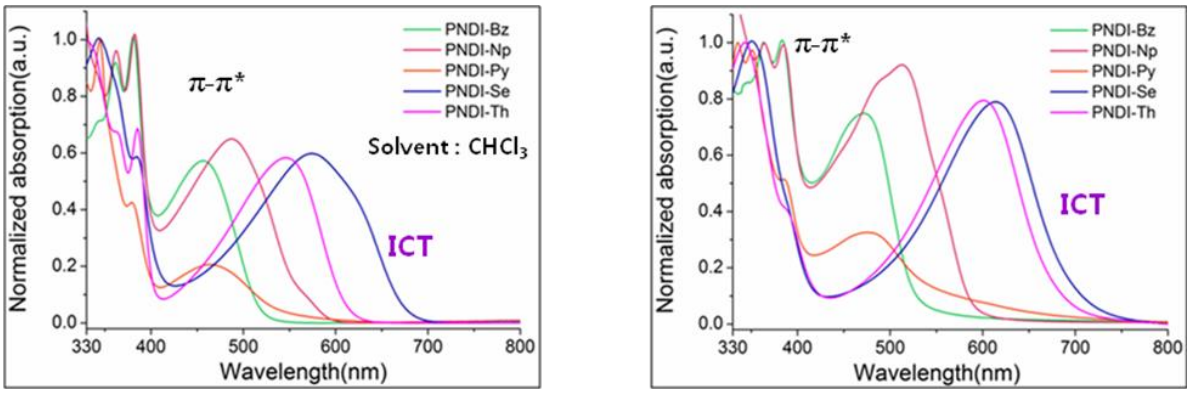

Figure 3.1 Normalized UV-Vis absorption spectra of NDI-based D-A copolymers in a) chloroform solution and b) as thin solid films.

As expected, when comparing acene- versus heteroacene-based copolymers, absorption onsets of **PNDI-Se** and **PNDI-Th** and the ICT bands are significantly red-shifted relative to the acene copolymers (**PNDI-Bz**, **PNDI-Np**, and **PNDI-Py**). This UV absorption characteristics of **PNDI-Se** and **PNDI-Th** are the reflection of a stronger donating ability of the heteroacenes units. Additionally, in the case of **PNDI-Se** and **PNDI-Th**, the intensity of ICT peaks compared with the shorter wavelength ones is observed to be enhanced, which means that the ICT effectively occurs in the heteroacene-based copolymers.

The optical bandgaps (E_g^{opt}) calculated by the absorption edge of the thin film are as follows, respectively: 2.36 eV for **PNDI-Bz**, 2.11 eV for **PNDI-Np**, 1.96 eV for **PNDI-Py**, 1.79 eV for **PNDI-Se**, and 1.83 eV for **PNDI-Th**. This calculation result means that a electron-donating ability of the donor co-units in NDI based copolymers predominantly affects the chromatic shifts and bandgaps, possibly being in the following order of the donating trend:

PNDI-Bz < **PNDI-Np** < **PNDI-Py** < **PNDI-Th** < **PNDI-Se**. In contrast, very intriguingly, the vibronic features of absorption band for **PNDI-Bz**, **PNDI-Np**, and **PNDI-Py** observed in the high-energy region are far more resolved relative to **PNDI-Th** and **PNDI-Se**, suggesting that all the acene-based copolymers have more stiff and well-defined backbones in the solid state.[51,52]

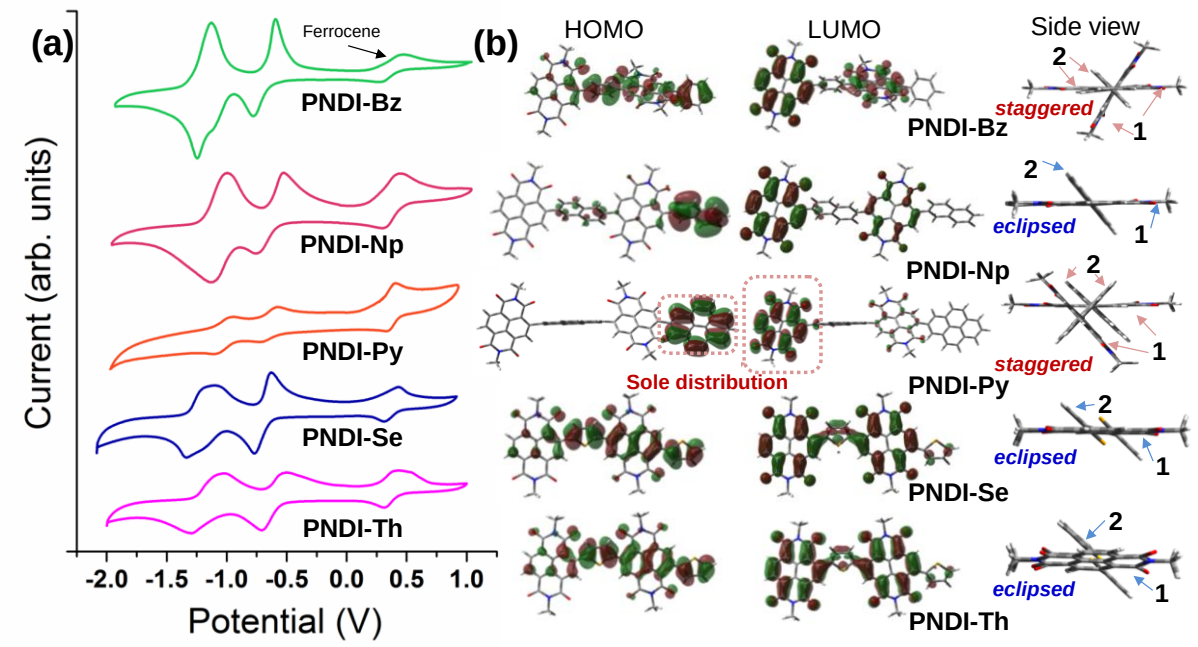

Figure 3.2 a) Cyclic voltammograms of NDI-based D-A copolymers in thin films drop-cast on a platinum working electrode and tested in n-Bu4NPF6/CH3CN solution (scan rate, 50 mVs-1). b) Calculated molecular orbitals and optimized geometry for the model dimers of NDI-based copolymers, respectively (B3LYP/6-31G*). (1) and (2) are used to symbolize the NDI acceptor and donor portions, respectively, for clarity of either staggered or eclipsed conformation. The side chains were replaced with methyl groups to simplify the calculation.

In order to achieve efficient transport of holes and electrons, it is needed to delocalize the electron-density-state and control the appropriate levels of HOMO and LUMO of organic semiconducting materials, respectively. Therefore, the electrochemistry and associated electronic structures of the NDI-based D-A copolymers were investigated as thin films using

cyclic voltammetry (CV) (Figure 3.2 a)). Although two clear reversible reduction peaks are detected for each copolymer during the cathodic sweep, there are no oxidation peaks within the solvent operating window (± 2V) during the anodic sweep, regardless of scan rate. Thus, the HOMO energy levels are calculated from the LUMO energy levels and the optical bandgaps and all the redox data are listed in Table 3.1. All of the five copolymers are analyzed to have similar LUMO levels from -3.72 ~ -3.82 eV due to the dominant NDI contribution to the backbone, while the HOMO energies show a strong dependence on the donor co-units used. The n-channel charge transport ability is attributed to the low-lying LUMO levels of all the NDI-based copolymers. Apparently, a significant increase in the HOMO levels on changing from acene to heteroacene units is observed, indicating the destabilization of HOMOs with increasing the electron donating ability. Judging from the CV analysis results, it can be concluded that the empirical electron-donating strength of donor co-units is manifested in the sequence of Bz < Np < Py < Th < Se, which is essentially consistent with the aforementioned trend based on the optical properties of the copolymers in the same order. It is worthy noting that the relative high-lying HOMO levels (-5.65 ~ -5.73 eV) of the copolymers **PNDI-Se**, **PNDI-Th**, and **PNDI-Py**, suggest that they may validate favorable properties of charge transport for holes, possibly being useful as semiconductors for ambipolar OFETs.

Density functional theory (DFT) computation (B3LYP/6-31G*) studies were also conducted for the additional insights into the electronic features, distributions of the HOMO and LUMO, and geometry-optimized structures of the NDI-based copolymers, depending on the variation of molecular structures affected by the donor partners (Figure 3.2 b)). The alkyl chains attached to NDI moiety in the copolymers were replaced by methyl groups to reduce the time

required for calculation. In the case of the acene-containing copolymers, the localized isosurfaces of both HOMOs and LUMOs are observed; where the HOMO isosurfaces mostly span over the donor counterparts and the LUMO electron densities are mostly localized upon the electron accepting NDI core. On the other hand, interestingly the isosurfaces of HOMOs and LUMOs of the heteroacene-containing copolymers are well spread over the whole backbone. Our proposed ambipolar behaviors above are partly supported by this extensive delocalizations of both the HOMOs and LUMOs for **PNDI-Se**, **PNDI-Th**. Particularly, in the case of **PNDI-Py** with the extended π-conjugation length in the single basic unit, the isosurfaces of electron densities are localized solely on either of the two same donors in HOMO or of the two same acceptors in LUMO, probably being accountable for the Py slightly prohibiting the effective conjugation system as well as ICT along the main backbone due to the large dihedral angle between NDI and Py blocks (see the side view in Figure 3.2 b)). Despite the highly extended degree of π-conjugation length in the basic unit of **PNDI-Py**, this geometry is proposed as the additional reason for its observed wider bandgap than those of the copolymers containing single heteroacene units (Se and Th). As the repeating units are getting more increased, the tendency of such unequally localized HOMO and LUMO distributions are getting clearer (see the calculated model trimers in Figure 3.3).

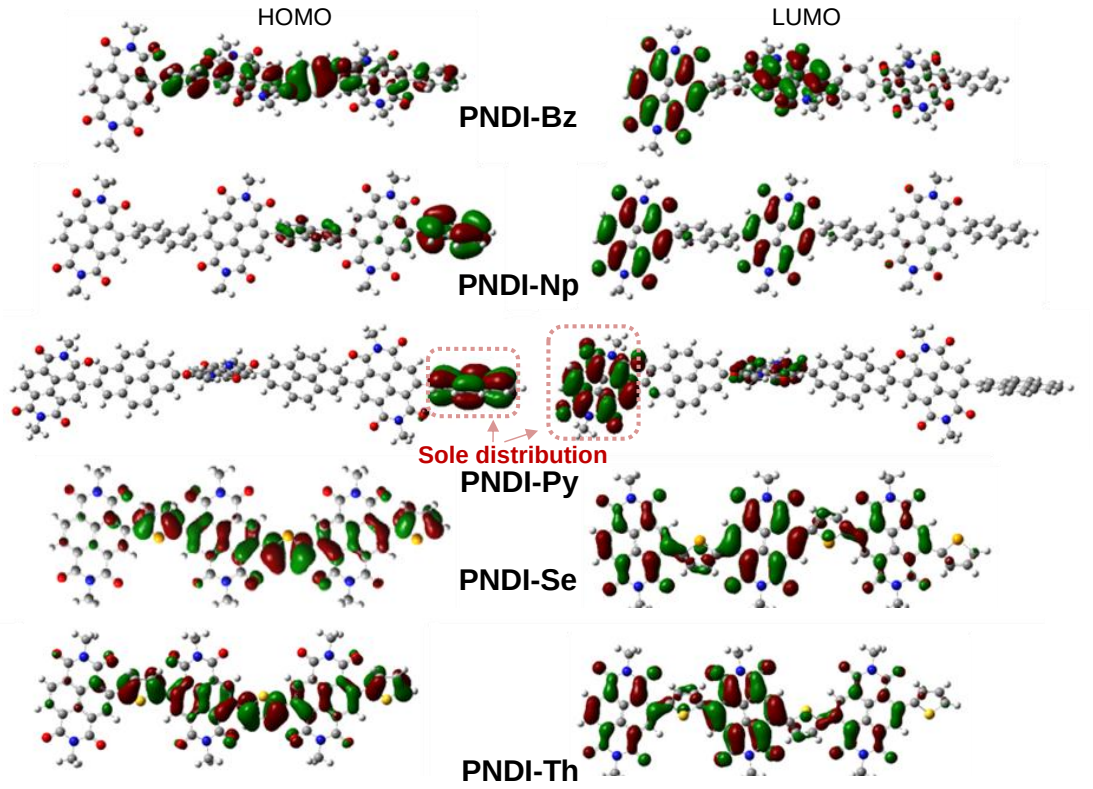

Figure 3.3 Calculated molecular orbitals for the model trimers of NDI copolymers, respectively (B3LYP/6-31G*)

Furthermore, in the case of **PNDI-Np**, **PNDI-Se**, and **PNDI-Th**, it is quite intriguing that the adjacent donor and acceptor units are mutually rotated in the same direction, called '***eclipsed***', whereas both **PNDI-Bz** and **PNDI-Py** show a '***staggered***' conformation where the moiety planes are toward the left and right of each other with about 60^{o} torsion angle. Judging from our current understanding of the computational results, it can be concluded that alongside electron-donating characteristics of the donors, their structural features such as geometry, conjugation length, and size considerably affect the charge distribution, frontier orbitals, and backbone curvature in NDI-based copolymers, most likely affecting the interchain π-π stacking, lamellar packing, and crystallinity.

3.3.3. Electrical Performance of OFETs Based on NDI Copolymers

For the evaluation of electrical properties of NDI copolymers, OFET devices in bottom-gate top-contact configuration (Figure 3.4 a)) were fabricated. The device fabrication process and details about characterization are well described in Experimental Section.

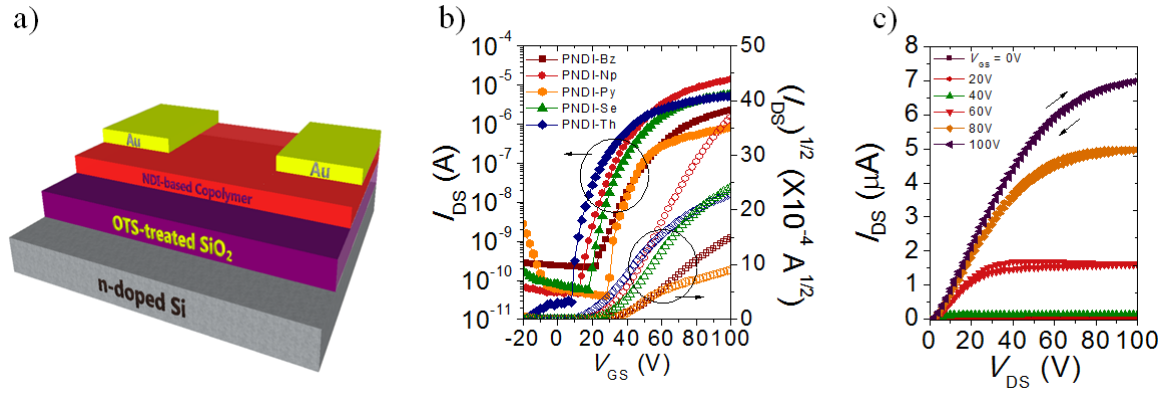

Figure 3.4 a) Schematic illustration of OFET in BGTC structure. b) Optimized n-channel transfer characteristics of OFETs based on annealed NDI copolymer thin films. c) Output characteristics of the best-performing n-channel **PNDI-Np** OFET annealed at 150 ℃.

The current-voltage (I-V) characteristics of NDI-based copolymer OFETs prepared at different annealing conditions are presented in Table 3.2.

Table 3.2 *I-V* characteristics of NDI-based copolymer OFETs obtained at different annealing temperatures.

		n-channel				*p*-channel			
Polymer	T_a [℃]	I_{on}/I_{off}	V_{th} [V]	$\mu_{e,avg}$[b] [cm^2/V·s]	$\mu_{e,max}$[c] [cm^2/V·s]	I_{on}/I_{off}	V_{th} [V]	$\mu_{h,avg}$[b] [cm^2/V·s]	$\mu_{h,max}$[c] [cm^2/V·s]
PNDI-Bz	N/A[a]	9.7×10^{3}	22.6	2.8×10^{-3}	4.9×10^{-3}	-[d]	-	-	-
	120	1.3×10^{5}	44.3	3.3×10^{-3}	5.3×10^{-3}	-	-	-	-
	150	1.1×10^{4}	37.0	5.5×10^{-3}	8.0×10^{-3}	-	-	-	-
	180	1.3×10^{5}	30.4	4.1×10^{-3}	5.7×10^{-3}	-	-	-	-
	220	3.0×10^{5}	26.4	2.1×10^{-3}	2.6×10^{-3}	-	-	-	-
PNDI-Np	N/A	3.0×10^{5}	30.0	1.0×10^{-2}	1.6×10^{-2}	-	-	-	-
	120	8.3×10^{4}	28.2	2.1×10^{-2}	2.6×10^{-2}	-	-	-	-
	150	2.7×10^{5}	30.6	4.0×10^{-2}	5.6×10^{-2}	-	-	-	-
	180	3.0×10^{3}	27.9	3.6×10^{-2}	5.6×10^{-2}	-	-	-	-
	220	2.1×10^{5}	27.3	1.6×10^{-2}	2.2×10^{-2}	-	-	-	-
PNDI-Py	N/A	3.9×10^{4}	24.5	1.2×10^{-3}	2.7×10^{-3}	-	-	-	-
	120	4.7×10^{4}	31.4	4.5×10^{-3}	7.6×10^{-3}	1.1×10^{2}	-109.5	8.7×10^{-5}	7.4×10^{-4}
	150	5.2×10^{5}	36.2	3.6×10^{-3}	7.5×10^{-3}	6.7×10^{1}	-120.8	1.5×10^{-4}	9.3×10^{-4}
	180	2.0×10^{6}	13.9	2.6×10^{-3}	4.9×10^{-3}	6.2×10^{1}	-89.7	5.0×10^{-5}	4.0×10^{-4}
	220	4.6×10^{5}	17.7	2.2×10^{-3}	4.8×10^{-3}	5.3×10^{1}	-82.8	7.5×10^{-5}	3.6×10^{-4}
PNDI-Se	N/A	3.5×10^{4}	28.1	6.0×10^{-3}	7.9×10^{-3}	-	-	-	-
	120	5.9×10^{4}	32.7	1.5×10^{-2}	2.2×10^{-2}	-	-	-	-
	150	1.8×10^{5}	31.3	9.1×10^{-3}	1.7×10^{-2}	-	-	-	-
	180	9.6×10^{4}	14.3	7.5×10^{-3}	1.0×10^{-2}	-	-	-	-
	220	3.0×10^{5}	21.4	8.2×10^{-3}	1.3×10^{-2}	1.2×10^{1}	-140.6	6.5×10^{-5}	2.2×10^{-5}
PNDI-Th	N/A	1.5×10^{5}	14.0	3.8×10^{-3}	7.6×10^{-3}	-	-	-	-
	120	5.5×10^{4}	29.2	6.1×10^{-3}	8.7×10^{-3}	-	-	-	-
	150	6.7×10^{5}	17.0	1.1×10^{-2}	1.9×10^{-2}	-	-	-	-
	180	6.2×10^{5}	-2.9	1.0×10^{-2}	1.7×10^{-2}	-	-	-	-
	220	3.1×10^{5}	-9.2	1.1×10^{-2}	3.2×10^{-2}	7.8×10^{2}	-113.6	1.2×10^{-4}	6.9×10^{-4}

[a]The thermal annealing was not applied. [b]The average and [c]the maximum mobility of the OFET devices (L = 50 μm and W = 1000 μm). [d]The p-channel behavior was not observed.

For the more clear annealing effects, the dependence of average electron mobilities on the annealing temperature is listed in Figure 3.5.

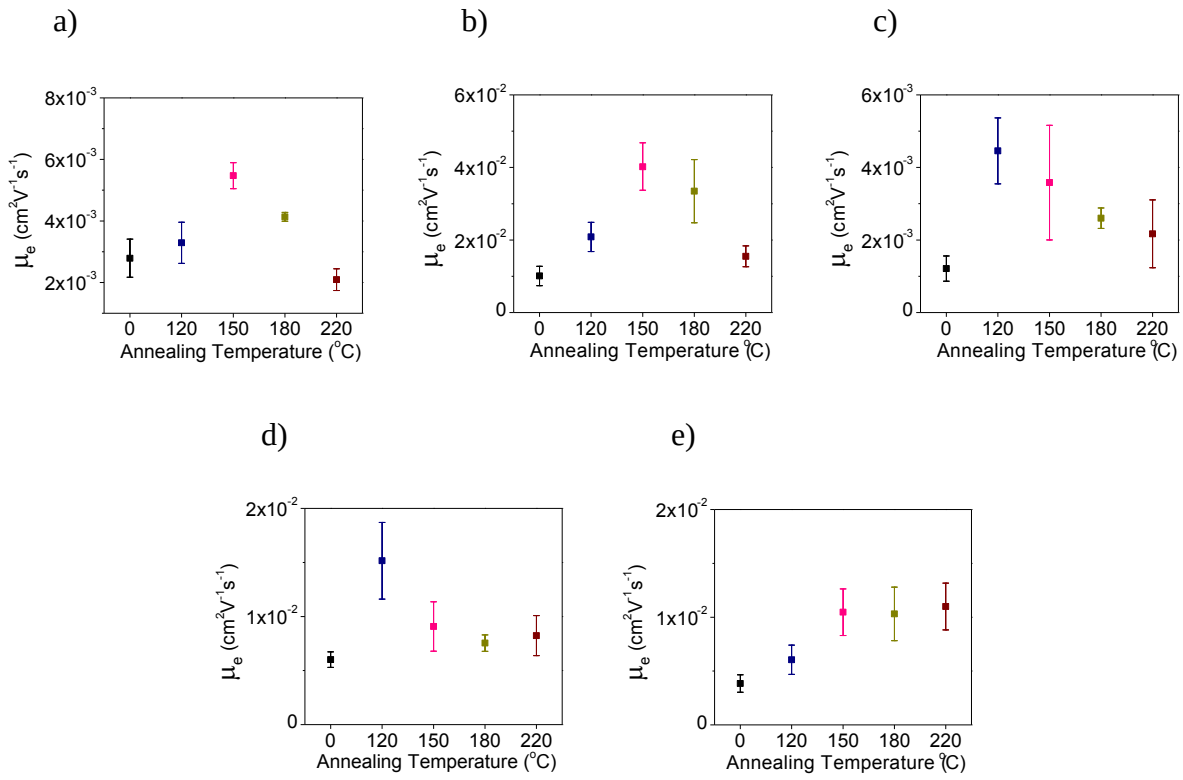

Figure 3.5 Average electron mobility of the films based on a) **PNDI-Bz**, b) **PNDI-Np**, c) **PNDI-Py**, d) **PNDI-Se**, e) **PNDI-Th** as a function of annealing temperature.

All the as-prepared films of NDI copolymers showed only unipolar n-channel field-effect behaviors with electron mobilities ranging from 10^{-3} to 10^{-2} $cm^2V^{-1}s^{-1}$. the electron mobilities generally increased compared with those of the as-prepared thin films, after annealing at elevated temperatures. At an annealing temperature of 150℃, the optimized n-channel performance was exhibited for **PNDI-Bz**, **PNDI-Np**, and **PNDI-Th**, and 120 ℃ for **PNDI-Py** and **PNDI-Se**, respectively. Among the NDI copolymers, **PNDI-Np** exhibited the maximum n-channel field-effect mobility of up to 5.63×10^{-2} $cm^2V^{-1}s^{-1}$. The optimized n-

channel transfer characteristics of OFETs based on the annealed NDI copolymer thin films are shown in Figure 3.4 b), while the typical transfer curves of as-cast NDI copolymer thin films are presented in Figure 3.6.

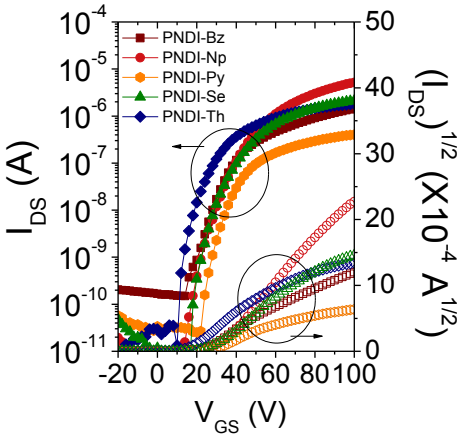

Figure 3.6 Typical transfer curves of OFETs based on the as-cast NDI copolymer films.

The output characteristics of the best-performing n-channel **PNDI-Np** OFET showed well-defined field-effect modulations with a small degree of hysteresis (Figure 3.4 c)).

It is noticeable that although the LUMO level (-3.78 eV) of **PNDI-Np** is less favorable for electron injections with regard to the gold contacts, **PNDI-Np** exhibited the maximum electron mobility, compared with **PNDI-Se** with the lowest-lying LUMO (-3.82 eV). In the case of **PNDI-Py**, due to its low molecular weight as well as '*staggered*' geometry between the donor and acceptor units, its electrical performance is analyzed not to be good enough probably. This indicates that, for such narrow LUMO windows just like these NDI copolymers, the charge transport may be influenced more significantly by other factors such as geometric and morphological features. More intriguingly, **PNDI-Bz** and **PNDI-Np** showed only unipolar n-channel charge transport, whereas after annealing at a high temperature **PNDI-Py**, **PNDI-Se**, and **PNDI-Th** could exhibit ambipolar charge transport (Table 3.2 and

Figure 3.7). These analysis results are enough to explain the predictions from the relatively high-lying HOMO levels (-5.65 ~ -5.73 eV) of **PNDI-Se**, **PNDI-Th**, and **PNDI-Py**, where hole injection barriers relative to gold contacts are lower than those of **PNDI-Bz** and **PNDI-Np**. Additionally, ambipolar charge transport may be facilitated by the more distributions of LUMO and HOMO isosurfaces over the repeat unit of the heteroacene-containing copolymers.

a) b) c)

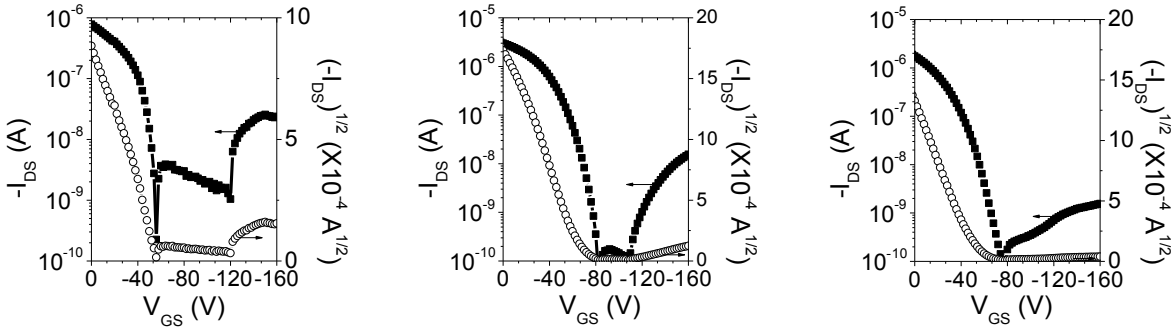

Figure 3.7 Transfer characteristics of (a) **PNDI-Py** annealed at 120 ℃, (b) **PNDI-Th** and (b) **PNDI-Se** annealed at 220 ℃ at hole-enhancement operation.

3.3.4. Thin Film Microstructure Analyses

The investigation of the crystallinity and molecular organization in NDI copolymer thin films were analyzed by Out-of-plane X-ray diffraction (XRD). XRD patterns of the annealed thin films of the NDI-based polymers are presented in Figure 3.8 and the XRD data are summarized in Tale 2.3.

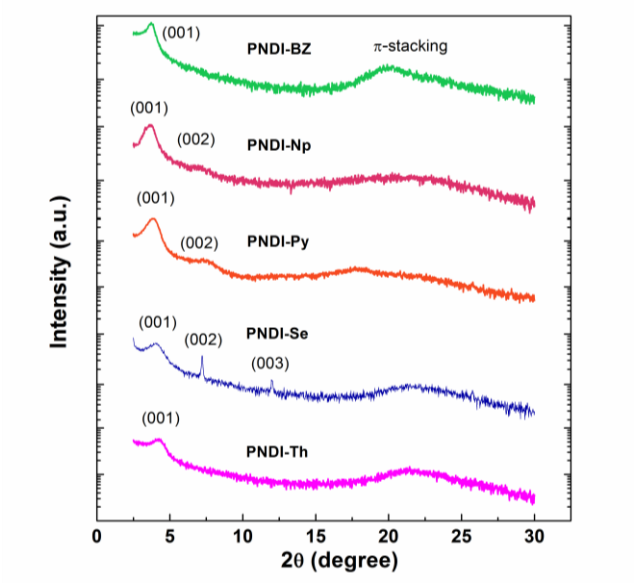

Figure 3.8 Out-of-plane X-ray diffraction (XRD) patterns of the annealed NDI copolymer thin films that show the best n-channel performance.

Table3.3 Peak assignments for the out-of-plane XRD patterns of as-cast and annealed NDI-based polymer films.

		As-cast Film		**Annealed Film[a]**	
Polymer	(00n)	2θ (°)	*d(001)*-spacing (Å)	2θ (°)	*d(001)*-spacing (Å)
PNDI-Bz	(001)	3.34	26.43	3.78	23.36
	(002)	-	-	-	-
	(003)	-	-	-	-
	π-stacking	19.68	4.51	19.66	4.51
PNDI-Np	(001)	3.68	23.99	3.70	23.86
	(002)	7.26	-	7.06	-
	(003)	-	-	-	-
	π-stacking	-	-	-	-
PNDI-Py	(001)	3.94	22.41	3.88	22.75
	(002)	7.32	-	7.30	-
	(003)	-	-	-	-
	π-stacking	-	-	-	-
PNDI-Se	(001)	3.73	23.69	4.00	22.08
	(002)	7.38	-	7.22	-
	(003)	12.23	-	12.01	-
	π-stacking	21.32	4.16	21.46	4.14
PNDI-Th	(001)	3.98	22.18	4.18	21.12
	(002)	-	-	-	-
	(003)	-	-	-	-
	π-stacking	21.3	4.17	21.42	4.15

[a]The annealing temperature was chosen as the condition for the best n-channel performance: *i.e.*, **PNDI-Bz** (150 ℃), **PNDI-Np** (150 ℃), **PNDI-Py** (120 ℃), **PNDI-Se** (120 ℃), **PNDI-Th** (150 ℃).

The as-cast NDI copolymer thin films exhibited a relatively broad primary diffraction peak at 2θ = 3.34° ~ 3.98°, corresponding to the *d*(*001*)-spacing values of 22.18 Å ~ 26.43 Å (Figure 3.9). Most *d*(*001*)-spacing values of NDI copolymers thin films were reduced ranging from 21.12 Å to 23.86 Å indicating that a denser lamellar packing formed after annealing. However, it is noteworthy that, unlike other NDI copolymers, **PNDI-Py** thin films showed a slightly increased *d(001)*-spacing value from 22.41 Å to 22.75 Å after annealing.

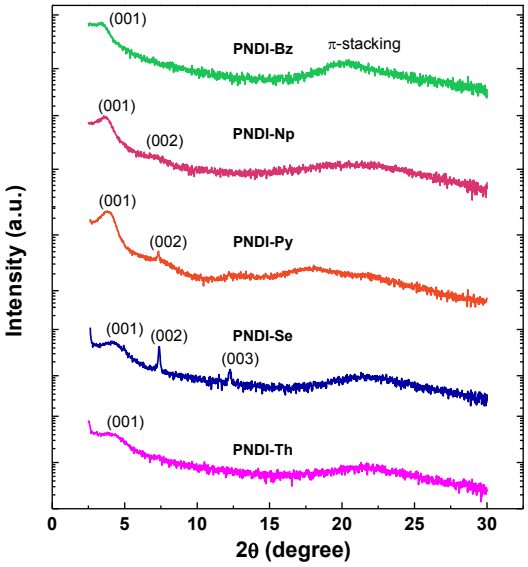

Figure 3.9 Out-of-plane X-ray diffraction (XRD) patterns of the as-cast NDI copolymer thin films.

Judging from the DFT calculations, pyrene units have the tendency to rotate more easily with regard to the NDI π-planar axis. It has been known that such easier molecular relaxations can result in less dense molecular packing and interdigitation.[53] Nonetheless, after annealing **PNDI-Py** thin films also exhibited higher mobilities. It is considered that the co-facing stack area of π-planes becomes larger although the pyrene moiety tends to be slightly tilted after annealing. NDI copolymers with bulky co-units (**PNDI-Np**, **PNDI-Py**) did not show any

discernible π-π stacking peak, whereas NDI copolymers to have the less bulky co-units (**PNDI-Se**, **PNDI-Th**, and **PNDI-Bz**) relatively showed a broad π-π stacking peak centered at 2θ = ~20°. Thus it is suggested that less bulky co-units tend to adopt face-on orientations more easily. It is worthy noting that out-of-plane XRD patterns in the **PNDI-Se**, **PNDI-Th**, and **PNDI-Bz** films exhibited broad π-π stacking peaks, which have lower intensities and larger *d*-spacing values (4.14 ~ 4.51Å) compared with those of other high-performance NDI-based polymers (3.59 ~ 3.80 Å).[54,55] Therefore, it is carefully considered that existence of π-π stacking with relatively long π-planar distance cannot effectively induce efficient 3-D charge transport,[34,56] and thus long-range molecular ordering and morphological characteristics become more important factors for achieving high mobility. The thin film morphologies of NDI copolymers were investigated using tapping-mode atomic-force microscopy (AFM). Nanofibrillar networks were observed in the as-cast film of **PNDI-Bz**, whereas small granular domains were detected in the as-cast films of other NDI copolymers (Figure 3.10).

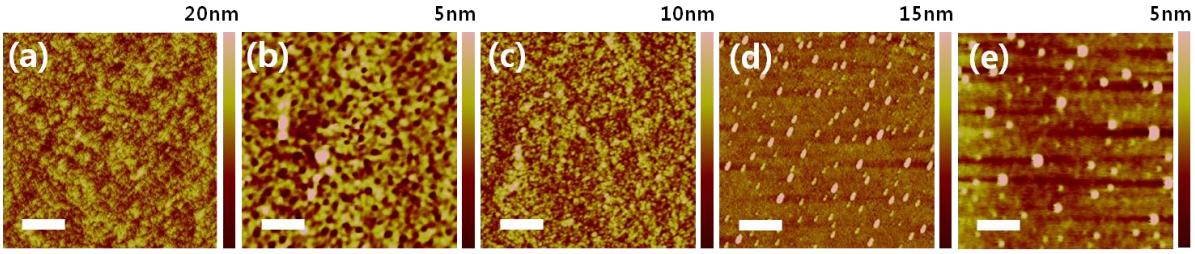

Figure 3.10 AFM height images of (a) **PNDI-Bz**, (b) **PNDI-Np**, (c) **PNDI-Py**, (d) **PNDI-Se**, (e) **PNDI-Th** as-cast films. Scale bar = 1 μm.

This is presumably closely related to the higher charge carrier mobility of as-cast **PNDI-Np** films than those of other NDI copolymer films. Interestingly, all the NDI copolymers formed relatively larger fibrillar network grains after thermal treatment (Figure 3.11). The enhanced

mobilities after thermal treatment can thus be attributed to the morphological factors. This also indicates that significant molecular reorganizations can take place in NDI-copolymer thin films with relatively rigid frameworks.

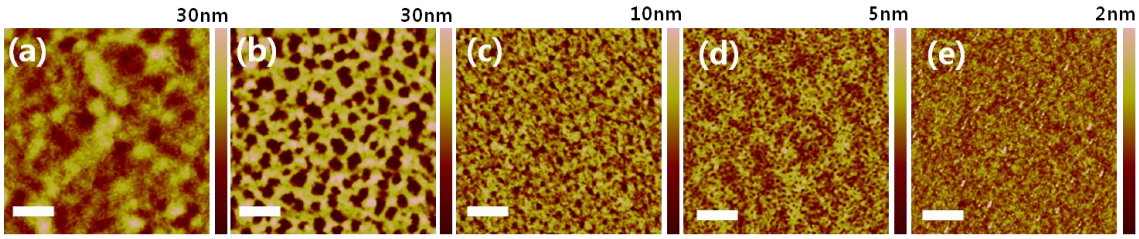

Figure 3.11 AFM height images of (a) **PNDI-Bz**, (b) **PNDI-Np**, (c) **PNDI-Py**, (d) **PNDI-Se**, (e) **PNDI-Th** polymer films annealed at temperatures for the best n-channel performance. Scale bar = 1 μm.

3.4. Conclusion

Despite the growing number of reports on NDI-oligothiophene copolymers, the present NDI-based 'thiophene-free' D-A copolymers (**PNDI-Bz**, **PNDI-Np**, **PNDI-Py**, and **PNDI-Se**) together with the reference thiophene-based copolymer (**PNDI-Th**) represent a big step toward a clear structure-property relationship regarding the structural features as well as electron-donating characteristics of the counterpart co-monomers for OFETs based on rylenes. **PNDI-Se** and **PNDI-Th** are regarded as 'heteroacene'-based copolymers incorporated strong donors for a more pronounced ICT within D-A main backbones, while the donor units of **PNDI-Bz**, **PNDI-Np**, **PNDI-Py** classified as 'acene'-based copolymers are moderate electron-donating ability. The results of this study suggest that and electrochemical properties and NDI-based D-A copolymers show good correlation with increasing the donor strengths from Bz, Np, Py, Th to Se. Besides, there is an obvious trend of the tuned polarity of the majority charge carriers in accordance to the electron-donating ability of the donor co-units primarily due to the change of the HOMO levels, where the copolymers (**PNDI-Bz** and **PNDI-Np**) exhibit unipolar n-channel transport, whereas the others with relatively high-lying HOMO levels (**PNDI-Py**, **PNDI-Se**, and **PNDI-Th**) have ambipolar transport characteristics. More intriguingly, the acene-based centrosymmetric copolymer **PNDI-Np** shows a higher electron mobility (5.63×10^{-2} $cm^2V^{-1}s^{-1}$) than those of the other copolymers with axisymmetric units, irrespective of the efficient ICT effects granted by strong electron donors. Not only have such intriguing findings shed considerable light on the geometric skeletons of the donors rather than their overall donating ability in a set of NDI D-A copolymer systems, but also have brought into sharp focus on the apparent importance of the molecular packing and

intermolecular interaction induced by the physical structures of donors for achieving high mobilities in OFETs based on NDI copolymers.

3.5. Experimental Section

3.5.1. Materials

All the chemicals and reagents were purchased from Sigma-Aldrich, Alfa Aesar chemical company, Tokyo Chemical Industry Co., Ltd. and used without any further purification. THF was freshly dried over sodium and benzophenone, prior to use.

3.5.2. Instruments for characterization

^{1}H and ^{13}C NMR were recorded on a Varian VNRS 600 MHz spectrometer using deuterated chloroform ($CDCl_3$) with TMS as an internal standard. Chemical shifts were given in parts per million (ppm) and coupling constants (*J*) in Hertz (Hz). Elemental analyses were carried out with a Flesh 2000 elemental analyzer. The molecular weight of the copolymers were determined by gel permeation chromatography (GPC) with an Agilent 1200 series and miniDAWN TREOS using tetrahydrofuran (THF) as the eluent against PS standard. UV-Vis absorption spectra in solution and in thin film were recorded on a Varian Carry 5000 UV-Vis-NIR spectrophotometer. The electrochemical properties were characterized by VersaSTAT3 Princeton Applied Research Potentiostat in a three-electrode cell system with platinum as the working electrode, a platinum wire counter electrode and $Ag/AgNO_3$ as the reference electrode. The electrolytic solution employed were 0.1 M tetra-*n*-butylammonium hexafluorophosphate (*n*-Bu_4NPF_6) in dry acetonitrile under Ar atmosphere. The reference electrode was calibrated using a ferrocene/ferrocenium redox couple as an internal standard, whose oxidation potential is set at -4.8 eV with respect to zero vacuum level. The HOMO energy levels were obtained from the equation E_{HOMO} (eV) = LUMO - E_g^{opt}. The LUMO

levels of copolymers were obtained from the equation E_{LUMO} (eV) = -4.8- ($E_{1/2red}^{first}$- $E_{1/2ox}^{Fc/Fc+}$).

3.5.3. General procedure for copolymerizations via either (a) Stille- or Suzuki-type coupling. *(a)*: 2,6-dibromonaphthalene diimides (Br2-NDI, compound 3) (0.254 mmol) and distannyl compound (compound 6 and 8) (0.254 mmol) were taken in a Schlenk tube under argon atmosphere with 4 mL of anhydrous toluene. The mixture was degassed for 20 min followed by addition of $Pd_2(dba)_3$ (3.5 mg, 3.82 μmol) and P(*o*-tolyl)$_3$ (5.81 mg, 19.1 μmol). The mixture was heated at 100 ℃ for 72 h. After cooling to room temperature, the crude copolymers were precipitated from ammonia solution-methanol (100ml:700ml) and collected, followed by washing with methanol. Further purification was accomplished by successive Soxhlet extractions with methanol, acetone, hexane and chloroform. The chloroform fraction was washed with ethylenediaminetetraacetic acid (EDTA) saturated solution then the extracted chloroform fraction was concentrated by evaporation and re-precipitated in methanol. The resulting dark green colored solid was collected and dried overnight under vacuum. The copolymers were characterized by ^{1}H NMR, GPC, and elemental analysis.

(b): A mixture of Br2-NDI (compound 3) (0.254 mmol), diboronic ester compound (compound 9 and 10) (0.254 mmol), $Pd(PPh_3)_4$ (4.4 mg, 3.80 μmol) were taken together in a Schlenk flask. K_3PO_4 (K_2CO_3) (2.66 mmol) in toluene (4 ml) with demineralized water (1.33 ml) were added to this solution and the reaction mixture was heated at 100 ℃ under vigorous stirring for 72 h. Following the procedure described above for the purification and characterization.

Poly((N,N'-bis(2-octyldodecyl)-1,4,5,8-naphthalene diimide-2,6-diyl)-alt-1,4-benzene) ***(PNDI-Bz)***: Isolated yield = 192 mg (84%). GPC analysis M_n = 30.8 kDa, M_w = 102.1 kDa, and PDI = 3.31 (against PS standard,). ^{1}H NMR ($CDCl_3$, 600 MHz): δ ppm 8.89-8.74 (br, 2H), 7.89-7.16 (m, br, 4H), 4.16 (br, 4H), 2.03 (br, 2H), 1.82-1.24 (br, 64H), 0.87-0.82 (br, 12H). Anal. Calcd for $C_{60}H_{90}N_2O_4$: C, 79.77; H, 10.04; N, 3.10 Found: C, 79.47; H, 9.83; N, 3.10.

Poly((N,N'-bis(2-octyldodecyl)-1,4,5,8-naphthalene diimide-2,6-diyl)-alt-2,6-naphthalene) ***(PNDI-Np)***: Isolated yield = 269 mg (93%). GPC analysis M_n = 18.4 kDa, M_w = 51.8 kDa, and PDI = 2.81 (against PS standard,). ^{1}H NMR ($CDCl_3$, 600 MHz): δ ppm 8.84 (br, 2H), 8.06-7.43 (m, br, 6H), 4.16 (br, 4H), 2.04 (br, 2H), 1.86-1.24 (br, 64H), 1.02-0.85 (br, 12H). Anal. Calcd for $C_{64}H_{92}N_2O_4$: C, 80.62; H, 9.73; N, 2.94 Found: C, 80.56; H, 9.57; N, 2.86.

Poly((N,N'-bis(2-octyldodecyl)-1,4,5,8-naphthalene diimide-2,6-diyl)-alt-2,7-pyrene) ***(PNDI-Py)***: Isolated yield = 98 mg (38%). GPC analysis M_n = 3.3 kDa, M_w = 4.6 kDa, and PDI = 1.39 (against PS standard,). ^{1}H NMR ($CDCl_3$, 600 MHz): δ ppm 8.94 (br, 2H), 8.29-8.06 (m, 8H), 4.03 (s, 4H), 1.94 (s, 2H), 1.53-1.20 (br, 64H), 0.86-0.81 (br, 12H). Anal. Calcd for $C_{70}H_{94}N_2O_4$: C, 81.82; H, 9.22; N, 2.73 Found: C, 81.50; H, 9.01; N, 2.63.

Poly((N,N'-bis(2-octyldodecyl)-1,4,5,8-naphthalenedicarboximide-2,6-diyl)-2,5-selenophene) ***(PNDI-Se)***: Isolated yield = 224 mg (94%). GPC analysis M_n = 87.8 kDa, M_w = 758.5 kDa, and PDI = 8.63 (against PS standard,). ^{1}H NMR ($CDCl_3$, 600 MHz): δ ppm 9.01 (s, 2H), 7.65 (s, 2H), 4.16 (s, br, 4H), 2.04 (s, br, 2H), 1.26-1.20 (br, 64H), 0.88-0.81 (br, 12H). Anal. Calcd for $C_{58}H_{88}N_2O_4S$: C, 72.85; H, 9.28; N, 2.93 Found: C, 72.77; H, 9.21; N, 2.95.

Poly((N,N'-bis(2-octyldodecyl)-1,4,5,8-naphthalenedicarboximide-2,6-diyl)-2,5-thiophene) ***(PNDI-Th)***: Isolated yield = 200 mg (82%). GPC analysis M_n = 62.7 kDa, M_w = 317.9 kDa,

and PDI = 5.07 (against PS standard,). ^{1}H NMR ($CDCl_3$, 600 MHz): δ ppm 8.97 (s, 2H), 7.45(s, 2H), 4.15 (br, 4H), 2.02 (br, 2H), 1.38-1.89 (br, 64H), 0.85-0.80 (br, 12H). Anal. Calcd for $C_{58}H_{88}N_2O_4S$: C, 76.60; H, 9.75; N, 3.08 Found: C, 76.79; H, 9.70; N, 3.14.

Fabrication and characterization of OFETs: Bottom-gate top-contact OFET devices based on the NDI copolymers were fabricated on a highly *n*-doped Si substrate with thermally grown 300-nm-thick SiO_2 layer (C_i = 10 nFcm^{-2}), where the highly *n*-doped Si and SiO_2 layer were used as the gate electrode and dielectric, respectively. The surface of SiO_2/Si wafer was modified with *n*-octadecyltrimethoxysilane (OTS), as reported previously.[57] After cleaning the SiO_2/Si wafers with piranha solution (a 7:3 mixture of H_2SO_4 and H_2O_2), OTS solution (3 mM in trichloroethylene) was spin-coated on the SiO_2/Si substrate at 3000 rpm for 30 s. The OTS-coated wafers were exposed to ammonia vapor in a desiccator for 12 h. Then, the wafers were rinsed with toluene, acetone, and isopropyl alcohol. The contact angle of OTS-treated wafers measured with deionized water was about 110°. NDI copolymers were dissolved in anhydrous chlorobenzene (~5 mg mL^{-1}) and stirred at 80 ℃ at least for 12 h. Then, the solution was drop-cast on the OTS-treated SiO_2/Si substrate. The drop-casting method was chosen to prepare thin films, because the wettability of chlorobenzene solution is poor on the highly crystalline OTS-treated SiO_2/Si substrate and the drop-casting method tends to yield a higher crystallinity in the films.[55,57] Drop-cast films were annealed on a hot plate at various temperatures (120 ℃, 150 ℃, 180 ℃, and 220 ℃) for 30 min. Gold electrodes (40 nm) were thermally evaporated through a shadow mask. The channel length (L) and width (W) were 50 μm and 1000 μm, respectively. The current-voltage characteristics were measured in a N_2-filled glove box by using a Keithley 4200 semiconductor parametric analyzer. The field-effect mobility was calculated in the saturation regime using the following equation:

$$I_{DS} = ½ (W/L)\mu C_i(V_G - V_T)^2$$

where I_{DS} is the drain current, W and L are the semiconductor channel width and length, respectively, μ is the mobility, C_i is the capacitance per unit area of the gate dielectric, and V_G and V_T are the gate voltage and threshold voltage, respectively.

3.6. References

(1) Park, J. H.; Jung, E. H.; Jung, J. W.; Jo, W. H. *Adv. Mater.* **2013**, *25*, 2583.

(2) Kang, I.; An, T. K.; Hong, J.-A.; Yun, H.-J.; Kim, R.; Chung, D. S.; Park, C. E.; Kim, Y.-H.; Kwon, S.-K. *Adv. Mater.* **2013**, *25*, 524.

(3) Usta, H.; Newman, C.; Chen, Z.; Facchetti, A. *Adv. Mater.* **2012**, *24*, 3678.

(4) Lei, T.; Dou, J.-H.; Pei, J. *Adv. Mater.* **2012**, *24*, 6457.

(5) Lei, T.; Dou, J.-H.; Ma, Z.-J.; Yao, C.-H.; Liu, C.-J.; Wang, J.-Y.; Pei, J. *J. Am. Chem. Soc.* **2012**, *134*, 20025.

(6) Lee, J. S.; Son, S. K.; Song, S.; Kim, H.; Lee, D. R.; Kim, K.; Ko, M. J.; Choi, D. H.; Kim, B.; Cho, J. H. *Chem. Mater.* **2012**, *24*, 1316.

(7) Kronemeijer, A. J.; Gili, E.; Shahid, M.; Rivnay, J.; Salleo, A.; Heeney, M.; Sirringhaus, H. *Adv. Mater.* **2012**, *24*, 1558.

(8) Kanimozhi, C.; Yaacobi-Gross, N.; Chou, K. W.; Amassian, A.; Anthopoulos, T. D.; Patil, S. *J. Am. Chem. Soc.* **2012**, *134*, 16532.

(9) Chen, Z.; Lee, M. J.; Shahid Ashraf, R.; Gu, Y.; Albert-Seifried, S.; Meedom Nielsen, M.; Schroeder, B.; Anthopoulos, T. D.; Heeney, M.; McCulloch, I.; Sirringhaus, H. *Adv. Mater.* **2012**, *24*, 647.

(10) Chen, H.; Guo, Y.; Yu, G.; Zhao, Y.; Zhang, J.; Gao, D.; Liu, H.; Liu, Y. *Adv. Mater.* **2012**, *24*, 4618.

(11) Tsao, H. N.; Cho, D. M.; Park, I.; Hansen, M. R.; Mavrinskiy, A.; Yoon, D. Y.; Graf, R.; Pisula, W.; Spiess, H. W.; Müllen, K. *J. Am. Chem. Soc.* **2011**, *133*, 2605.

(12) Mohebbi, A. R.; Yuen, J.; Fan, J.; Munoz, C.; Wang, M. f.; Shirazi, R. S.; Seifter, J.; Wudl, F. *Adv. Mater.* **2011**, *23*, 4644.

(13) Mei, J.; Kim, D. H.; Ayzner, A. L.; Toney, M. F.; Bao, Z. *J. Am. Chem. Soc.* **2011**, *133*, 20130.

(14) Li, Y.; Sonar, P.; Singh, S. P.; Soh, M. S.; van Meurs, M.; Tan, J. *J. Am. Chem. Soc.* **2011**, *133*, 2198.

(15) Lei, T.; Cao, Y.; Fan, Y.; Liu, C.-J.; Yuan, S.-C.; Pei, J. *J. Am. Chem. Soc.* **2011**, *133*, 6099.

(16) Ha, J. S.; Kim, K. H.; Choi, D. H. *J. Am. Chem. Soc.* **2011**, *133*, 10364.

(17) Bronstein, H.; Chen, Z.; Ashraf, R. S.; Zhang, W.; Du, J.; Durrant, J. R.; Shakya Tuladhar, P.; Song, K.; Watkins, S. E.; Geerts, Y.; Wienk, M. M.; Janssen, R. A. J.; Anthopoulos, T.; Sirringhaus, H.; Heeney, M.; McCulloch, I. *J. Am. Chem. Soc.* **2011**, *133*, 3272.

(18) Zhang, W.; Smith, J.; Watkins, S. E.; Gysel, R.; McGehee, M.; Salleo, A.; Kirkpatrick, J.; Ashraf, S.; Anthopoulos, T.; Heeney, M.; McCulloch, I. *J. Am. Chem. Soc.* **2010**, *132*, 11437.

(19) Li, Y.; Singh, S. P.; Sonar, P. *Adv. Mater.* **2010**, *22*, 4862.

(20) Li, J.; Zhao, Y.; Tan, H. S.; Guo, Y.; Di, C.-A.; Yu, G.; Liu, Y.; Lin, M.; Lim, S. H.; Zhou, Y.; Su, H.; Ong, B. S. *Sci. Rep.* **2012**, *2*, 754.

(21) Yan, H.; Chen, Z.; Zheng, Y.; Newman, C.; Quinn, J. R.; Dötz, F.; Kastler, M.; Facchetti, A. *Nature* **2009**, *457*, 679.

(22) Steyrleuthner, R.; Schubert, M.; Jaiser, F.; Blakesley, J. C.; Chen, Z.; Facchetti, A.; Neher, D. *Adv. Mater.* **2010**, *22*, 2799.

(23) Baeg, K.-J.; Khim, D.; Jung, S.-W.; Kang, M.; You, I.-K.; Kim, D.-Y.; Facchetti, A.; Noh, Y.-Y. *Adv. Mater.* **2012**, *24*, 5433.

(24) Rao, M.; Ponce Ortiz, R.; Facchetti, A.; Marks, T. J.; Narayan, K. S. *J. Phys. Chem. C.* **2010**, *114*, 20609.

(25) Caironi, M.; Newman, C.; Moore, J. R.; Natali, D.; Yan, H.; Facchetti, A.; Sirringhaus, H. *Appl. Phys. Lett.* **2010**, *96*, 183303.

(26) Blakesley, J. C.; Schubert, M.; Steyrleuthner, R.; Chen, Z.; Facchetti, A.; Neher, D. *Appl. Phys. Lett.* **2011**, *99*, 183310.

(27) Chen, T.-G.; Huang, B.-Y.; Chen, E.-C.; Yu, P.; Meng, H.-F. *Appl. Phys. Lett.* **2012**, *101*, 033301.

(28) Caironi, M.; Bird, M.; Fazzi, D.; Chen, Z.; Di Pietro, R.; Newman, C.; Facchetti, A.; Sirringhaus, H. *Adv. Funct. Mater.* **2011**, *21*, 3371.

(29) Fazzi, D.; Caironi, M.; Castiglioni, C. *J. Am. Chem. Soc.* **2011**, *133*, 19056.

(30) Lange, I.; Blakesley, J. C.; Frisch, J.; Vollmer, A.; Koch, N.; Neher, D. *Phys. Rev. Lett.* **2011**, *106*, 216402.

(31) Rivnay, J.; Toney, M. F.; Zheng, Y.; Kauvar, I. V.; Chen, Z.; Wagner, V.; Facchetti, A.; Salleo, A. *Adv. Mater.* **2010**, *22*, 4359.

(32) Sciascia, C.; Martino, N.; Schuettfort, T.; Watts, B.; Grancini, G.; Antognazza, M. R.; Zavelani-Rossi, M.; McNeill, C. R.; Caironi, M. *Adv. Mater.* **2011**, *23*, 5086.

(33) Schuettfort, T.; Huettner, S.; Lilliu, S.; Macdonald, J. E.; Thomsen, L.; McNeill, C. R. *Macromolecules* **2011**, *44*, 1530.

(34) Rivnay, J.; Steyrleuthner, R.; Jimison, L. H.; Casadei, A.; Chen, Z.; Toney, M. F.; Facchetti, A.; Neher, D.; Salleo, A. *Macromolecules* **2011**, *44*, 5246.

(35) Fabiano, S.; Chen, Z.; Vahedi, S.; Facchetti, A.; Pignataro, B.; Loi, M. A. *J. Mater. Chem.* **2011**, *21*, 5891.

(36) Osaka, I.; Sauvé, G.; Zhang, R.; Kowalewski, T.; McCullough, R. D. *Adv. Mater.* **2007**, *19*, 4160.

(37) Ando, S.; Nishida, J.-i.; Tada, H.; Inoue, Y.; Tokito, S.; Yamashita, Y. *J. Am. Chem. Soc.* **2005**, *127*, 5336.

(38) Jenekhe, S. A.; Lu, L.; Alam, M. M. *Macromolecules* **2001**, *34*, 7315.

(39) Zhou, H.; Yang, L.; You, W. *Macromolecules* **2012**, *45*, 607.

(40) Cho, S.; Lee, J.; Tong, M.; Seo, J. H.; Yang, C. *Adv. Funct. Mater.* **2011**, *21*, 1910.

(41) Lee, J.; Han, A. R.; Hong, J.; Seo, J. H.; Oh, J. H.; Yang, C. *Adv. Funct. Mater.* **2012**, *22*, 4128.

(42) Dutta, G. K.; Han, A. R.; Lee, J.; Kim, Y.; Oh, J. H.; Yang, C. *Adv. Funct. Mater.* **2013**, n/a.

(43) Guo, X.; Kim, F. S.; Seger, M. J.; Jenekhe, S. A.; Watson, M. D. *Chem. Mater.* **2012**, *24*, 1434.

(44) Guo, X.; Watson, M. D. *Org. Lett.* **2008**, *10*, 5333.

(45) Durban, M. M.; Kazarinoff, P. D.; Luscombe, C. K. *Macromolecules* **2010**, *43*, 6348.

(46) Thalacker, C.; Röger, C.; Würthner, F. *J. Org. Chem.* **2006**, *71*, 8098.

(47) Letizia, J. A.; Salata, M. R.; Tribout, C. M.; Facchetti, A.; Ratner, M. A.; Marks, T. J. *J. Am. Chem. Soc.* **2008**, *130*, 9679.

(48) Kim, B.; Yeom, H. R.; Yun, M. H.; Kim, J. Y.; Yang, C. *Macromolecules* **2012**, *45*, 8658.

(49) Kim, J.; Han, A. R.; Seo, J. H.; Oh, J. H.; Yang, C. *Chem. Mater.* **2012**, *24*, 3464.

(50) Coventry, D. N.; Batsanov, A. S.; Goeta, A. E.; Howard, J. A. K.; Marder, T. B.; Perutz, R. N. *Chem. Commun.* **2005**, *0*, 2172.

(51) Braun, D.; Heeger, A. J. *Appl. Phys. Lett.* **1991**, *58*, 1982.

(52) Balan, B.; Vijayakumar, C.; Saeki, A.; Koizumi, Y.; Tsuji, M.; Seki, S. *Polym. Chem.* **2013**, *4*, 2293.

(53) Chen, Z.; Lemke, H.; Albert-Seifried, S.; Caironi, M.; Nielsen, M. M.; Heeney, M.; Zhang, W.; McCulloch, I.; Sirringhaus, H. *Adv. Mater.* **2010**, *22*, 2371.

(54) Jimison, L. H.; Toney, M. F.; McCulloch, I.; Heeney, M.; Salleo, A. *Adv. Mater.* **2009**, *21*, 1568.

(55) Lee, J.; Han, A. R.; Kim, J.; Kim, Y.; Oh, J. H.; Yang, C. *J. Am. Chem. Soc.* **2012**, *134*, 20713.

(56) Fabiano, S.; Musumeci, C.; Chen, Z.; Scandurra, A.; Wang, H.; Loo, Y.-L.; Facchetti, A.; Pignataro, B. *Adv. Mater.* **2012**, *24*, 951.

(57) Ito, Y.; Virkar, A. A.; Mannsfeld, S.; Oh, J. H.; Toney, M.; Locklin, J.; Bao, Z. *J. Am. Chem. Soc.* **2009**, *131*, 9396.

A Balanced Face-On to Edge-On Texture Ratio in Naphthalene Diimide-Based Polymers with Hybrid Siloxane Chains Directs Highly Efficient Electron Transport

4.1. Abstract

Structure-property relationships associated with a hybrid siloxane-terminated hexyl chain (SiC6), photophysics, molecular packing, thin-film morphology, and charge carrier transport are reported for two novel naphthalene diimide (NDI)-based polymers; P(NDI2SiC6-T2) consists of NDI and bithiophene (T2) repeating units, while for P(NDI2SiC6-TVT), the (*E*)-2-(2-(thiophen-2-yl)-vinyl)thiophene (TVT) units are introduced into the NDI-based backbone. The analysis of the optical spectra shows that the pre-aggregation of these polymers in solution is highly sensitive to the choice of solvent, such that the films prepared by using different solvents can be 'tuned' with regard to their degrees and types of the aggregates. In-depth morphology investigations (atomic force microscopy (AFM), grazing incidence X-ray diffraction (GIXD), and near-edge X-ray absorption fine structure (NEXAFS)) combined with device optimization studies are used to probe the interplay between molecular structure, molecular packing, and OFET mobility. It is found that the polymer films cast as a coating from chloroform (CF) solvent favor a mixed face-on and edge-on orientation, while 1-chloronaphthalene (CN)-cast films favor an almost entirely edge-on orientation, resulting in a difference in mobility between CF- and CN-cast devices. Within this work, the annealed P(NDI2SiC6-T2) device fabricated from CF, despite showing a less densely packed organization, shows the highest electron mobility of up to 1.04 $cm^2/V{\cdot}s$ due to a highly balanced face-on to edge-on ratio. This work, for the first time, advances our

understanding for how the balanced face-on to edge-on ratio plays a dramatic role in facilitating charge transport, opening a new charge-transport mechanism in electronic devices.

4.2. Introduction

Significant efforts have been made toward the development of solution-processable polymeric materials for organic field-effect transistors (OFETs) because of their facile processability in solution at a relatively low temperature, which can open a new paradigm in application for flexible electronics and device manufacturing through cost-effective graphic art printing processes.[1-9] Current state-of-the-art polymers have been developed for use in *p*-channel OFETs with hole mobilities surpassing 10 $cm^2/V{\cdot}s$;[1,10-12] however, the distinct lack of high-performance, ambient-stable, solution processed *n*-channel OFETs has hindered the development of low cost organic complementary circuits.[13-23] Therefore, not only is the development of reliable *n*-channel polymeric semiconductors a crucial issue, but also a challenge for this type of polymers is a deep understanding and control of the layer morphology in organic electronics.

A breakthrough in *n*-channel polymers occurred with the development of P(NDI2OD-T2) polymer, containing naphthalene diimide (NDI) and bithiophene (T2) repeating units, by Facchetti and co-workers, demonstrating unprecedented OFET characteristics with electron mobility of up to 0.85 $cm^2/V{\cdot}s$ in the device architecture.[24,25] Interestingly, P(NDI2OD-T2) thin films predominantly formed a dense in-plane molecular packing with only weak out-of-plane π-stacking order. Although the P(NDI2OD-T2) showed a best OFET characteristics with such face-on textures,[26] there were several attempts to achieve its out-of-plane ordering, which would be expected to exhibit better charge carrier mobility characteristics.[27-29] However, in previous reports, the out-of-plane ordered structures in P(NDI2OD-T2) – which can be obtained by lowering surface energy *via* surface treatment and high temperature

thermal annealing – reduced the electron mobility by an order of magnitude (10^{-2} $cm^2/V{\cdot}s$) from that of the pristine device.[30]

A more recent study by Fabiano and co-workers clearly indicated that the edge-on orientation of a few layers of P(NDI2OD-T2) derived from the Langmuir-Schäfer method shows the low electron mobility of ~ 10^{-3} $cm^2/V{\cdot}s$ relative to that of the face-on orientation ($\mu_{electron}$ = 0.1 ~ 0.5 $cm^2/V{\cdot}s$).[28,31] These results challenge the traditional assumption that high carrier mobility is unambiguously linked to the high crystallinity morphology of the edge-on orientation for obtaining in-plane strong π-π stacking.[29,32-36] Very recently, the hindrance of the electron injection from the source/drain electrodes – which is attributed to the vertically aligned long branched side chains (2-octyldodecyl solubilizing groups (2OD)) that have the same direction with the P(NDI2OD-T2) backbones – is proposed as the main reason for the poor OFET characteristics in the edge-on orientated P(NDI2OD-T2) thin film.[19]

As a result, P(NDI2OD-T2) OFETs with preferential face-on orientation showed a relatively low Rc for electron injection due to a shorter hopping distance between the charge injection electrode and the frontier orbitals of P(NDI2OD-T2). In terms of this understanding, the best morphology to achieve both high mobility and low Rc in P(NDI2OD-T2) is a mixture of face-on orientation at the contact region and edge-on orientation in the channel region. Indeed, a remarkably improved electron mobility was reported for (*E*)-2-(2-(thiophen-2-yl)-vinyl)thiophene (TVT)-containing NDI polymer (P(NDI2OD-TVT) that co-exists with face-on and edge-on orientations.[18,19]

Apart from the molecular engineering of the conjugated backbones, recently, it was demonstrated that manipulating the side chains has a big impact on molecular packing, film microstructure, and charge transport.[2,3,37-39] Although there is currently a relatively large side

chain toolbox, systematic investigation on siloxane-terminated alkyl side chain-dependent molecular packing and OFET performance for NDI-based polymers is a fascinating topic because: (i) the siloxane-terminated alkyl side chain is referred to as a hybrid organic–inorganic material in which the hybridization of organic and inorganic building blocks can combine their particular advantages; (ii) the previous investigations of the siloxane solubilizing groups are limited to the study of unipolar *p*-channel and *p*-channel dominant semiconductors;[1-3,40] studies on the critical role of siloxane-based hydrid side chains on charge transport properties for *n*-channel organic semiconductors are thus highly desired; and (iii) advancing our understanding of the multifunctional nature of hybrid side chains is essential for academic research and innovative industrial applications.

Herein, we describe the introduction of hybrid siloxane-terminated hexyl chains (SiC6) onto the NDI-T2 and NDI-TVT polymer backbones, to afford P(NDI2SiC6-T2) and P(NDI2SiC6-TVT), respectively (Scheme 4.1). By utilizing a combination of OFET characterizations, atomic force microscopy (AFM), grazing incidence X-ray diffraction (GIXD), and near-edge X-ray absorption fine structure (NEXAFS) spectroscopy, in-depth study on the siloxane-based side chain-dependent molecular packing and charge transport of P(NDI2SiC6-T2) and P(NDI2SiC6-TVT) is thoroughly carried out. We discovered that the polymer film-packing orientation can be controlled by changing the solvent used for the device fabrication; chloroform (CF)-cast films favored a mixed face-on and edge-on orientation, while 1-chloronaphthalene (CN)-cast films favored an almost entirely edge-on packing relative to the substrate. An exciting electron mobility greater than 1 $cm^2/V{\cdot}s$ is observed for the annealed P(NDI2SiC6-T2) films fabricated from CF solvent, despite the relatively poor packing registry along both lamellar and π-stacking directions. This intriguing result is a clear

indication of how the co-existence of face-on and edge-on orientations and a balanced face-on to edge-on ratio has a strong impact on the electron transport properties.

4.3. Results and Discussion

4.3.1. Synthetic Strategies, Synthesis and Characterization

Scheme 4.1 Synthesis of P(NDI2SiC6-T2) and P(NDI2SiC6-TVT).[a]

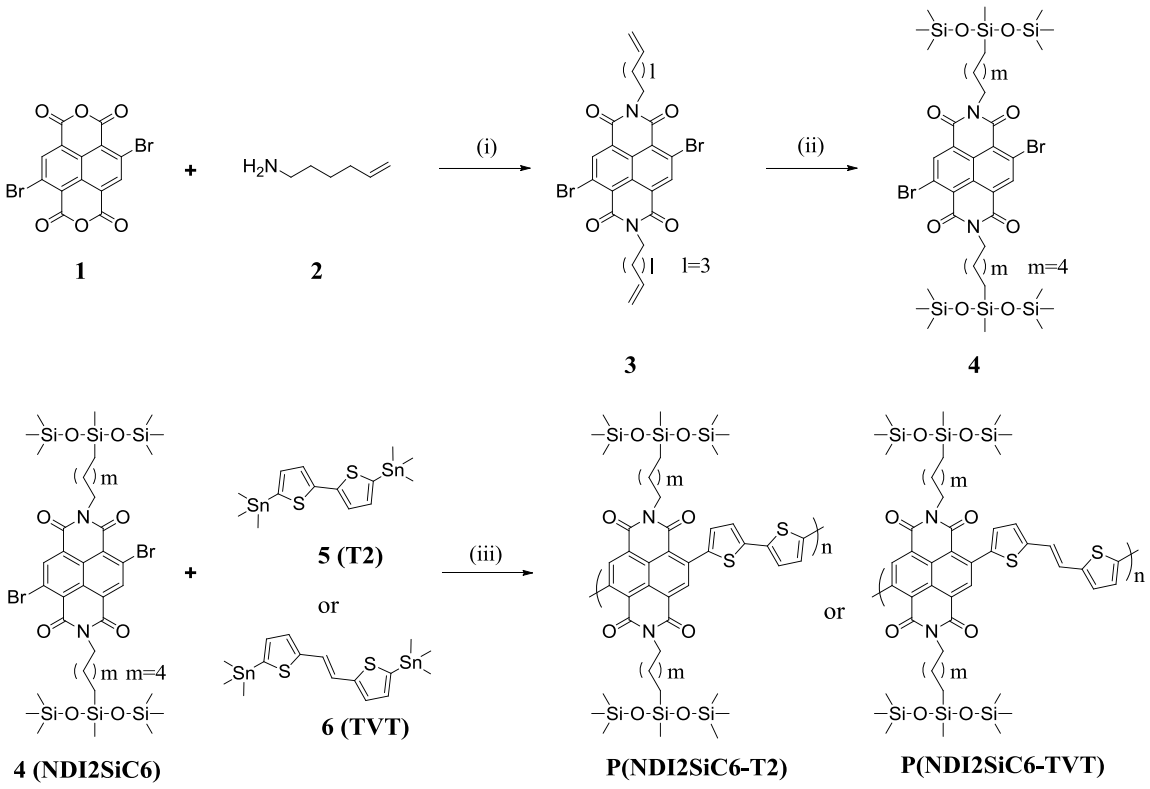

[a]Reagents and conditions: (i) Acetic acid, 120 ℃, 29% (ii) 1,1,1,3,5,5,5-heptamethyltrisiloxane, Karstedt catalyst ($C_8H_{18}OPtSi_2$, Pt 2% xylene solution), toluene, 90 °C, 26% (iii) $Pd_2(dba)_3$, P(*o*-tolyl)$_3$, toluene, 110 °C, 48h; P(NDI2SiC6-T2) (29%) and P(NDI2SiC6-TVT) (73%)

The synthetic routes to solution-processable polymers based on NDI consisting exclusively of SiC6 solubilizing groups are outlined in Scheme 4.1 and the detailed procedures and characterization data are described in the Experimental Section. Briefly, *N,N'*-bis(hex-5-en-l-yl)-2,6-dibromonaphthalene-1,4,5,8-tetracarboxylic diimide (3) was synthesized by condensation of 2,6-dibromonaphthalene-1,4,5,8-tetracarboxylic dianhydride (1) with 6-amino-1-hexene (2) that was obtained by Gabriel synthesis using 6-bromo-1-hexene and

potassium phthalimide salt. Then, hydrosilylation of the terminal alkene with 1,1,1,3,5,5,5-heptamethyltrisiloxane was achieved in the presence of Karstedt catalyst, generating highly soluble NDI monomer (NDI2SiC6) with SiC6 solubilizing chains. A Stille-coupling polymerization between bis-stannylated co-monomers, T2 or TVT and NDI2SiC6 was employed to afford P(NDI2SiC6-T2) and P(NDI2SiC6-TVT). Both polymers were obtained as dark solids after careful purification by precipitation in methanol and subsequent Soxhlet extraction with methanol, acetone, hexane, and chloroform. Molecular weights of the polymers were determined by gel permeation chromatography (GPC), using polystyrene standards as calibrants with THF as eluent (Table 4.1). In contrast to the high solubility of P(NDI2SiC6-T2) in common organic solvents, P(NDI2SiC6-TVT) is less soluble in THF. Therefore, the reported GPC data only represent the soluble fractions of each sample in THF.

Table 4.1 Optical and electrochemical properties of P(NDI2SiC6-T2) and P(NDI2SiC6-TVT).

Polymer	M_n(kDa) / PDI[a]	λ_{max} soln (nm) Room temp.[b]			Elevated temp.[c]		λ_{max} film (nm)[d]		E_g^{opt} (eV)[e]	LUMO (eV)[f]	HOMO (eV)[g]
		CF	TCB	CN	TCB	CN	CF	CN			
P(NDI2SiC6-T2)	32 / 2.02	709	717	632	628	611	714	712	1.44	-3.83	-5.27
P(NDI2SiC6-TVT)	15 / 3.28	747	736	652	643	646	730	729	1.40	-3.96	-5.36

[a]GPC versus polystyrene standards in THF as eluent; [b]Solution absorption spectra at 25 °C; [c]Solution absorption spectra over 80 °C for TCB and CN as solvent; [d]Thin film absorption spectra from spin-cast from TCB and CN solution; [e]Optical energy gap estimated from the absorption onset of the thin films; [f]Cyclic voltammetry determined with Fc/Fc^+ as an internal reference (LUMO = -4.8 - ($E_{1/2red}^{first}$ - $E_{1/2ox}^{Fc/Fc+}$)) using thin film prepared with CF solution; [g]Estimated from HOMO = LUMO – E_g^{opt}.

4.3.2. Photophysical and Electrochemical Properties and Computational Stuedies

It is well-known that optical properties of NDI-based materials can be widely tuned, e.g, by changing solubilizing groups or solvents, due to the different types and degrees of their

aggregation.[17,41,42] Thereby, to gain the detailed optical picture in our new class of polymers, we recorded the absorption spectra of P(NDI2SiC6-T2) and P(NDI2SiC6-TVT) both in solution and as thin films, by using different solvents, such as chloroform (CF), trichlorobenzene (TCB) and 1-chloronaphthalene (CN); the relevant data are collected in Table 4.1.

Both NDI-based polymers showed similar dual absorption bands in any solution and films: one broad absorption peak in the low-energy region (500–950 nm), corresponding to the strong charge transfer (CT) transition, and another one in the high-energy region (330–470 nm) arising from π-π* transitions (see Figure 4.1).

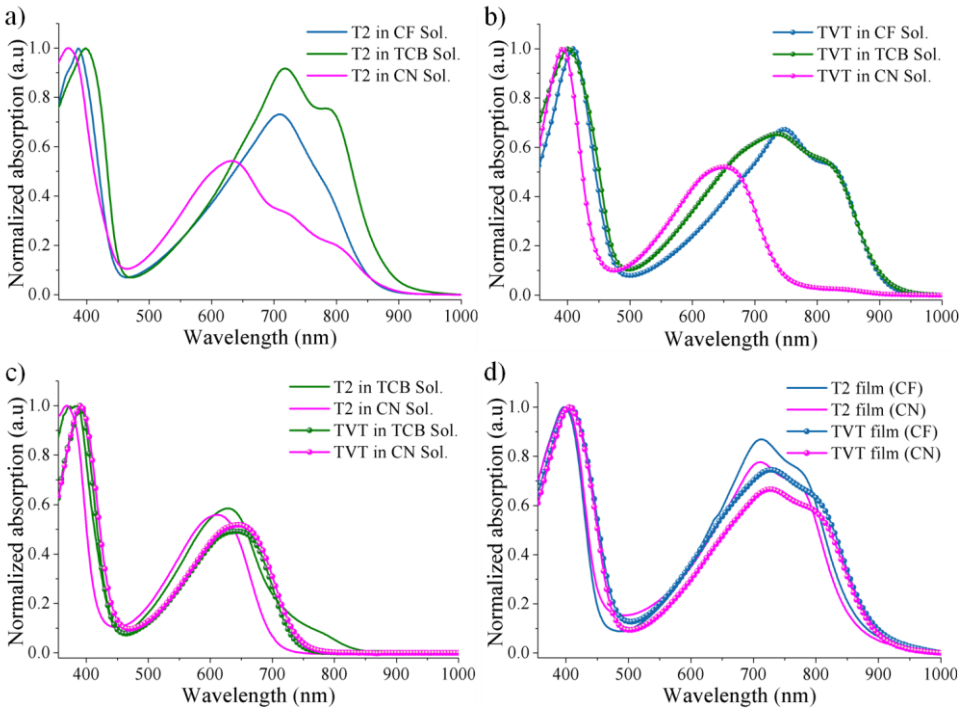

Figure 4.1 UV-Vis absorption spectra of P(NDI2SiC6-T2) and P(NDI2SiC6-TVT) in a) CF, TCB and CN for P(NDI2SiC6-T2) at room temperature. b) CF, TCB and CN for P(NDI2SiC6-TVT) at room temperature. c) TCB and CN over 80 °C for each polymer. d) as thin solid films fabricated with CF and CN for each polymer.

Both the solution and film spectra of P(NDI2SiC6-TVT) are red-shifted relative to those of P(NDI2SiC6-T2), which is commonly explained by the extended conjugation length as well as enhanced CT effects in TVT units.[18,19] Interestingly, both polymers show marked red-shifted absorptions in CF or TCB, when compared to those in CN. In addition, the spectra of the polymer solutions at an elevated temperature (80 ^{o}C) exhibit a broad and featureless band centered at 632 nm for P(NDI2SiC6-T2) and 652 nm for P(NDI2SiC6-TVT), respectively, which is similar to the corresponding absorption profiles seen in each polymer in CN. Therefore, in both cases, this is solid evidence that the chain aggregation occurring in CN is apparently rather weak or even absent, while a pre-aggregated state prevails in the other solvents like CF and TCB. Additionally, a continuous decrease of the fraction of the polymers in the aggregated state can be induced by raising temperature.

Although the chromatic shifts of both polymer films spin-coated from CN are quite identical to the corresponding ones of the most structured spectra observed in CF, the intensities of the CT bands are somewhat increased when going from CN to CF. This indicates that both polymers show a pronounced tendency to aggregate during film formation, regardless of the solvents, but the aggregate content and type would be dependent on the chosen solvent. Optical band gaps (E_g^{opt}s), estimated from the absorption onset of polymer films, are listed in Table 4.1.

The electronic energy levels of both polymers were measured by cyclic voltammetry (CV) calibrated using a ferrocene/ferrocenium redox couple as an internal standard, showing only two reversible reduction waves within the solvent operating window (± 2V) (see Figure 4.2). Thus, using their E_g^{opt}s and LUMO values, we calculated their HOMO levels and the data are summarized in Table 4.1. Notably, it was found that the replacement of T2 with TVT

simultaneously changed the HOMO and LUMO levels of the polymer, resulting in a narrower bandgap in P(NDI2SiC6-TVT) with respect to that in P(NDI2SiC6-T2).

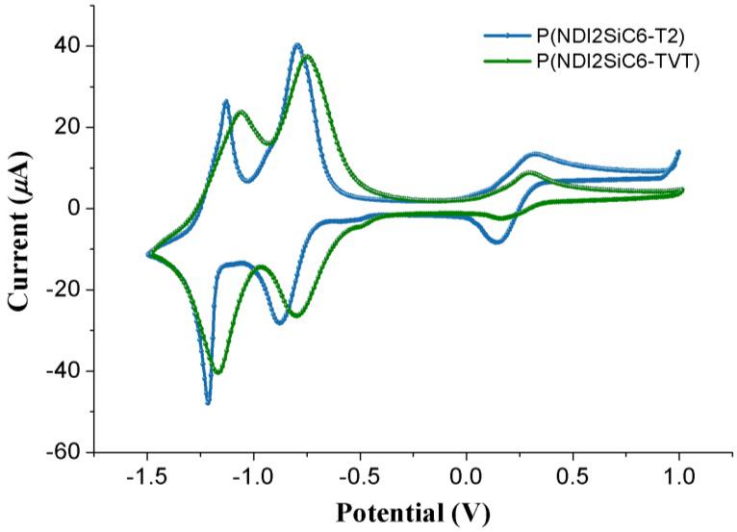

Polymer	E_{red}^{1}	$E_{1/2red}^{1}$	E_{red}^{2}	$E_{1/2red}^{2}$	E_{ox} of Ferrocene	$E_{1/2ox}$ of Ferrocene
P(NDI2SiC6-T2)	-0.796 -0.873	-0.834	-1.13 -1.21	-1.17	0.320 0.145	0.232
P(NDI2SiC6-TVT)	-0.752 -0.796	-0.774	-1.06 -1.16	-1.11	0.298 0.166	0.232

Figure 4.2 Cyclic voltammograms of P(NDI2SiC6-T2) and P(NDI2SiC6-TVT) thin films prepared by drop-casting on a platinum working electrode using CF solution and measured in *n*-Bu_4NPF_6/CH_3CN solution (scan rate = 100 mV/s).

The optimized geometries and electron density distributions of the NDI-based trimers were calculated at B3LYP/6-31G* level (Figure 4.3). The dihedral angles between thiophene and neighboring vinylene or thiophene units are $\theta_{T\text{-}Vinyl}$ = 4.09° and $\theta_{T\text{-}T}$ = 3.92°, respectively together with the similar angles (θ = 36.6–37.4°) between NDI and neighboring thiophene units in both cases. This result demonstrates that the incorporation of vinyl groups into

polymer backbones has a negligible influence on the dihedral angles between NDI and adjacent thiophene units. For both the model oligomers, the HOMOs show a high electron density around the thiophene units, whereas the LUMOs are localized on the NDI unit, similar to those of many other donor-accepter polymers.

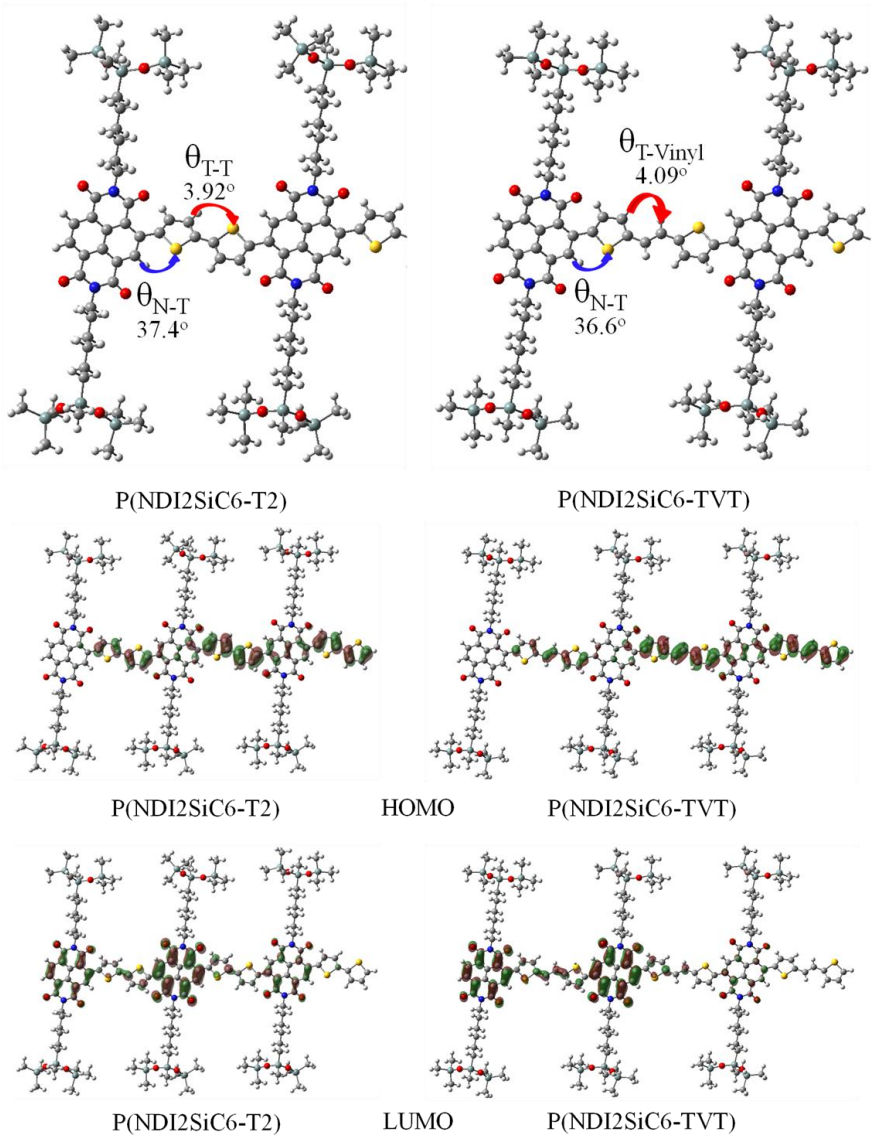

Figure 4.3 Dihedral angles and isosurfaces of the intact trimer model for P(NDI2SiC6-T2) and P(NDI2SiC6-TVT) calculated by DFT, respectively (B3LYP/6-31G*).

4.3.3. Electrical Performance of OFETs

We fabricated top-gate, bottom-contact (TG/BC) OFETs based on P(NDI2OD-T2), P(NDI2SiC6-T2), and P(NDI2SiC6-TVT). For the sake of comparison, P(NDI2OD-T2) was used as a reference polymer. The polymer thin films (20–22 nm) were prepared by spin-coating of the NDI polymer solutions in CF (4 mg/mL) – in which the most enhanced solvent inducing pre-aggregation is shown – and sequentially annealed at 100, 200, and 300 ^{o}C for 30 min in a nitrogen-filled glove box.

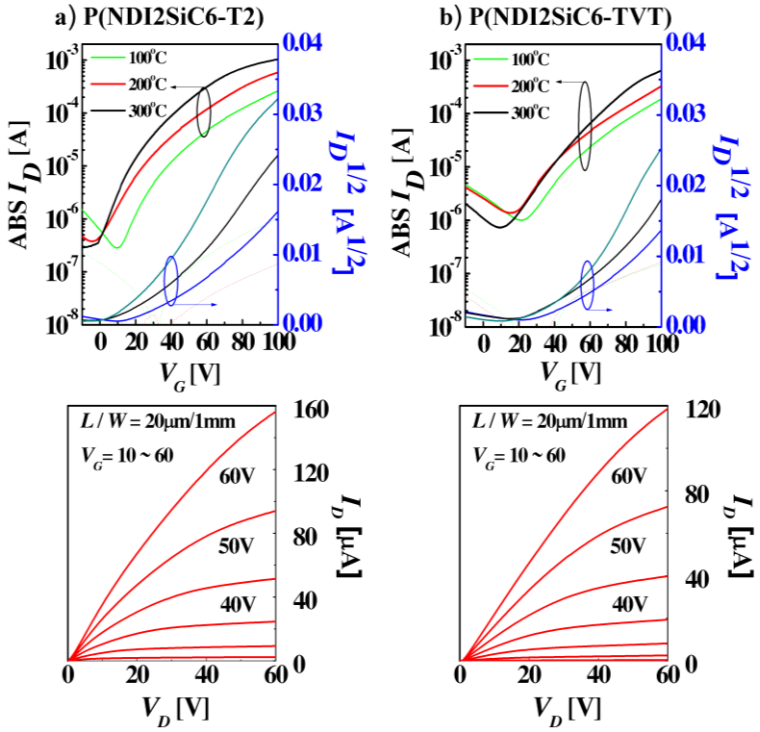

Figure 4.4 Current−voltage ($I-V$) characteristics of the OFETs fabricated with a) P(NDI2SiC6-T2) and b) P(NDI2siC6-TVT) using CF as solvent and output characteristics of the devices annealed at 300 ^{o}C.

Figure 4.4 shows typical transfer and output characteristics of P(NDI2SiC6-T2) and P(NDI2SiC6-TVT) OFETs. Both P(NDI2SiC6-T2) and P(NDI2SiC6-TVT) OFETs exhibited typical *n*-channel OFET characteristics and the electron mobilities of both devices were

progressively improved by the increased annealing temperature. After annealing at 300 °C, the maximum mobility of the P(NDI2SiC6-T2) was determined to be as high as 1.04 $cm^2/V{\cdot}s$, which was slightly higher than that of P(NDI2SiC6-TVT) devices (μ_{elec} = 0.93 $cm^2/V{\cdot}s$) (see Table 4.2).

Table 4.2 Parameters of the TG/BC OFETs with different annealing temperature.

Semiconductor[a]	Annealing Temp/Time [°C/min]	$\mu_{e,avg}$ [$cm^2/V{\cdot}s$][b]	V_{Th} [V]	$I_{on/off}$
P(NDI2SiC6-T2) (CF solvent)	100/ 30	0.43 (± 0.14)	25.1 (± 4.00)	10^3
	200/ 30	0.79 (± 0.25)	22.4 (± 3.50)	10^3
	300/ 30	1.04 (± 0.21)	21.6 (± 4.17)	10^3
P(NDI2SiC6-TVT) (CF solvent)	100/ 30	0.38 (± 0.11)	38.7 (± 4.00)	10^3
	200/ 30	0.62 (± 0.21)	36.4 (± 3.50)	10^3
	300/ 30	0.93 (± 0.20)	33.6 (± 4.17)	10^3
P(NDI2SiC6-T2) (CN solvent)	100/ 30	0.27 (± 0.32)	23.7 (± 3.80)	10^3
	200/ 30	0.48 (± 0.22)	23.3 (± 3.80)	10^3
	300/ 30	0.85 (± 0.23)	20.6 (± 4.70)	10^3
P(NDI2SiC6-TVT) (CN solvent)	100/ 30	0.33 (± 0.20)	25.6 (± 4.10)	10^3
	200/ 30	0.43 (± 0.20)	28.4 (± 4.10)	10^3
	300/ 30	0.78 (± 0.25)	31.6 (± 4.67)	10^3

[a]Semiconductor OFET devices fabricated by spin-coating onto Au S/D electrodes using CF and CN as solvent. [b]The average mobilities of the OFET devices were measured with L = 20 μm, W = 1000 μm and V_D = 100 V. All electrical characteristics were obtained from the top-gate based transistors more than twenty devices.

These exciting high mobilities are three times higher than that of the optimized reference polymer (P(NDI2OD-T2)) (μ_{elec} = 0.32 $cm^2/V{\cdot}s$, see Figure 4.5). The highly improved electron mobilities for P(NDI2SiC6-T2) and P(NDI2SiC6-TVT) devices can be explained by their deep-lying LUMOs (-3.83 ~ -3.96 eV), facilitating electron injection from the high work-function Au (-4.8 ~ -5.1 eV) to polymer films, however this is not the exclusive reason. The varied molecular packing/crystallinity of the polymers should be strongly correlated to

their high mobility values, which will be discussed in a subsequent thin-film morphology study. The variation of FET mobilities is highly dependent on contact resistance. Thus, to evaluate contact effects, we applied the Y-function method (YFM) described previously.[43] The detailed description of the specific analysis and equations employed are found in Experimental Section. The YFM enables us to precisely obtain the R_c and low-field mobility (μ_0) from individual devices. The relevant data are listed in Table 4.3.

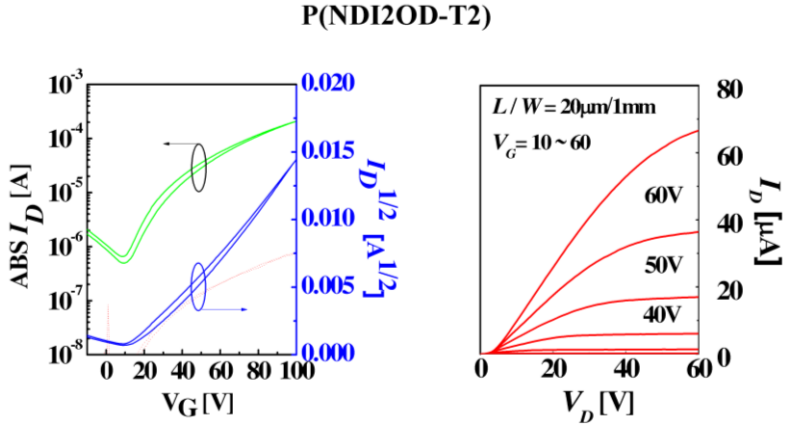

Figure 4.5 Current−voltage (I−V) characteristics of the OFETs fabricated with P(NDI2OD-T2) using CF as solvent and output characteristics of the devices annealed at 100 °C. Semiconductor OFET device fabricated by spin-coating onto Au S/D electrodes exhibited electron mobility, 0.32 $cm^2/V{\cdot}s$ (V_D = 100 V).

Table 4.3 Contact resistances of the TG/BC OFETs fabricated with P(NDI2SiC6-T2), P(NDI2SiC6-TVT), and P(NDI2OD-T2) varying annealing temperature.

Semiconductor	Annealing Temp/Time [°C/min]	Low-field mobility (μ_o) [$cm^2/V{\cdot}s$]	V_{Th} [V]	Contact resistance [MΩ]
P(NDI2SiC6-T2) (CN solvent)	100/30	1.55×10^{-3}	38.4	63.1
	200/30	8.67×10^{-3}	32.7	22.6
	300/30	5.33×10^{-3}	29.6	12.25
P(NDI2SiC6-TVT) (CN solvent)	100/30	6.5×10^{-4}	43.4	120
	200/30	1.56×10^{-4}	39.8	58.6
	300/30	7.7×10^{-3}	36.8	28.2
P(NDI2OD-T2)	100/30	9.75×10^{-4}	26.1	35.7

In both OFETs, the R_c values were gradually reduced as a function of the increased temperature. At each temperature, P(NDI2SiC6-T2) OFETs showed higher R_c values than those of the corresponding P(NDI2SiC6-TVT) OFETs (Figure 4.6). These findings agree very well with the trends of the changed mobilities described above.

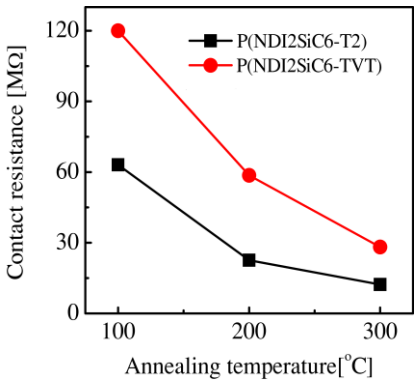

Figure 4.6 Contact resistance of the OFET devices upon different annealing temperatures.

Furthermore, we expanded the OFETs analyses to both P(NDI2SiC6-T2) and P(NDI2SiC6-TVT) films prepared from CN that mostly inhibits their pre-aggregations, because the dependence for each of the analyzed films was observed upon changing CF to CN, as already described in the previous section.

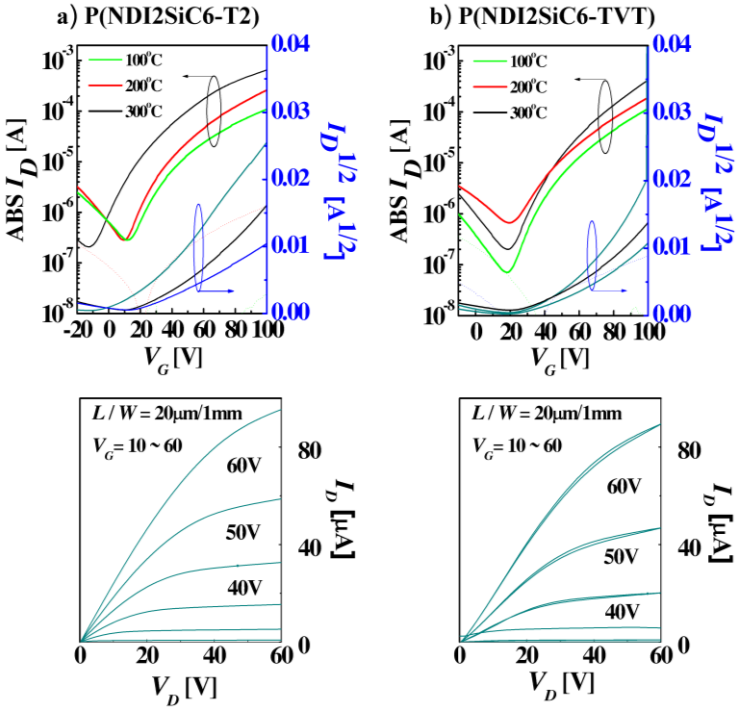

Figure 4.7 Current−voltage (*I*−*V*) characteristics of the OFETs fabricated with a) P(NDI2SiC6-T2) and b) P(NDI2SiC6-TVT) using CN as solvent and output characteristics of the devices annealed at 300 °C.

As was observed for the OFETs fabricated from CF, both polymer films formed when employing CN as solvent followed a similar tendency to increased mobilities with elevated annealing temperature over the range of 100 to 300 °C (Figure 4.7); P(NDI2SiC6-T2) (μ_{elec} = 0.85 cm^2/V·s) showed slightly higher electron mobility than that of P(NDI2SiC6-TVT) (μ_{elec} = 0.78 cm^2/V·s) (see Table 4.2). Obviously, it should be noted that the CF-cast films – which show the micro structured absorption spectra – revealed somewhat superior mobilities in general relative to the performances of the corresponding CN-cast OFET devices. These results corroborate that the film-packing orientations are influenced upon solvent selection (changing from CN to CF) since the molecular packing (degree of crystallinity and preference of ordering along the different crystallographic directions) strongly impacts the electronic coupling between molecules and the resulting charge carrier mobility.[44,45]

4.3.4. Thin-Film Morphology and Nanostructural Order

Firstly, information about the surface topography of the films fabricated from CF was gained with atomic force microscopy (AFM) images. As shown in Figure 4.8, the morphologies for both polymers are highly sensitive to annealing temperature, resulting in a clear visualization of the periodic structure of the fibril-like domains in both samples annealed at 300 ^{o}C.

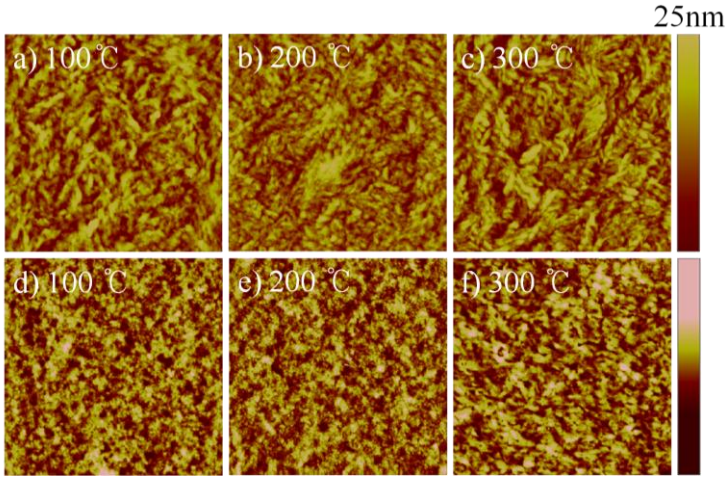

Figure 4.8 AFM height images of P(NDI2SiC6-T2) and P(NDI2SiC6-TVT) thin film prepared with CF at each annealed temperature. a), b) and c) represent P(NDI2SiC6-T2) thin film, d), e) and f) represent P(NDI2SiC6-TVT) thin film (4×4μm size).

Furthermore, to determine the extent of co-facial π-stacking, crystallinity, and polymer-packing orientation relative to the substrate, we characterized the as-spun and annealed films at 300 ^{o}C for P(NDI2SiC6-T2) and P(NDI2SiC6-TVT) prepared from both CN and CF, respectively, by using grazing incidence X-ray diffraction (GIXD) measurement. These studies can allow access to the origin of the high electron mobility and the reasons why variations in deposition conditions, such as annealing and solvent, lead to different mobility values. Typical out-of-plane and in-plane diffraction curves and the detailed crystallographic parameters extracted from those GIXD patterns are shown in Figure 4.9 and Table 3.4, respectively.

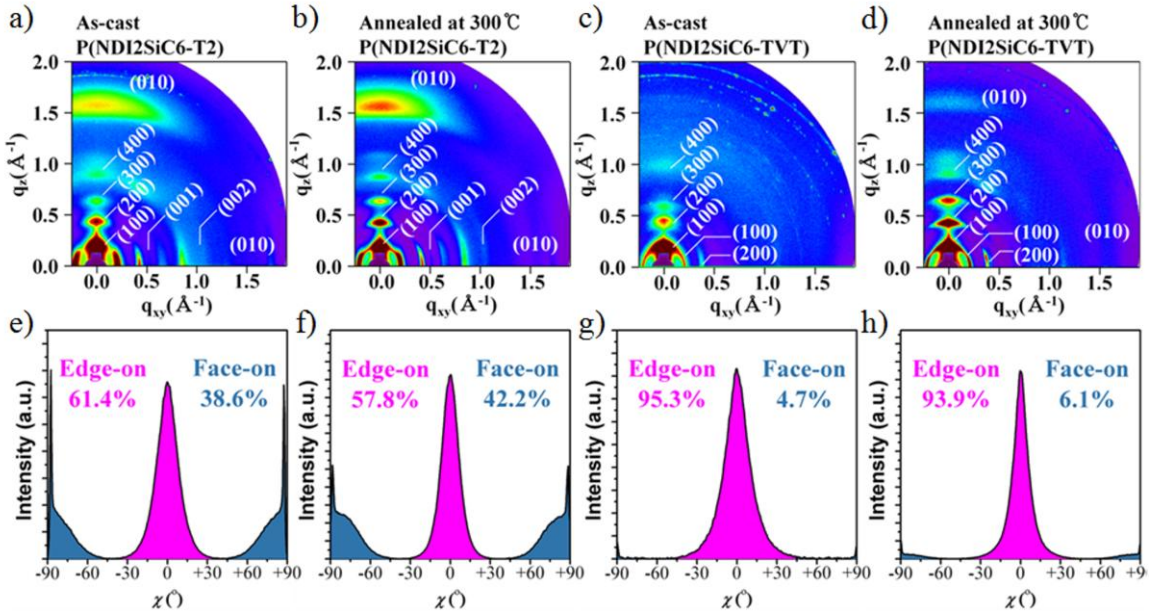

Figure 4.9 GIXD images and crystallite population of as-cast and annealed at 300 °C films fabricated by spin coating method using CF solution. a) and b) represent thin film of P(NDI2SiC6-T2), and c) and d) represent thin film of P(NDI2SiC6-TVT) under each condition; e)-h) are the corresponding pole figures.

Table 4.4 Crystallographic parameters calculated from GIXD profiles.

Preparation condition	Crystallographic parameters		P(NDI2SiC6-T2)	P(NDI2SiC6-TVT)
As-cast CF (solvent)	(100)	*q* (Å^{-1})	0.213	0.228
		d-spacing (Å)	29.5	27.6
	π–π	*q* (Å^{-1})	1.603	N/D[a]
		d-spacing (Å)	3.92	N/A[b]
Annealing at 300 °C CF (solvent)	(100)	*q* (Å^{-1})	0.223	0.232
		d-spacing (Å)	28.2	27.1
	π–π	*q* (Å^{-1})	1.62	1.63
		d-spacing (Å)	3.88	3.85
As-cast CN (solvent)	(100)	*q* (Å^{-1})	0.233	0.202
		d-spacing (Å)	27.0	31.1
	π–π	*q* (Å^{-1})	N/D[a]	N/D
		d-spacing (Å)	N/A[b]	N/A
Annealing at 300 °C CN (solvent)	(100)	*q* (Å^{-1})	0.228	0.199
		d-spacing (Å)	27.6	31.6
	π–π	*q* (Å^{-1})	N/D	N/D
		d-spacing (Å)	N/A	N/A

[a]Any discernible π–π stack peak was not detected in as-cast thin film. [b]The *d*-spacings could not be calculated due to the absence of π–π stack peak in as-cast thin film. All electrical characteristics were obtained from the top-gate based transistors more than twenty devices.

Both as-spun P(NDI2SiC6-T2) and P(NDI2SiC6-TVT) films in CF exhibited well-defined multiple (*h*00) diffraction patterns along the q_z (out-of-plane) axis corresponding to a highly ordered lamellar structure; (i) the observed lamellar *d*-spacing of P(NDI2SiC6-TVT) (27.6 Å) is slightly smaller than that of P(NDI2SiC6-T2) (29.5 Å) and (ii) a (*010*) diffraction peak arising from π-π stacking is clearly observed for P(NDI2SiC6-T2), while this peak is not found in P(NDI2SiC6-TVT).

When both the P(NDI2SiC6-T2) and P(NDI2SiC6-TVT) films were annealed at 300 ^{o}C, the peaks in the diffraction pattern became more defined and visible, suggesting the formation of more closed lamellar structures. For both annealed films coated from CF, two perpendicular features with *q* vectors compatible with the (*100*) and (*010*) peaks obtained with GIXD can be observed, confirming the co-existence of face-on and edge-on orientations.

We are able to quantify the crystallite orientation distribution using an intensity-corrected pole figure plot along the (*200*) diffraction peaks described previously.[1] Briefly, for each pole figure (see Figure 4.9), the integrated intensity is as a function of χ along the arcs, where χ (-90^{o} to 90^{o}) is defined as the semicircular angle between the crystallite orientation and the surface normal.[27]

The near vertical-cut (χ = 0^{o}) and horizontal-cut (χ = ± 90^{o}) are associated with the edge-on and face-on crystallites, respectively, where the area ratio of the two peaks (χ = 0^{o}–45^{o} and χ = 45^{o}–90^{o}) can be used to quantitatively access the portion of each crystallinity structure. The CF-pristine P(NDI2SiC6-T2) films show a clear bi-modal distribution (edge-on (61.4%) vs face-on (38.6%), whereas the CF-pristine P(NDI2SiC6-TVT) films have mainly edge-on structure (95.3%). In both cases, the thermal annealing slightly increases the face-on crystallite population (42.2% for P(NDI2SiC6-T2) and 6.1% for P(NDI2SiC6-TVT)) while

maintaining their majority crystallite population and trend. These increases of face-on crystallite population after thermal annealing were estimated to be induced by the orientational preference of NDI-based polymers in cast film.[17]

Near-edge X-ray absorption fine structure (NEXAFS) spectroscopy provides information regarding the molecular orientation of the conjugated core complementary to GIXD. Therefore, the angle-dependent Carbon K-edge NEXAFS was performed on the as-cast and annealed (300 ^{o}C) films fabricated using CF solution. Figure 4.10 shows the corresponding NEXAFS spectra collected in the incident X-ray angle range between 30 (~ parallel to film surface) and 85 (~ nominal to film surface) degrees.

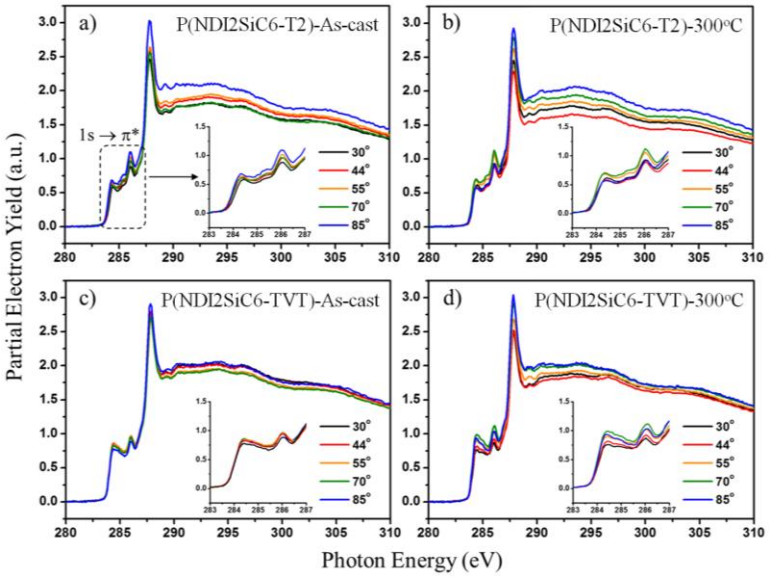

Figure 4.10 Angle-dependent Carbon K-edge NEXAFS spectra of as-cast and annealed at 300°C films fabricated by spin coating method using CF solution. a) and b) represent thin film of P(NDI2SiC6-T2), and c) and d) represent thin film of P(NDI2SiC6-TVT) under each condition. Insets show the magnified region of peaks corresponding to the resonant transitions of 1s → π* antibonding orbitals.

The lowest energy peaks appearing around 285 eV below the ionization step are associated with transitions from C-1s orbitals to π* antibonding orbitals.[35,46] Since the resonance intensity of this transition is sensitive to the orientation of the transition dipole moment (TDM) with respect to the polarization of the incident X-ray beam, angular dependence of the intensity of these π* resonances can be used to determine molecular orientation of the conjugated backbone. For example, if there is a strong angular dependence of the π* resonance intensity with the largest value at normal incident angle (90^o) to the film surface, this indicates that the conjugated plane is highly oriented and tilts away from the substrate in an edge-on orientation. However, all of the spectra show little angular dependence of the π* resonance intensity, as shown in the insets of Figure 4.10. The lack of strong angular dependence in the π* resonance could be associated either with a well-balanced face-on to edge-on ratio as proved by our GIXD results. Thermal annealing of the as-cast films leads to the slightly increased peak intensities at high incident angles (i.e., nominal to substrate).

We expanded the GIXD analysis to films prepared from CN. All CN-cast polymer films show a similar diffraction pattern regardless of the thermal treatment; although it is possible to discern the presence of faint (*h00*) diffraction peaks in the out-of-plane, being assignable to lamellar stacking oriented randomly with respect to the substrate, the (*010*) diffraction peaks are not seen both in the q_z and q_{xy} vectors (see Figure 4.11 and Table 3.4). This suggests that the CN-cast films before and after annealing possess a rather amorphous microstructure with almost exclusively edge-on population, substantiating the results obtained from the optical spectra above; the CN-cast films showed the less structured absorption spectra than those of CF-cast films.

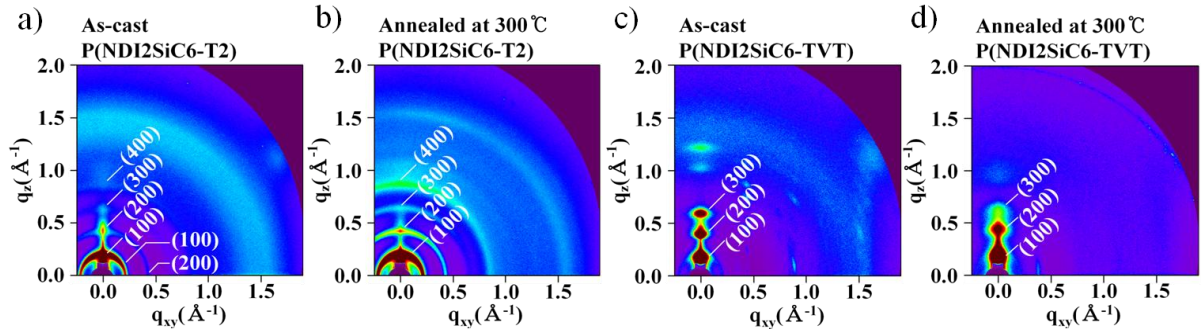

Figure 4.11 GIXD images of as-cast and annealed at 300 °C films fabricated by spin coating method using CN solution. a) and b) represent thin film of P(NDI2SiC6-T2), and c) and d) represent thin film of P(NDI2SiC6-TVT) under each condition.

By incorporating GIXD and NEXAFS results with the device performances, we propose that the charge transport in NDI-based polymers strongly correlates with not only the co-existence of face-on and edge-on crystalline domains but also the balanced face-on to edge-on ratios in NDI-based polymer, though π-π stacking distance and the packing conformation can directly affect the interpolymer chain carrier transport.[47] This finding is extremely significant since previous studies of polymer-packing orientation have mainly focused on how to adopt the preferential orientation order and the denser packing by tailoring structures and fabrication processing, and not on how to create the balanced mixture stacking structures with face-on and edge-on oriented molecules.

4.4. Conclusion

With taking into account the cooperative properties and synergistic effects derived from hybridization of organic and inorganic species, a hybrid siloxane-terminated hexyl chain (SiC6) has been incorporated onto the NDI-based backbone to generate P(NDI2SiC6-T2) and P(NDI2SiC6-TVT), respectively. We have shown distinct changes in the optical absorptions of these two polymers in solution when varying the organic solvent. Among the tested solvents, in both polymer cases, the most structured and red-shifted spectra are measured in CF, while the chain pre-aggregations in CN are almost absent. The intensities of the CT bands of the polymer films spin-coated from CF and CN solvents are slightly different, meaning that their aggregate content and type would be dependent on the chosen solvent. A combination of detailed electrical measurements by using OFET characterization and thin-film morphology studies (AFM, GIXD, and NEXAFS) reveals that the nature of the CF- and CN-cast films of each polymer has a significant influence on film morphology and molecular packing, thus affecting the charge transport properties. Regardless of the annealing treatment, both P(NDI2SiC6-T2) and P(NDI2SiC6-TVT) devices fabricated from CF solvent show a mixed face-on and edge-on orientation whereas the corresponding CN-cast films exhibit a rather amorphous microstructure with almost exclusively edge-on population, indicating the significant role of the chosen solvent on molecular assembly properties for NDI-based polymers. The co-existence of face-on and edge-on orientations in the CF-cast films is responsible for their higher electron transport mobilities than those of the corresponding CN-cast films. In particular, the annealed P(NDI2SiC6-T2) films from CF, despite showing less packed ordering along both the lamellar and π-stacking directions, have a highly balanced face-on to edge-on ratio (42.2% : 57.8%), resulting in the best electron mobility of up to 1.04

$cm^2/V{\cdot}s$. When the data from our current study are considered, for the first time, it is evident that the balanced face-on to edge-on ratio rather than the preferential orientation order and the strong π-stacking is a critical factor that governs charge transport, which provides a new test bench for the charge-transport mechanism.

4.5. Experimental Section

4.5.1 Materials

All chemicals and reagents were purchased from Sigma-Aldrich, Alfa Aesar chemical company, Tokyo Chemical Industry Co., Ltd., and used without any further purification. Dry THF was freshly distilled from reflux over sodium and benzophenone, prior to use.

4.5.2. Instruments for characterization

^{1}H and ^{13}C NMR were recorded on a Varian VNRS 600 MHz spectrometer using deuterated chloroform ($CDCl_3$) with TMS as an internal standard. Chemical shifts were given in parts per million (ppm) and coupling constants (*J*) in Hertz (Hz). Elemental analyses were carried out with a Flesh 2000 elemental analyzer. The molecular weights of the polymers were determined by gel permeation chromatography (GPC) with an Agilent 1200 series and miniDAWN TREOS using tetrahydrofuran (THF) as the eluent against PS standard. UV-Vis absorption spectra in solution and in thin film were recorded on a UV-1800 SHIMADZU UV Spectrophotometer. The electrochemical properties were characterized by VersaSTAT3 Princeton Applied Research Potentiostat in a three-electrode cell system with platinum as the working electrode, a platinum wire counter electrode and $Ag/AgNO_3$ as the reference electrode. The electrolytic solution employed was 0.1 M tetra-*n*-butylammonium hexafluorophosphate (n-Bu_4NPF_6) in dry acetonitrile under Ar atmosphere. The reference electrode was calibrated using a ferrocene/ferrocenium redox couple as an internal standard, whose oxidation potential is set at -4.8 eV with respect to zero vacuum level. The HOMO energy levels were obtained from the equation E_{HOMO} (eV) = LUMO - E_g^{opt}. The LUMO levels of polymers were obtained from the equation E_{LUMO} (eV) = -4.8- ($E_{1/2red}^{first}$- $E_{1/2ox}^{Fc/Fc+}$).

4.5.3. Synthesis of comomomers and polymers

*Preparation of N,N'-bis(hex-5-en-1-yl)-2,6-dibromo-1,4,5,8-naphthalenediimide (**3**):* 3.21 g (7.53 mmol) of 2,6-dibrmo-1,4,5,8-naphthalenetetracarboxylic dianhydride (**1**) was added to 80 ml of anhydrous acetic acid then stirred at room temperature for 30 minutes under argon atmosphere. 1.6g (18.79 mmol) of 6-amino-1-hexene (**2**) was carefully added dropwise to the solution of **1** in acetic acid then the reaction mixture was heated to reflux for 24 hours. The reaction mixture was cooled down to room temperature and extracted with water and chloroform. The organic layer was dried with $MgSO_4$ then concentrated under reduced pressure. The pale yellow solid product was obtained by column chromatography using chloroform as eluent. ^{1}H NMR ($CDCl_3$ 600 MHz): δ ppm 8.99 (s, 2H), 5.84-5.79 (m, 2H), 5.04-5.02 (d, *J* = 17.1Hz, 2H), 4.98-4.96 (d, *J* = 10.2Hz, 2H), 4.21 (t, *J* = 7.71Hz, 4H), 2.15 (m, 4H), 1.76 (m, 4H), 1.55 (m, 4H). ^{13}C NMR ($CDCl_3$, 150 MHz): δ ppm 161.07, 139.42, 138.59, 128.69, 128.05, 125.66, 124.42, 115.28, 41.75, 33.71, 27.71, 26.66. Anal. Calc'd for $C_{26}H_{24}Br_2N_2O_4$: C, 53.08; H, 4.11; N, 4.76. Found: C, 53.09; H, 4.30; N, 4.76.

*Preparation of N,N'-bis(1,1,1,3,5,5,5-heptamethyltrisiloxane)-2,6-dibromo-1,4,5,8-naphthalenediimide (**4**):* Compound **3** (1.1 g, 1.87 mmol) and 1,1,1,3,5,5,5-heptamethyltrisiloxane (1.0 g, 4.49 mmol) were dissolved in anhydrous toluene then 60 mg of Karstedt catalyst ($C_8H_{18}OPtSi_2$, Pt 2% xylene solution) was added dropwise. The reaction mixture was heated to 80 ^{o}C then stirred for 24 hours. The reaction mixture was cooled to room temperature then concentrated under reduced pressure. The pale yellow solid product was obtained by column chromatography (eluent: chloroform/hexane = 4/1). ^{1}H NMR ($CDCl_3$ 600 MHz): δ ppm 8.99 (s, 2H), 4.19 (t, *J* = 7.70Hz, 4H), 1.73 (m, 4H), 1.42-1.33 (m, 12H), 0.459 (t, *J* = 7.35Hz, 4H), 0.2-0.08 (s, 42H). ^{13}C NMR ($CDCl_3$, 150 MHz): δ ppm

161.01, 139.34, 128.63, 128.00, 125.65, 124.39, 41.94, 33.22, 28.22, 27.16, 23.37, 17.92, 2.21, 0.036. Anal. Calc'd for $C_{40}H_{68}Br_2N_2O_8Si_6$: C, 46.49; H, 6.63; N, 2.71. Found: C, 46.53; H, 6.64; N, 3.00.

Preparation of polymers P(NDI2SiC6-T2) and P(NDI2SiC6-TVT): Under argon atmosphere, a mixture of dibrominated NDISiC6 (**4**, 413 mg, 0.400 mmol for P(NDI2SiC6-T2) or 150 mg, 0.145 mmol for P(NDI2SiC6-TVT)), bis-stannylated co-monomer (**5**, 197 mg, 0.400 mmol for P(NDI2SiC6-T2) or **6**, 75.2 mg, 0.145 mmol for P(NDI2SiC6-TVT)), $Pd_2(dba)_3$ (5.5 mg, 6 μmol for P(NDI2SiC6-T2) or 2.0 mg, 2.18 μmol for P(NDI2SiC6-TVT)), and P(*o*-tolyl)$_3$ (9.1 mg, 30 μmol for P(NDI2SiC6-T2) and 3.3mg, 10.8 μmol for P(NDI2SiC6-TVT)) was dissolved in degassed anhydrous toluene (6 ml for P(NDI2SiC6-T2), 4 ml for P(NDI2SiC6-TVT)) and stirred at 90 ^{o}C for 2 days. After reaction, the solids precipitated by dropwise addition of reaction mixture to 800 ml of methanol were collected by filtration then dried in vacuum drying oven. The crude polymers were purified by Soxhlet extraction with methanol, acetone, hexane, and chloroform sequentially for the removal of low molecular weight product. The chloroform fraction was extracted with EDTA saturated aqueous solution and distilled water three times then dried with anhydrous $MgSO_4$. The dried chloroform solution was concentrated under reduced pressure for the precipitation of polymer in methanol. The purified polymers were collected by filtration, washed with methanol and dried in a vacuum drying oven leading to dark greenish blue solid.

Poly((N,N'-bis(1,1,1,3,5,5,5-heptamethyltrisiloxane)-1,4,5,8-naphthalenediimide-2,6-diyl)-alt-5,5'-bithiophene) (P(NDI2SiC6-T2)): 120 mg of isolated polymer was obtained with 28.9% yield. GCP analysis M_n = 32 kDa, M_w = 65 kDa, and PDI = 2.02 (against PS standard) obtained. ^{1}H NMR ($CDCl_3$ 600 MHz): δ ppm 8.82 (s, 2H), 7.36 (s, 2H), 7.32 (s, 2H), 4.15 (m,

4H), 2.16 (m, 4H), 1.71-1.0 (br, 12H), 0.87-0.20 (br, 46H). Anal. Calc'd for $C_{48}H_{72}N_2O_8S_2Si_6$: C, 55.55; H, 6.99; N, 2.70. Found: C, 55.26; H, 6.89; N, 2.55.

Poly((N,N'-bis(1,1,1,3,5,5,5-heptamethyltrisiloxane)-1,4,5,8-naphthalenediimide-2,6-diyl)-alt-5,5'-(E)-2-(2-(thiophene-2-yl)-vinyl)thiophene) (P(NDI2SiC6-TVT)): 110 mg of isolated polymer was obtained with 73.3% yield. GPC analysis M_n = 15 kDa, M_w = 50 kDa, and PDI = 3.28 (against PS standard) obtained. ^{1}H NMR ($CDCl_3$ 600 MHz): δ ppm 8.80 (m, 2H), 7.28-7.16 (m, 6H), 4.14 (m, 4H), 2.03 (m, 4H), 1.70-1.0 (br, 12H), 0.88-0.20 (br, 46H). Anal. Calc'd for $C_{50}H_{74}N_2O_8S_2Si_6$: C, 56.45; H, 7.01; N, 2.63. Found: C, 56.72; H, 6.95; N, 2.59.

4.5.4. Fabrication and characterization of OFETs

TG/BC structure OFETs were fabricated on Corning Eagle 2000 glass substrate. After the conventional photolithography process of developing photoresist layer for source/drain electrode patterning, a 3 nm-thick Ni adhesion layer and a 13 nm-thick Au contacting layer were deposited followed by the lift-off of photoresist. The substrates with patterned Au/Ni electrodes were cleaned sequentially with an ultrasonic bath in deionized water, acetone, and isopropanol for 10 min each. The polymer thin films (20–22 nm thickness) were prepared from hybrid siloxane–NDI polymer solution in chloroform or 1-chloronaphthalene (4 mg/mL) using spin-coating methods, and sequentially thermal annealed at 100, 200, 300 ℃ for 30 min in a nitrogen (N_2)-filled glove box. PMMA polymer dielectric was purchased from Sigma-Aldrich and used without further purification. The PMMA was dissolved in *n*-butyl acetate (nBA) at 80 mg/ml concentration and then spin-coated on the polymer layer followed by a thermal baking at 80 ℃ for ~30 min in the same N_2-filled glove box to remove the

residual solvents. The device fabrication was completed by deposition of aluminum (Al) as top-gate electrodes (~50 nm thick) via thermal evaporation using metal shadow masks.

Contact resistance of OFETs: Y-function method (YFM) is considered as a fast and precise alternative method for obtaining R_c. From the transfer characteristics of the OFETs, I_d in the linear regime can be described as in following equation:

$$I_d = \frac{W}{L} C_i (V_g - V_{Th}) \frac{\mu_0}{1+\theta(V_g - V_{Th})} \times V_d \qquad (1)$$

where C_i is the dielectric capacitance per unit area, and μ_o is the low-field mobility. θ is the mobility attenuation factor, which consists of the extrinsic factors caused by the surface roughness and phonon scattering (θ_o) and contact resistance [$\theta^* = (W/L)\mu_o C_i R_c$]. Assuming a constant R_c, the transconductance (g_m) can be expressed as

$$g_m = \frac{\delta I_d}{\delta V_g} = \frac{W}{L} C_i \frac{\mu_0}{[1+\theta(V_g - V_{Th})]^2} \times V_d \qquad (2)$$

θ can be obtained by plotting $1/g_m^{1/2}$ versus V_g at a strong charge accumulation, where a linear behavior is obtained. Assuming that θ_o is negligible, R_c can be calculated, as summarized in Table 4.3. Note that the negative value of θ, is presumably due to the gate-field enhanced mobility, which is compensated for by the conventional mobility attenuation.

Near edge X-ray absorption fine structure (NEXAFS) characterization: Carbon K-edge NEXAFS measurements were carried out at the U7A NIST beamline of the National Synchrotron Light Source at Brookhaven National Laboratory. The NEXAFS spectra were collected in partial electron yield (PEY) mode with a Channeltron electron multiplier detector with the entrance grid bias set to -150 V to enhance the surface sensitivity. A toroidal spherical grating monochromator with 600 lines mm^{-1} was used, yielding an energy resolution of approximately 0.10 eV. A carbon mesh was used for energy calibration using

the carbon K-edge π*C=C transition of graphite at 285.10 eV. The incident beam angle with respect to the sample was controlled in the range of 20 90° to obtain orientation information. The PEY signals were normalized using the incident beam intensity obtained from the photoemission yield of a clean Au grid to eliminate the effects of beam fluctuations and monochromator absorption features. All spectra were processed using standard pre- and post-edge normalization methods, as described in previously published work.[48] The pre-edge jump was subtracted to zero, followed by post-edge normalization, which consisted of dividing the pre-edge normalized spectra by the edge jump intensity obtained far above the C K-edge, beyond 320 eV. The pre- and post-edge normalization was performed using the Athena program.

4.6. Reference

(1) Kim, G.; Kang, S.-J.; Dutta, G. K.; Han, Y.-K.; Shin, T. J.; Noh, Y.-Y.; Yang, C. *J. Am. Chem. Soc.* **2014**, *136*, 9477.

(2) Lee, J.; Han, A.-R.; Kim, J.; Kim, Y.; Oh, J. H.; Yang, C. *J. Am. Chem. Soc.* **2012**, *134*, 20713.

(3) Lee, J.; Han, A.-R.; Yu, H.; Shin, T. J.; Yang, C.; Oh, J. H. *J. Am. Chem. Soc.* **2013**, *135*, 9540.

(4) Baeg, K.-J.; Caironi, M.; Noh, Y.-Y. *Adv. Mater.* **2013**, *25*, 4210.

(5) Olivier, Y.; Niedzialek, D.; Lemaur, V.; Pisula, W.; Müllen, K.; Koldemir, U.; Reynolds, J. R.; Lazzaroni, R.; Cornil, J.; Beljonne, D. *Adv. Mater.* **2014**, *26*, 2119.

(6) Henson, Z. B.; Mullen, K.; Bazan, G. C. *Nat. Chem.* **2012**, *4*, 699.

(7) Tsao, H. N.; Cho, D. M.; Park, I.; Hansen, M. R.; Mavrinskiy, A.; Yoon, D. Y.; Graf, R.; Pisula, W.; Spiess, H. W.; Müllen, K. *J. Am. Chem. Soc.* **2011**, *133*, 2605.

(8) Sirringhaus, H. *Adv. Mater.* **2014**, *26*, 1319.

(9) Mei, J.; Diao, Y.; Appleton, A. L.; Fang, L.; Bao, Z. *J. Am. Chem. Soc.* **2013**, *135*, 6724.

(10) Tseng, H.-R.; Phan, H.; Luo, C.; Wang, M.; Perez, L. A.; Patel, S. N.; Ying, L.; Kramer, E. J.; Nguyen, T.-Q.; Bazan, G. C.; Heeger, A. J. *Adv. Mater.* **2014**, *26*, 2993.

(11) Li, J.; Zhao, Y.; Tan, H. S.; Guo, Y.; Di, C.-A.; Yu, G.; Liu, Y.; Lin, M.; Lim, S. H.; Zhou, Y.; Su, H.; Ong, B. S. *Sci. Rep.* **2012**, *2*.

(12) Kang, I.; Yun, H.-J.; Chung, D. S.; Kwon, S.-K.; Kim, Y.-H. *J. Am. Chem. Soc.* **2013**, *135*, 14896.

(13) Newman, C. R.; Frisbie, C. D.; da Silva Filho, D. A.; Brédas, J.-L.; Ewbank, P. C.; Mann, K. R. *Chem. Mater.* **2004**, *16*, 4436.

(14) Chua, L.-L.; Zaumseil, J.; Chang, J.-F.; Ou, E. C. W.; Ho, P. K. H.; Sirringhaus, H.; Friend, R. H. *Nature* **2005**, *434*, 194.

(15) Oh, J. H.; Lee, H. W.; Mannsfeld, S.; Stoltenberg, R. M.; Jung, E.; Jin, Y. W.; Kim, J. M.; Yoo, J.-B.; Bao, Z. *Proc. Natl. Acad. Sci. U.S.A.* **2009**, *106*, 6065.

(16) Usta, H.; Risko, C.; Wang, Z.; Huang, H.; Deliomeroglu, M. K.; Zhukhovitskiy, A.; Facchetti, A.; Marks, T. J. *J. Am. Chem. Soc.* **2009**, *131*, 5586.

(17) Steyrleuthner, R.; Di Pietro, R.; Collins, B. A.; Polzer, F.; Himmelberger, S.; Schubert, M.; Chen, Z.; Zhang, S.; Salleo, A.; Ade, H.; Facchetti, A.; Neher, D. *J. Am. Chem. Soc.* **2014**, *136*, 4245.

(18) Chen, H.; Guo, Y.; Mao, Z.; Yu, G.; Huang, J.; Zhao, Y.; Liu, Y. *Chem. Mater.* **2013**, *25*, 3589.

(19) Kim, R.; Amegadze, P. S. K.; Kang, I.; Yun, H.-J.; Noh, Y.-Y.; Kwon, S.-K.; Kim, Y.-H. *Adv. Funct. Mater.* **2013**, *23*, 5719.

(20) Anthony, J. E.; Facchetti, A.; Heeney, M.; Marder, S. R.; Zhan, X. *Adv. Mater.* **2010**, *22*, 3876.

(21) Sun, B.; Hong, W.; Yan, Z.; Aziz, H.; Li, Y. *Adv. Mater.* **2014**, *26*, 2636.

(22) Sonar, P.; Singh, S. P.; Li, Y.; Soh, M. S.; Dodabalapur, A. *Adv. Mater.* **2010**, *22*, 5409.

(23) Di Pietro, R.; Fazzi, D.; Kehoe, T. B.; Sirringhaus, H. *J. Am. Chem. Soc.* **2012**, *134*, 14877.

(24) Yan, H.; Chen, Z.; Zheng, Y.; Newman, C.; Quinn, J. R.; Dötz, F.; Kastler, M.; Facchetti, A. *Nature* **2009**, *457*, 679.

(25) Chen, Z.; Zheng, Y.; Yan, H.; Facchetti, A. *J. Am. Chem. Soc.* **2008**, *131*, 8.

(26) Rivnay, J.; Toney, M. F.; Zheng, Y.; Kauvar, I. V.; Chen, Z.; Wagner, V.; Facchetti, A.; Salleo, A. *Adv. Mater.* **2010**, *22*, 4359.

(27) Rivnay, J.; Steyrleuthner, R.; Jimison, L. H.; Casadei, A.; Chen, Z.; Toney, M. F.; Facchetti, A.; Neher, D.; Salleo, A. *Macromolecules* **2011**, *44*, 5246.

(28) Fabiano, S.; Musumeci, C.; Chen, Z.; Scandurra, A.; Wang, H.; Loo, Y.-L.; Facchetti, A.; Pignataro, B. *Adv. Mater.* **2012**, *24*, 951.

(29) Caironi, M.; Bird, M.; Fazzi, D.; Chen, Z.; Di Pietro, R.; Newman, C.; Facchetti, A.; Sirringhaus, H. *Adv. Funct. Mater.* **2011**, *21*, 3371.

(30) Fabiano, S.; Yoshida, H.; Chen, Z.; Facchetti, A.; Loi, M. A. *ACS Appl. Mater. Interfaces.* **2013**, *5*, 4417.

(31) Cheng, X.; Noh, Y.-Y.; Wang, J.; Tello, M.; Frisch, J.; Blum, R.-P.; Vollmer, A.; Rabe, J. P.; Koch, N.; Sirringhaus, H. *Adv. Funct. Mater.* **2009**, *19*, 2407.

(32) Sirringhaus, H.; Brown, P. J.; Friend, R. H.; Nielsen, M. M.; Bechgaard, K.; Langeveld-Voss, B. M. W.; Spiering, A. J. H.; Janssen, R. A. J.; Meijer, E. W.; Herwig, P.; de Leeuw, D. M. *Nature* **1999**, *401*, 685.

(33) Chabinyc, M. L.; Toney, M. F.; Kline, R. J.; McCulloch, I.; Heeney, M. *J. Am. Chem. Soc.* **2007**, *129*, 3226.

(34) Jimison, L. H.; Salleo, A.; Chabinyc, M. L.; Bernstein, D. P.; Toney, M. F. *Phys. Rev. B* **2008**, *78*, 125319.

(35) Schuettfort, T.; Thomsen, L.; McNeill, C. R. *J. Am. Chem. Soc.* **2012**, *135*, 1092.

(36) Li, Y.; Sonar, P.; Singh, S. P.; Soh, M. S.; van Meurs, M.; Tan, J. *J. Am. Chem. Soc.* **2011**, *133*, 2198.

(37) Zhang, F.; Hu, Y.; Schuettfort, T.; Di, C.-a.; Gao, X.; McNeill, C. R.; Thomsen, L.; Mannsfeld, S. C. B.; Yuan, W.; Sirringhaus, H.; Zhu, D. *J. Am. Chem. Soc.* **2013**, *135*, 2338.

(38) Lei, T.; Dou, J.-H.; Pei, J. *Adv. Mater.* **2012**, *24*, 6457.

(39) Ha, Y.-g.; Emery, J. D.; Bedzyk, M. J.; Usta, H.; Facchetti, A.; Marks, T. J. *J. Am. Chem. Soc.* **2011**, *133*, 10239.

(40) Mei, J.; Kim, D. H.; Ayzner, A. L.; Toney, M. F.; Bao, Z. *J. Am. Chem. Soc.* **2011**, *133*, 20130.

(41) Steyrleuthner, R.; Schubert, M.; Howard, I.; Klaumünzer, B.; Schilling, K.; Chen, Z.; Saalfrank, P.; Laquai, F.; Facchetti, A.; Neher, D. *J. Am. Chem. Soc.* **2012**, *134*, 18303.

(42) Schubert, M.; Dolfen, D.; Frisch, J.; Roland, S.; Steyrleuthner, R.; Stiller, B.; Chen, Z.; Scherf, U.; Koch, N.; Facchetti, A.; Neher, D. *Adv. Energy. Mater.* **2012**, *2*, 369.

(43) Baeg, K.-J.; Bae, G.-T.; Noh, Y.-Y. *ACS Appl. Mater. Interfaces.* **2013**, *5*, 5804.

(44) Coropceanu, V.; Cornil, J.; da Silva Filho, D. A.; Olivier, Y.; Silbey, R.; Brédas, J.-L. *Chem. Rev.* **2007**, *107*, 926.

(45) Brédas, J.-L.; Cornil, J.; Beljonne, D.; dos Santos, D. A.; Shuai, Z. *Acc. Chem. Res.* **1999**, *32*, 267.

(46) Gann, E.; McNeill, C. R.; Szumilo, M.; Sirringhaus, H.; Sommer, M.; Maniam, S.; Langford, S. J.; Thomsen, L. *J. Chem. Phys.* **2014**, *140*, 164710.

(47) Rivnay, J.; Noriega, R.; Northrup, J. E.; Kline, R. J.; Toney, M. F.; Salleo, A. *Phys. Rev. B* **2011**, *83*, 121306.

(48) Lee, S.-W.; Bak, S.-M.; Lee, C.-W.; Jaye, C.; Fischer, D. A.; Kim, B.-K.; Yang, X.-Q.; Nam, K.-W.; Kim, K.-B. *J. Phys. Chem. C* **2014**, *118*, 2834.